# EXPOSURE FROM THORON, RADON AND MODELLING INDOOR GAMMA RADIATION DOSE IN HOMA BAY COUNTY, KENYA

**WILLIS OTIENO GOR ODONGO (M.SC)**

**I84/28545/2018**

**THESIS SUBMITTED IN FULFILLMENT OF THE REQUIREMENTS FOR THE AWARD OF THE DEGREE OF DOCTOR OF PHILOSOPHY (NUCLEAR PHYSICS) IN THE SCHOOL OF PURE AND APPLIED SCIENCE OF KENYATTA UNIVERSITY**

**JULY, 2023**

## DECLARATION

This thesis is my original work and has not been presented for the award of a degree or any other award in any other university.

**Signature**_____ **Date** 04/07/2023
**Willis Otieno Gor Odongo**
**I84/28545/2018**

### SUPERVISORS

We confirm that the work reported in this thesis was carried out by the candidate under our supervision:

**Signature**_____ **Date** 05/07/2023
**Dr. Margaret W. Chege**
Department of Physics,
Kenyatta University.

**Signature**_____ **Date** 05/07/2023
**Dr. Nadir Hashim**
Department of Physics,
Kenyatta University.

**Signature**_____ **Date** 04/07/2023
**Prof. Shinji Tokonami**
Department of Radiation Measurement and Physical Dosimetry,
Institute of Radiation Emergency Medicine,
Hirosaki University.
Japan.

## DEDICATION

This work is dedicated to my late parents, Shadrack Odongo and Rose Atieno

## ACKNOWLEDGEMENTS

I am sincerely grateful to my research supervisors, Dr. Margaret Chege, Dr. Nadir Hashim, and Prof. Shinji Tokonami, for their relentless support, guidance, advice, and motivation throughout the research work. I greatly appreciate the whole team of the Institute of Radiation Emergency Medicine at Hirosaki University for the provision of the radon detectors alongside the analysis process. I also thank the whole of Kenyatta University Physics Department members for their guidance during my Physics seminar presentations. Special thanks go to all the Physics laboratory technicians, led by Chief laboratory technologist Fredrick Mudimba for their technical support during this research work. My gratitude also goes to my fellow postgraduate colleagues Catherine Nyambura and Charles Rotich of Kenyatta University, who greatly assisted with their experience and expertise in experimental measurements and data analysis. I would also greatly appreciate Mr. Joram Kihumba and Mr. David Opere for their fieldwork support in Homa, Ruri and Lake Victoria. I also greatly appreciate the support of the local administrators of the Homa and Ruri regions. A lot of appreciation to the Water Resource Management Authority (WARMA) for the assistance with the RAD7 detector. I also greatly appreciate my wife, sons and daughter for their moral and financial support, prayers and sacrifices to ensure I get adequate time and resources for this work. I also wish to greatly thank Kisii University for the conducive work environment that allowed me to do this research. Many thanks to my colleagues Dr. Carlford Otieno and Dr. Daniel Ketui for their support while working at the institution. Much appreciation also goes to the residents and local administration of Homa and Ruri for their acceptance. Above all am sincerely grateful to Almighty God for the good health and wisdom he granted me the whole of this period.

# TABLE OF CONTENTS

## LIST OF TABLES

## LIST OF FIGURES

## LIST OF ABBREVIATIONS AND ACRONYMS

| | |
|---|---|
| **AAS** | Atomic Absorption Spectrophotometer |
| **CR-39** | Colombia Resin number 39 |
| **DNA** | Deoxyribonucleic Acid |
| **DSS** | Digital sampling system |
| **EC** | European council |
| **EETC** | Equilibrium equivalent thoron concentration |
| **ERR** | Excess relative risk |
| **EU** | European Union |
| **GRS** | Generic reactor safety |
| **HBRA** | High background radiation area. |
| **IAEA** | International atomic energy agency |
| **IARC** | International agency for research on cancer |
| **ICRP** | International commission on radiation protection |
| **IQ** | Intelligent quotient |
| **ISO** | International Organization for Standardization |
| **LLD** | Lower limit of detection |
| **MCA** | Multichannel Analyzer |
| **MDA** | Minimum detectable activity |
| **MOH** | Ministry of Health (Kenya) |
| **NaI(TI)** | Thallium Activated sodium iodide detector |
| **NORM** | Naturally occurring radioactive materials. |

| | |
|---|---|
| **NRC- BEI**R | National research council on biological effects of ionization radiation |
| **PCA-P** | Principal component analysis |
| **PCI** | Peripheral component interconnect standard |
| **RAD7** | Radon in air detector number 7 |
| **RADUET** | Radon–thoron discriminative monitors |
| **RBM** | Red bone marrow |
| **SSNTD** | Solid state nuclear track detector |
| **TDS** | Total dissolved solids |
| **TSS** | Total suspended solids |
| **UNSCEAR** | United nations scientific committee on effects of atomic radiation |
| **USEPA** | United States environmental protection agency |
| **WHO** | World health organization |

## ABSTRACT

Homa and Ruri hills in Homa Bay County, Kenya, are associated with high background radiation levels. Presently, they are experiencing high human settlement. Maize is the major food crop and Lake Victoria is the major water source. There is no sufficient data on radiation exposure from indoor gamma, air ($^{222}$Rn and $^{220}$Rn) crops and water. The main objective of this research is to determine human exposure to ionizing radiation associated with natural radioactivity in dwellings, water and crops, besides assessing the risk of heavy metals from contamination of Lake Victoria waters and modeling indoor gamma absorbed dose due to non-secular equilibrium in $^{232}$Th decay series. Terrestrial radioactivity measurements were done using NaI (Tl) detector. Indoor $^{222}$Rn, $^{220}$Rn, and $^{220}$Rn progenies were measured using RADUET and EETC monitors while $^{222}$Rn in water was measured using big bottle system coupled with RAD7. For heavy metal analysis, AAS was used. A mathematical model on absorbed gamma dose was developed and validated. The modelled and measured absorbed doses in the dwellings registered a reasonable agreement. The modelled absorbed dose was 15% less than the experimental one, which considers secular equilibrium in the $^{232}$Th decay series. The total annual effective dose from indoor air in Ruri was 4.9±0.7 mSv/y$^{1,}$ nearly 1.5 times that of Homa. The average $^{222}$Rn concentration in Lake Victoria in Homa was 14.8 Bq/L, 10% higher than in Ruri. The average $^{222}$Rn ingested annual effective dose was 60% lower than the recommended WHO reference level of 100 μSv/y$^{1}$ in both regions. Arguably, heavy-metal lead was the main contaminant in Lake Victoria around the study region as the average incremental lifetime cancer risk for heavy metals was above the WHO limit of $1 \times 10^{-4}$ by a factor of 5 for adults in both Ruri and Homa, respectively. The total annual effective dose from indoor air, building materials, food stuff maize, and Lake Victoria in Homa was 45% lower than Ruri, which was 12.6±2.1 mSv/y, each contributing about 45%, 30%, 24%, and 1% of the dose respectively in both regions. These results indicate potential health risk of human exposure to ionizing radiations in these regions as the reported values in some of the considered dwellings and maize samples were above the ICRP and WHO safe limits. Indoor air was the major contributor to radiation exposure; thus, houses in the regions should be properly ventilated. Non-secular equilibrium in the $^{232}$Th decay series should be considered in determining absorbed gamma dose in earthen dwellings to avoid overestimation.

# CHAPTER ONE: INTRODUCTION

## 1.1 Background information

Ruri and Homa hills are considered among the high background radiation areas in Kenya as established by Opiyo *et al.,* 2009 and Otwoma *et al*., 2013 respectively, they are both located in Homa Bay county in the south western part of Kenya. The major categories of the natural exposure as a result of the high background radiation in this area include external exposure from primordial radionuclides $^{226}$Ra $^{232}$Th and $^{40}$K in the building material, inhalation of radon and thoron alongside the ingestion of food crops and water. The level of human exposure to ionizing radiation from radioactivity in earthen building materials, indoor air (radon and thoron), water (radon), crops (maize) was determined in this work in Homa and Ruri. A model of gamma absorbed dose rate as a result of the non-secular equilibrium in $^{232}$Th decay series due to thoron release which is prevalent with highly porous building materials like the earthen ones studied in this work was also developed. Lastly, this research work also analysed the non-radioactive physio-chemical parameters i.e., concentration of selected heavy metals, electrical conductivity, temperature and pH in Lake Victoria waters around Homa and Ruri regions.

The primordial radionuclides are not uniformly distributed in the environment but occur in varying quantities in rock and soil as characterized by the geology of a region (Eisenbud *et al.,* 1997). Therefore, it is important to determine their levels in soil and rocks which constitutes major building materials in Homa and Ruri, maize which is the major food crop grown in the study region as well as their corresponding individual contributions to the

total radiation dose. It is also necessary to determine the levels of indoor radon and thoron in these regions given the high levels of their parent radionuclide $^{226}$Ra and $^{232}$Th respectively for purposes of radiation protection.

The natural radionuclides decay to emit radon gas and gamma radiation to certain levels depending on their quantities in the building materials, which vary based on the type and nature of the building material. Therefore, external radiation exposure exists due to the emitted gamma rays in the dwellings and internal exposure from inhalation of the radon isotopes. Consequently, there is a need for radiological impact assessment for building materials used in Homa and Ruri to develop control measures, policies and mitigation on the radiological effects on the human population and environment (Karangelos *et al.*, 2004; Kumar *et al.*, 2014). International organizations such as the International Commission on Radiological Protection (ICRP, 2007; WHO, 2009; IAEA-TRS 474, 2013; Euratom, 2014) have adopted and developed measures to mitigate radiation exposures through the formulation of standards, guidelines, and legislation for reference levels, action levels, building codes, radiological protection principles, and dose rate measurement protocols, all of which are yet to be emphasized and applied in rural Kenya based on the data from such studies.

These radionuclides are transferred to plants through uptake by the roots when dissolved in the water alongside other minerals and nutrients. Human consumption of food crops through the ingestion pathway gets the radionuclides into the body. Consequently, high concentrations of these radionuclides in food crops are unsafe for human health

(Asaduzzaman *et al.*, 2015). It is necessary to determine the levels of terrestrial radionuclides in maize which is the major food crop grown in the study region.

The gamma absorbed dose rate model is based on the fact that it mainly arises from the short-lived progeny of $^{222}$Rn and $^{220}$Rn in $^{226}$Ra and $^{232}$Th decay series, respectively. Their release on the house's outer and inner walls reduces them in the building material. The ones exhaled from the house's exterior wall are all lost to the surrounding air, while the ones exhaled from the inner walls of the house get controlled by removal through ventilation and deposition. Their progenies are ions; thus, some attach to water or other polarized molecules in the house. Therefore, the release of $^{222}$Rn and $^{220}$Rn affects secular equilibrium in $^{226}$Ra and $^{232}$Th decay series, respectively, which consequently reduces the amount of $^{222}$Rn, $^{220}$Rn, and their progenies contributing to the indoor gamma absorbed dose rate. $^{220}$Rn has always been ignored due to its short half-life of 55.6 s and thus decays before getting to the room space from the concrete walls. However, this is not true for the case of a typical earthen dwelling common in regions of Homa and Ruri characterized by many cracks, high porosity, and elevated levels of parent radionuclide $^{232}$Th, resulting in an enhanced $^{220}$Rn release rate.

The radon isotopes [Radon ($^{222}$Rn) and thoron ($^{220}$Rn)] account for 52% of the general public's exposure to natural radiation sources (UNSCEAR, 2008). The generation and distribution pattern of these isotopes in soils are linked to geological conditions such as; $^{226}$Ra and $^{232}$Th content in surrounding bedrocks and soils which has already been established to be high in both Homa and Ruri. $^{222}$Rn has a half-life of 3.8 days and is produced in the decay chain of $^{226}$Ra within the $^{238}$U decay chain, as shown in appendix I.

$^{220}$Rn has a half-life of 55.6 seconds and is produced in the decay of $^{224}$Ra decay process in the $^{232}$Th decay chain, as shown in appendix II (Crameri *et al.,* 1989).

These isotopes are emitted into the void spaces between the grains, transported by diffusion and advection/convection, and eventually exhaled from the soil into dwellings and water sources like lakes, rivers, shallow wells, and boreholes. Ventilation and air conditioning ducts are the various routes through which these isotopes can seep into indoor spaces (WHO, 2009). For the typical Kenyan rural earthen houses considered in this study, the cracks on the floor and walls easily allow the radon isotopes to seep into the house (Chege *et al.,* 2019). $^{220}$Rn was initially ignored because of its short half-life, thus can largely decay before getting to living space. However, emerging studies have indicated $^{220}$Rn can be a risk and even a major contributor to inhaled dose, particularly in earthen dwellings, which has more cracks and pores on the walls and floor, making it easier for emanated $^{220}$Rn to diffuse to the living space before decay compared to concrete one. Therefore, the likelihood of $^{220}$Rn having a higher concentration in earthen dwellings is very high, as has already been observed in soil-walled dwellings in China (Shang *et al.,* 2005) and Ghana (Quashie *et al.,* 2011). Earthen dwellings are common in many parts of rural Kenya, Homa and Ruri being part of the same. $^{220}$Rn has a very short half-life and is not evenly distributed in the house. Therefore, long-lived progenies like $^{212}$Pb and $^{212}$Bi are used to determine its inhaled dose assessment accurately. These concentrations are collectively expressed in the equivalent equilibrium concentration (EEC) known as Equilibrium Equivalent Thoron Concentration (EETC) for thoron progeny. They are directly measured using EETC monitors (Tokonami, 2020).

The exhalation rate of both $^{222}$Rn and $^{220}$Rn contributes immensely to their reaching outer space from building materials and the ground. It depends on the content of the parent radionuclides $^{226}$Ra for $^{222}$Rn and $^{232}$Th for $^{220}$Rn, the soil porosity, the size of the grains, the emanation coefficient, and morphology (Khan *et al.,* 2012). Therefore, the exhalation of $^{222}$Rn and $^{220}$Rn directly contributes to their indoor concentration from soil and highly porous earthen building materials making up rural houses in Homa and Ruri (UNSCEAR, 2000).

Lake Victoria is the major domestic water source in both Homa and Ruri, natural water like the one for a lake has dissolved $^{222}$Rn which gets to water through soil and rock by diffusion, convection flow, or dissolved gas (Somalai *et al.,* 2007). Its levels in the water depends and the amount of the parent radionuclide $^{226}$Ra (William *et al.,* 1991) The worldwide average $^{222}$Rn concentration for surface water sources lakes 0.4 Bq/l (WHO, 2008). $^{222}$Rn gets to the human body through direct ingestion or inhalation. Direct ingestion of the dissolved $^{222}$Rn in water leads to radiation exposure to the stomach lining. Dissolved $^{222}$Rn in water diffuses to the surrounding indoor air from the water sources or from the water transported to the house for domestic use from the sources leading to its increased indoor concentration resulting in radiation dose to the lungs when inhaled (Somalai *et al.,* 2007).

Quality and clean water are basic for good human health; contaminants like heavy metals get into the human body by ingesting drinking water containing traces of heavy metals (Salwa *et al.,* 2016). Homa and Ruri are both adjacent to Lake Victoria, the following

activities may introduce these heavy metals to its water, urban centers like Homa bay town might improperly discharge sewerage and industrial wastes, which may contain higher levels of heavy metals, into water sources. Secondly, the use of fertilizers and pesticides to improve agricultural production on the farms along the lake majorly in Homa hill region may allow the release of heavy metals and excess essential elements into domestic water sources through erosion or uptake by plants. Thirdly, mining areas such as the ones in Rachuonyo south uses metals such as mercury alongside other heavy metals and essential elements, which might get eroded into the lake water. The contaminated water, when used for irrigation, like in the case of lake water used to irrigate farms, these metals are taken up by the crops through their roots which consequently get consumed by humans.

Heavy metals like lead, arsenic and cadmium are carcinogenic, whereas iron, zinc, and nickel have non-carcinogenic effects. The non-carcinogenic metals affect the liver toxicity respiratory system and result in fertility disorders. Therefore, it is very important to continuously monitor the levels of heavy metals in water sources around regions having high anthropogenic activities.

**1.2 Study area**

Homa and Ruri hills both neighbors Lake Victoria, the largest freshwater lake in Africa and the second largest in the world. The two hills are approximately 46 km apart, with Homa Bay town being right between them.

Homa hill is mainly covered by a large carbonatite peninsula complex on the eastern shores of Lake Victoria with a series of cone sheets of carbonatites and breccias intrusions in the oldest rock in the nyanzian series and ijolites (Le Bas, 1977). Ruri hill is covered by the

Precambrian metabasaltic of the nyanzian type of rocks composed of ijolites and the nepheline syenites. The hill also has ring shaped intrusion of carbonatites of lower tertiary age, monazite and pyrochlore minerals associated with high $^{232}$Th levels (McCall, 1958).

Homa hill is located on latitude 0º 23´ 28´´ S and longitude 34º 29´ 21´´ E at an approximate elevation of 1,751 m above sea level. It encompasses a large carbonatite peninsula complex on the eastern shore of Lake Victoria with a series of cone sheets of carbonatites and breccias intrusions in the oldest rock in the Nyanzian series and ijolites (Le Bas *et al.*, 1977).

Ruri hill is on latitude 0º 32´ 37´´ S and longitude 34º 22´ 2´´ E at an elevation of approximately 1,545 m above sea level. It has the Precambrian metabasaltic of the Nyanzian type of rocks composed of ijolites and nepheline syenites, in addition to a ring-shaped intrusion composed of Carbonatites of lower tertiary age, monazite, and pyrochlore, minerals largely associated with elevated $^{232}$Th levels (McCall, 1958). Another hill, Asego hill, located near Homa Bay town, was studied as a control area since it is not an HBRA. It is located on latitude 0º 32' 18" S and longitude 34º 28' 10" E at an elevation of approximately 1,212 m above sea level.

Ruri and Homa hill are inhabited mainly by the Luo community and partly by the Luo Abasuba. The hills are experiencing increased encroachment, possibly because of the virgin fertile land on them and the growing population, thus demands more space for living. Rural communities across Kenya use locally available construction materials, and the region under study is no exception. The dwellings are majorly earthen and rectangular,

about 6 m by 7 m, and a height of 2 m with no ceiling as shown in figure 1.1. The main house is partitioned into two sections i.e., a smaller bedroom and a larger living room. There is a separate structure for kitchen. A small space locally known as “reru” in the Luo dialect is left between the roof and the house wall to allow free fresh air circulation as shown in figure 1.2

.

**Figure 1.1 : A snapshot of the sampled dwellings showing the rectangular shape**

**Figure 1.2 : Sampled dwelling revealing the gap (reru) between the roof and the wall the smeared wall**

The doors and windows are made of wood and mostly remain open during the day to improve the ventilation. The wall and floors of the houses are traditionally smeared with a mixture of cow dung and soil, locally known as “ongoro” to prevent the earthen wall from peeling off. Ongoro also seals the many cracks and pores on the walls, thus keeping the house warm.

Lake Victoria is the Africa's largest lake by area, the world's largest tropical lake, and the second-largest freshwater lake by surface area. In terms of volume, it is the world's ninth-largest continental lake, with approximately 2,424 $km^3$ of water and a maximum depth of 84 m with an average depth of 40 m. The lake has a surface area of approximately 59,947 $km^2$ divided among three countries, i.e., Kenya occupies 6% (4,100 $km^2$), Uganda 45% (31,000 $km^2$), and Tanzania 49% (33,700 $km^2$). It has a shoreline of

7,142 km (Okungu *et al.*, 2005). The lake serves as the primary water source for domestic use, irrigation, and fishing for the residents of the study area, as indicated in figure 1.3.


**Figure 1.3: A representation of the Lake Victoria shoreline in Homa. At the front-view, fishermen are preparing a boat to go fishing. At the background residents are fetching water and loading on donkeys as others are washing clothes**

This study only considered the Lake Victoria shoreline along Homa and Ruri hills in the Homa bay county Kenya which are both high natural radiation background areas for the radon ($^{222}$Rn) and heavy metal measurements. The shoreline along Homa Bay town (Asego) was also considered a control area.

### 1.3 Statement of the research problem

Regions around Homa and Ruri hills are both experiencing increased growth in human settlement, with readily available soil being used as a building material. Crops for consumption are grown in the same region, with Lake Victoria serving as the major water

source for the residents. Therefore, there is a potential radiation risk, given that people generally spend more time indoors and consume crops grown in the regions and the surrounding water. Despite this apparent risk, there is no sufficient data on the radiation exposure due to the terrestrial radionuclides from the earthen building materials, radon and thoron inside the local earthen dwellings, water and crops in Homa and Ruri, which this research seeks to determine. To the best of our knowledge, presently there is no model for the indoor gamma radiation dose based on the non-equilibrium condition of $^{232}$Th decay series as occasioned by $^{220}$Rn exhalation in typical rural Kenya earthen walled houses, which this research seeks to derive.

## 1.4 Objectives

### 1.4.1 General Objective

To determine human exposure to ionizing radiation associated with radioactivity in building materials, indoor air, water, crops, to model gamma absorbed dose due to non-secular equilibrium in $^{232}$Th decay series and non-radioactive physio-chemical parameters in Lake Victoria around Homa and Ruri in Homa bay county, Kenya.

### 1.4.2 Specific objectives

i. To measure natural activity concentration of $^{226}$Ra, $^{232}$Th & $^{40}$K in building materials and crops (maize).

ii. To model, gamma absorbed dose due to non-secular equilibrium in $^{232}$Th decay series.

iii. To determine radon and thoron exhalation rates from the building materials.

iv. To measure radon, thoron and thoron progeny concentration in the dwellings.

v. To determine radon concentration in Lake Victoria waters around the study region.

vi. To analyze non-radioactive physio-chemical parameters (concentration of selected heavy metals, electrical conductivity, temperature, and pH) in Lake Victoria waters around the study region.

**1.5 Rationale**

There is no sufficient data on indoor gamma radiation exposure, radon and thoron exposure indoors, and surrounding water sources around Homa and Ruri hills, even though they are claimed to be of high background radiation areas. The is an assumption that $^{220}$Rn short half-life may not allow it to get to the living space before it decays; this is not the case with highly porous building materials like earthen ones. Therefore, there is a need to model for gamma absorbed dose from $^{232}$Th decay series due to the non-secular equilibrium arising for $^{220}$Rn release in such building materials. The data generated from this research is solely significant for the purposes of risk awareness, planning and mitigation of management strategy for a better environment.

# CHAPTER TWO: LITERATURE REVIEW

## 2.1 Health Effects

### 2.1.1 Health effects of radiation exposure

Health effects are determined by the amount of radiation received as well as the length of exposure. Based on this criterion, radiation exposure impacts are divided into stochastic and non-stochastic effects. Stochastic effects are mostly linked to long-term exposure to low-level background radiation. In contrast, non-stochastic effects are linked to short-term exposure to high amounts of radiation (acute exposure). The human body is composed of cells that suffer biological and physical effects when exposed to ionizing radiation. These effects may result in complete cell death, partial cell damage, or modification. If a significant number of cells are affected in the body organ or tissues beyond a certain limit, then the death of the exposed individual might occur. If the radiation effect is not acute, the cells tend to restore themselves, which might not be perfect, leading to health complications like cancer, infertility, and damage to the exposed organs (ICRP, 2005).

When ionizing radiation exposure effects happen to the individual exposed, it is known as somatic effects. Somatic effects can either be prompt or delayed. Prompt effects are felt immediately after exposure, while delayed ones are felt many years after exposure. The latter are mostly linked to the development of cancers. On the other hand, if the radiation affects the descendants of the person exposed, then the effect is referred to as genetic. In this case, cell Deoxyribonucleic Acid (DNA) is altered, resulting in a change in genetic information referred to as gene mutation (UNSCEAR, 2000).

Radiation exposure can also be categorized as either chronic or acute. Acute exposure occurs when a large dose of more than 10 rad gets to the body within a short period, mostly from artificial sources like medical processes and nuclear accidents; Evidence of the acute exposure is visible after a few hours of exposure. However, Chronic exposure happens when an individual receives small amounts of radiation over a long period, which then allows enough restoration period for the damaged cells or substitution of the dead or malfunctioned ones (UNSCEAR, 1993).

Gamma-ray radiation exposure can cause cancer in practically all human tissues, although cancer risk in a given tissue depends on the radiation dose response. The referred article (UNSCEAR, 2013) indicates age-related elements that contribute to variances in radiation effects and dangers from childhood exposure to individual size and organs, as well as the rate of development at various ages, including physical activity. Yamaguchi's 1994 did an intensive investigation on the response of the isotropic radiation fields and calculated dose rate coefficients for six age groups. He concluded that the effective dose coefficients for infants were about 20% to 30% higher than those for adults; also, the effective dosage coefficients of UNSCEAR and ICRP are age-dependent (ICRP, 1995; UNSCEAR, 2008).

Radon isotopes and their decay products can cause serious health problems, especially in enclosed spaces like underground mines, caves, cellars, or poorly ventilated and poorly constructed dwellings. The chance that radon gas will build up to harmful levels is a source of anxiety for homeowners. The radon isotopes ($^{222}$Rn and $^{220}$Rn) decay to form relatively short-lived charged particulate progeny, emitting high-energy alpha particles that damage

lung cells. The decay products are electrically charged and deposit energy in the lung, hence transferring energy to the cellular structure of the surface of the bronchi and lungs, which strikes individual lung cells, causing either physical or chemical damage to DNA and cell death. While the body can tolerate and replace dead cells, damaged lung tissue cells can multiply and develop into lung cancer (James, 2006; WHO, 2009; ICRP, 2010). According to World Health Organization (WHO, 2009) exposure to radon isotopes is the leading cause of lung cancer in nonsmokers.

There is currently a significant scientific consensus that radiation-induced DNA damage plays a critical role in the development of carcinogenesis, even at low levels such as those resulting from normal, natural background radiation exposure (NRC, BEIR VII, 2006; ICRP, 2005). However, according to UNSCEAR 2013 Annex A, a repair mechanism requires a particular level of DNA damage to be activated; for example, after very low doses, the quantity of damage may be insufficient to trigger repair. Untreated lesions, on the other hand, may develop issues later in life. Some studies, however, indicate health benefits of exposure to low radiation levels; by acting as a stimulant to accelerate DNA damage repair, reduction of genetic instability, and enhance immune responses leading to cyto protection from low radiation (Cuttler, 2013; Feinendegen, 2012; Pandey, 2006).

### 2.1.2 Health effects of heavy metals in water

Most people in Kenya, especially in rural areas like Homa and Ruri, do not have access to safe drinking water and must rely on alternate sources such as groundwater extracted from hand-dug wells, boreholes, and surface waters like lakes and dams. Heavy metal pollution in these sources is hazardous and can harm human health and well-being when consumed.

Human kidney is the first organ to be affected by heavy metal poisoning, which depends on the type of metal and the dose received. Even at low levels, cadmium, lead, and radioactive heavy metals $^{226}$Ra may affect the renal organ as Manganese, and copper only affects it at higher quantities (Sabath *et al.,* 2012; Barbier et al., 2005; Kurttio *et al.,* 2002; Zamora *et al.,* 1998). Moreover, Cadmium is carcinogenic and can cause cancer, osteoporosis, and hearing loss (Nawrot *et al.,* 2006; Prasher, 2009; WHO, 2011). Lead poisoning also results in developmental delays in neonates and children, irreparable harm to the neurological and reproductive systems, high blood pressure, and persistent anaemia (Smith *et al.,* 1989). Very high levels of Manganese may result in children's intellectual impairment, leading to low intelligent quotient (IQ) scores (Momodu *et al.,* 2009). It is also connected to low libido and impotence, alongside manganism, a Parkinson's-like condition associated with muscle stiffness, weakness, and tremors (USEPA, 2004). High copper and zinc levels may lead to stomach cramps, skin irritations, vomiting, nausea, and anaemia (USEPA, 2003), and extremely high levels of magnesium (50mg/l) might generate unwanted laxative effects (WHO, 2011).

## 2.2 Studies on natural radioactivity in building materials and crops (maize)

### 2.2.1 Building materials

The impact of naturally occurring radionuclides $^{226}$Ra, $^{232}$Th, and $^{40}$K on construction materials and processed products to indoor exposure has been studied worldwide. The results show that naturally occurring radionuclides (NORM) is present in houses at varying levels (UNSCEAR, 2000; Moura *et al.,* 2001; Saad *et al.,* 2014). Radioactivity measurements on building materials in high background radiation areas in other parts of the world like Ramsar, Iran reported values more than the accepted limits for building

materials by Bavarnegin *et al.*, 2013, using high purity Germanium (HPGe) gamma-ray spectrometry. The samples had an average activity concentration of 179 Bq/Kg, 29 Bq/Kg, and 202 Bq/Kg for $^{226}$Ra, $^{232}$Th, and $^{40}$K respectively, radium equivalent of 144 Bq/Kg and gamma index of 0.53 Bq/Kg.

In Africa, the radiological investigation of building materials in high background radiation area north of the Nile Delta in Egypt using a Hyper-Pure Germanium (HPGe) detector by Mubarak *et al.*, 2017 reported an average activity concentration of 107 Bq/Kg, 201 Bq/Kg and 116 Bq/Kg for $^{226}$Ra, $^{232}$Th, and $^{40}$K respectively. The external hazard indices, radium equivalent activity, activity concentration indices, and alpha index (Iα) ranged between 0.32 – 2.04 Bq/Kg, 118.67 – 753.91 Bq/Kg, 0.42 –2.61 Bq/Kg, 0.18 – 0.89 Bq/Kg respectively, with some samples exceeding the upper limit of exposure.

Rock and soil samples collected from Homa hill gave an average value of the radioactivity concentrations of $^{40}$K, $^{226}$Ra, and $^{232}$Th of 915.6 Bq/kg, 195.3 Bq/kg, and 409.5 Bq/kg, respectively. The range of the annual effective dose for a person living in the Homa area varied from 28.6 to 1681.2, with a mean of 470.4 μSv. These results imply Homa hill has elevated levels of natural radioactivity; thus, the region is a high background radiation area (Otwoma *et al.*, 2012).

Gamma-ray spectrometric analyses of 21 rocks and soil samples from Ruri hills were done using high-purity germanium (HPGe) gamma-ray detector. The average activity concentrations of 1396.9 Bq/kg for $^{232}$Th, 178.7 Bq/kg for $^{238}$U, and 508.7 Bq/kg for $^{40}$K.

The Absorbed dose rates in the air outdoors at approximately l m above the ground had an overall mean value of 2325.84 nGy/h, and the annual effective dose rates had a mean of 5.705 mSv/y, assuming a 40% (0.4) occupancy factor. Thus, annual external effective dose rates at Ruri hill are much higher than the global average of 0.46 mSv/y (Achola *et al.*, 2012).

### 2.2.2 Radioactivity in crops (Maize)

Natural radionuclides get to crops when planted in high background radiation areas, from farm inputs such as fertilizers meant to enhance their productivity, or when the crops are grown in areas with nuclear accidents and fallouts. The radionuclides accumulate on the leaves, stem, or fruit part of the crop, which, when ingested, results in internal radiation dose effects. Most rural western parts of Kenya depend on maize as the main food crop, with fertilizer application used to boost its yield. Moreover, maize is grown in HBRA like Homa and Ruri; it would naturally take up these radionuclides; thus, their levels need to be known for safety recommendations.

Studies on the activity concentration of the natural radionuclides $^{226}$Ra, $^{232}$Th, and $^{40}$K in maize in different regions have been done worldwide. Studies in Minjingu, Tanzania, in maize plantations in the phosphate mining area. They reported an average concentration of 25.6 Bq/kg and 435 Bq/kg for $^{226}$Ra and $^{40}$K with an average annual effective dose rate of 2 mSv/y, nearly ten times above the (UNSCEAR, 2000) safe limit of 290 µSv/y. Thus, there was an apparent radiation health hazard from the consumption of maize from the studied region.

In Kenya, not much has been published on the measured natural radionuclides in maize, Maina *et al.,* 2008 did measurements of the concentration of natural radionuclides in foodstuffs used in the capital city Nairobi which indicated that maize meal which majorly originates from the rural parts of Kenya had an annual ingestion dose of 162 µSv/y which was nearly half the safe limit of 290 µSv/y (UNSCEAR, 2000). This may not be the case for high background radiation areas with naturally high levels of $^{226}$Ra, $^{232}$Th, and $^{40}$K, like in Homa and Ruri areas.

### 2.3 Models of indoor gamma radiation dose

The absorbed gamma dose in the air inside a room is determined by the mathematical linear equation by UNSCEAR,1993, as given by equation 2.1.

$$D = k_1 C_{Ra} + k_2 C_R + k_3 C_k \quad (2.1)$$

Where $C_{Ra}$, $C_{R,}$ and $C_K$ are activity concentrations of $^{226}$Ra, $^{232}$Th, and $^{40}$K in Bq/kg in the construction material, respectively, and $k_1$, $k_{2,}$ and $k_3$ are the specific dose rates, also referred to as the dose conversion factors in nGyh$^{-1}$/Bqkg$^{-1}$ for $^{226}$Ra, $^{232}$Th and $^{40}$K respectively.

These specific dose rates assume secular equilibrium in both $^{226}$Ra and $^{232}$Th decay series, thus the effects of both $^{222}$Rn and $^{220}$Rn, respectively. However, studies have shown that the exhalation of these radon isotopes ($^{222}$Rn and $^{220}$Rn) indeed affects the secular equilibrium of both $^{226}$Ra and $^{232}$Th.

Stranden, 1979 model on radioactivity in building materials and gamma radiation in dwellings of Norway using model rooms for calculations by standard numerical integration methods noted that there could be an overestimation of the absorbed gamma dose from

$^{226}$Ra decay series of up to 20% due to $^{222}$Rn release. This was based on studies on experiences with concrete calibration sources for radiometric field instruments by Løvborg *et al.,* 1978.

De Jong *et al.,* 2006 and 2008 developed a model on the effect of non-equilibrium status in $^{226}$Ra decay series due to $^{222}$Rn exhalation using computer codes Marmer and Micro-Shield, then applied a correction factor based on the Dutch construction materials. The correction factor for the effect of $^{222}$Rn exhalation was derived by describing its emanation, diffusion, and exhalation, then quantified this effect based on Dutch construction materials (concrete, sand-lime brick, gypsum, clay brick, and aerated concrete) using equation 2.2 (De Jong *et al.,* 2008).

$$D = k_1 A_{Ra}(1 - F_{Rn}) + k_2 A_{Th} + k_3 A_k \quad (2.2)$$

Where $(1 - F_{Rn})$ is the correction factor for $^{222}$Rn exhalation, and $F_{Rn}$ is the $^{222}$Rn release factor defined as the ratio between the amount of $^{222}$Rn exhaled from the building material per unit of time to the one generated within the building material. They reported a reduction in absorbed gamma dose rate due to $^{222}$Rn exhalation, which was an average of 5% for the Dutch building materials considered and highest in gypsum with a value of 9%. The model, however, ignored the non-equilibrium in the $^{232}$Th decay series as a result of $^{220}$Rn exhalation based on the short half-life of $^{220}$Rn.

Orabi, 2017 also modelled gamma absorbed dose in a room based on the effect of non-equilibrium in $^{226}$Ra decay series due to $^{222}$Rn release. The model mathematically formulated the steps involved in $^{222}$Rn emanation, diffusion inside the building material, and exhalation. It also explored factors affecting $^{222}$Rn release such as moisture, wall

coverings, and building material structure using the Monte Carlo N – Particle Transport (MCNP) simulation software on different building materials. The model corrected the gamma absorbed dose rate by multiplying the activity concentration of $^{226}Ra$ by the correction factor $(1 - F_{Rn})$ as given in equation 2.1. The results indicated a reduction in the absorbed dose rate by nearly a quarter of its uncorrected value. Thus, the release of $^{222}Rn$ significantly changed the gamma radiation absorbed dose rate from the $^{226}Ra$ decay series. Orabi model also assumed the effect of non-equilibrium in the $^{232}Th$ decay series due to $^{220}Rn$ release, a correction factor that this research model seeks to determine based on a typical Kenyan earthen dwellings.

High background radiation areas (Homa and Ruri) have elevated naturally occurring radionuclides (NORM) levels in the surrounding soil. Using such soil in the construction of dwellings increases the risk of indoor gamma radiation exposure to the residents. Accurate determination of this indoor gamma absorbed dose in such dwellings is therefore of great significance for safe and better housing techniques and policies in such regions. Earthen dwellings have high levels of $^{220}Rn$ exhalation from their walls compared to other building materials like concrete. Therefore, there exists a non-secular equilibrium state between $^{232}Th$ and its progenies as a result of $^{220}Rn$ release, which this research seeks to derive.

**2.4 Studies on radon isotopes**

The indoor concentration of the radon isotopes also depends their exhalation rate from building material, housing dimensions (surface area to volume ratio), and ventilation rate (Cozmuta *et al.*, 2003). He used the indoor concentrations of $^{222}Rn$ and $^{220}Rn$ daughters in

air, accounting for exhalation rates, building material diffusion processes, room dimensions, and ventilation rates. Furthermore, the EC Directive 2013/59 'Basic Safety Standards' mandates that Member States develop a national radon action plan that tackles long-term radon risks. The directive states that radon risk is primarily caused by the airtightness of the house envelope, ventilation rate, and radon potential (CEN, 2007; ESR, 2015). This is determined by combining radon soil gas concentration and soil gas permeability, where the radon soil gas concentration is determined by geology.

In Kenya, the above-stated regulations are yet to be strengthened based on ongoing research programs such as this current one, which will provide sufficient data for such. Implementing such acts is not so emphasized in houses constructed in rural areas in Kenya like Homa and Ruri, which significantly affects the ventilation levels of such rural dwellings, thus leading to high indoor radon levels for houses that are not adequately ventilated.

There has been increased worldwide research on indoor radon isotopes, Chen *et al.*, 2014 did measurements of $^{222}$Rn and $^{220}$Rn concentrations in 4000 residential homes in the 33 census metropolitan areas of Canada, and the results had an average $^{220}$Rn concentration of 9 Bq/m$^3$ and an average $^{222}$Rn concentration of 96 Bq/m$^{3,}$ more than double the (UNSCEAR, 2000) worldwide average indoor $^{222}$Rn concentration of 40 Bq/m$^3$. Serge *et al.* 2019 measured $^{222}$Rn, $^{220}$Rn, and $^{220}$Rn progeny in 71 Douala city, Cameroon dwellings using radon– thoron discriminative detectors (RADUET) for $^{222}$Rn and $^{220}$Rn and equilibrium equivalent thoron concentration (EETC) monitor for $^{220}$Rn progeny. The concentrations varied from 31 ± 1 Bq/m$^3$ to 436 ± 12

Bq/$m^3$, 4 ± 7 to 246 ± 5 Bq/$m^3$, and 1.5 ± 0.9 Bq/$m^3$ to 13.1 ± 9.4 Bq/$m^3$ for $^{222}$Rn, $^{220}$Rn, and $^{220}$Rn progeny respectively. The average indoor annual effective dose for $^{222}$Rn was 2.6 ± 0.1 mSv/$y^1$, while for $^{220}$Rn and its progeny was 1.0 ± 0.4 mSv/$y^1$. These results indicated that $^{220}$Rn contributed approximately 26% to the total annual effective dose, which is quite significant and thus should not be ignored.

Studies on indoor radon in Kenya have advanced with time using more advanced techniques, equipment, and more isotopes, i.e., $^{222}$Rn, $^{220}$Rn alongside the $^{220}$Rn progenies in different types of dwellings. For instance, Nyambura *et al*., 2019 studied the concentration levels of $^{222}$Rn, $^{220}$Rn, and $^{220}$Rn progeny in mud, metallic, and stonewalled houses in the Kilimambogo Central part of Kenya. The mean $^{222}$Rn concentration levels in mud, metallic, and stone dwellings were 67 ± 11 Bq/$m^3$, 60 ± 10 Bq/$m^3$, and 75 ± 10 Bq/$m^3$, respectively. The mean $^{220}$Rn concentration levels in the corresponding dwellings were 195 ± 36 Bq/$m^3$, 71 ± 24 Bq/$m^3$, and 161 ± 31 Bq/$m^3$, respectively. Equilibrium equivalent thoron concentration (EETC) was 12 ± 2 Bq/$m^3$, 3 ± 1 Bq/$m^3$, and 7 ± 1 Bq/$m^3$ for mud, metallic, and stone dwellings, respectively. These resulted in an annual effective dose for $^{222}$Rn 1.3 ± 0.2 mSv/$y^1$, 1.1 ± 0.1 mSv/$y^1$ and 1.4 ± 0.2 mSv/$y^1$ in mud, metallic and stone-walled houses, while those from $^{220}$Rn estimated from its progeny were 2.4 ± 0.4, 0.5 ± 0.1 mSv/$y^1$ and 1.5 ± 0.2 mSv/$y^1$ in the corresponding houses, respectively. The annual effective dose was below the WHO, 2009 reference level of 3 mSv/$y^1$.

The radon measurements have been extended to some of the high background radiation areas in Kenya, like the one by Chege *et al.,* 2015 in Mrima hill. The results for $^{222}$Rn and

$^{220}$Rn concentration measurements and the corresponding effective dose rates in mud dwellings had an average annual effective dose of 0.7 mSv/y$^{1}$ and 13.7 mSv/y$^{1,}$ respectively from a corresponding average indoor $^{222}$Rn and $^{220}$Rn concentration of 35 Bq/m$^{3}$ and 652 Bq/m$^{3}$ respectively.

A general survey of studies on $^{222}$Rn and $^{220}$Rn concentrations in Kenya by Chege *et al.,* 2019 has indicated high levels of the isotopes in earthen dwellings more than any other type of house. Measurements of the levels $^{226}$Ra and $^{232}$Th in south-western Kenya have recorded high values; thus, the dwellings are expected to have elevated indoor $^{222}$Rn and $^{220}$Rn levels. The studies involving indoor $^{222}$Rn and $^{220}$Rn are relatively few and of a small scale in Kenya. Therefore, there is an immediate need for extensive research on $^{222}$Rn and $^{220}$Rn to corroborate the risk projections as well as to provide sufficient baseline data for better nationwide mapping of indoor $^{222}$Rn and $^{220}$Rn risk-prone areas.

Measurements of $^{222}$Rn and $^{220}$Rn exhalation rates in the Halfa Aljadida area, Sudan, by Elzain *et al.,* 2019 using the can technique coupled with CR-39 reported average values of 1.7 mBq/m$^{2}$/s and 34.8 mBq/m$^{2}$/s respectively. The average values were below the world average of $^{222}$Rn and $^{220}$Rn by UNSCEAR 2008. There was a strong positive correlation between the radon isotopes and the source radionuclides $^{226}$Ra and $^{232}$Th, respectively. Studies in high background radiation areas of Mrima hill, in the coastal part of Kenya, by Chege *et al.,* 2015 using an accumulation chamber technique coupled with RAD7, reported exhalation rates ranging from below detection limit to 11.9 mBq/m$^{2}$/s with an arithmetic mean of 4.3 mBq/m$^{2}$/s for $^{222}$Rn and 2.5 Bq/m$^{2}$/s to 35.7 Bq/m$^{2}$/s with an arithmetic mean

of 19.8 Bq/$m^2$/s for $^{220}$Rn. A strong positive correlation was observed between the $^{220}$Rn exhalation rate and $^{232}$Th.

$^{222}$Rn gets dissolved in water from the bedrock of the water source; if these rocks have high levels of the parent radionuclide $^{226}$Ra, then this could consequently increase its levels dissolved in water. Its levels in ground waters are higher than in surface waters like lakes because the exposed surfaces increase degassing of the dissolved $^{222}$Rn by the blowing wind. For instance, $^{222}$Rn measurements in Lake Darbandikhan, Iraq, reported concentration values of 0.88 Bq/l with an average annual effective dose rate due to the water consumption of 1.6 µSv/y (Jafir *et al.*, 2016). Surface waters in Sudan reported a mean average concentration of 14.2 Bq/l (Elzain, 2014). In Kenya, groundwater radon measurements ranged between 0.8 and 371.7 Bq/l (Otwoma *et al.*, 1998). Measurements of groundwater levels in Homa hill had an average value of 49.4 Bq/l (Mayaka *et al*., 2015), a value below the EU recommended limit of 100 Bq/l.

**2.5 Studies on Heavy metal exposure in water**

Several studies have been carried out on the heavy metal levels in Winam gulf, which is simply the Lake Victoria extension into western Kenya, covering Kisumu and Homa bay counties. These studies have involved the measurement of different heavy metals at different points along the lake and times, thus forming an essential data source for the lake pollution control policy guideline. Outa *et al*., 2020 measured Ni, Cr, and Pb in water from Lake Victoria along Winum gulf. The mean levels on one of the sites in the Homa bay county shoreline known as Mainuga registered average concentrations of Pb, Cr and Ni were 1.1 µg/L, 0.4 µg/L, and 2.2 µg/L, respectively. Farms have been established along

several parts of the Lake Victoria shoreline, with the water from the Lake serving as the major water source for irrigation. This has necessitated the determination of levels of heavy metals in irrigation water and crops on such farms. Akenga *et al.* 2019 measured the levels of selected heavy metals (Mn, Cd, Pb, Zn, Fe, and Co) in irrigation water which is majorly sourced from Lake Victoria and managu *(Solanum Nigrum)* grown on irrigated farms in Homa hills. Inductive Coupled Plasma Optical Emission Spectroscopy was applied in this study. Water for irrigation had an average value for Mn, Cd, Pb, Zn, Fe, and Co reported 0.89 mg $L^{-1}$, 0.01 mg/L, 0.18 mg/L, 0.35 mg/L, 4.20 mg/L, and 0.04 mg/L respectively. In *Solanum Nigrum*, the average values were 10.16 mg/kg, 5.23 mg/kg, 4.02 mg/kg, 41.42 mg/kg, 479.56 mg/kg, and 11.41 mg/kg for Mn, Cd, Pb, Zn, Fe, and Co respectively. The levels of Cd, Mn, Fe, and Pb in *managu* were higher than the recommended WHO limit.

# CHAPTER THREE: THEORETICAL BACKGROUND

## 3.1 Radiation Detectors

### 3.1.1 Gamma-ray spectroscopy detectors

Gamma-ray detectors interact by absorbing the gamma-ray energy from the source and converting it into a voltage signal proportional to the source. The most common gamma-ray detectors are scintillation counters like the thallium-activated sodium iodide detector [NaI (Tl)] and semiconductor detectors like high purity germanium detector.

#### 3.1.1.1 Thallium-activated sodium iodide [NaI (Tl)] detector

It comprises a transparent scintillation material photomultiplier tube alongside other electronics such as a preamplifier, linear amplifier, oxford PCA- P software, and computer. It emits light whenever its scintillation material crystal atoms interact with gamma-ray radiation. Its photomultiplier tube comprises a photocathode, a focusing electrode, and several dynodes, which is a minimum of ten. The incident photons interact with the NaI (Tl) crystal by depositing energy through pair production, photoelectric effect, or Compton scattering based on its energy. This energy scintillates the single crystal of NaI (Tl) to generate the photons, which then dislodge the photoelectrons in the photocathode.

The dislodged electrons in the photocathode get accelerated to electrodes alongside acquiring more energy resulting in the re-emission of secondary electrons. Electrons produced in the photocathode get accelerated to the dynode series with the emission of secondary electrons, which also get accelerated through the dynode series by the electric field to the last dynode, as shown in figure 3.1.

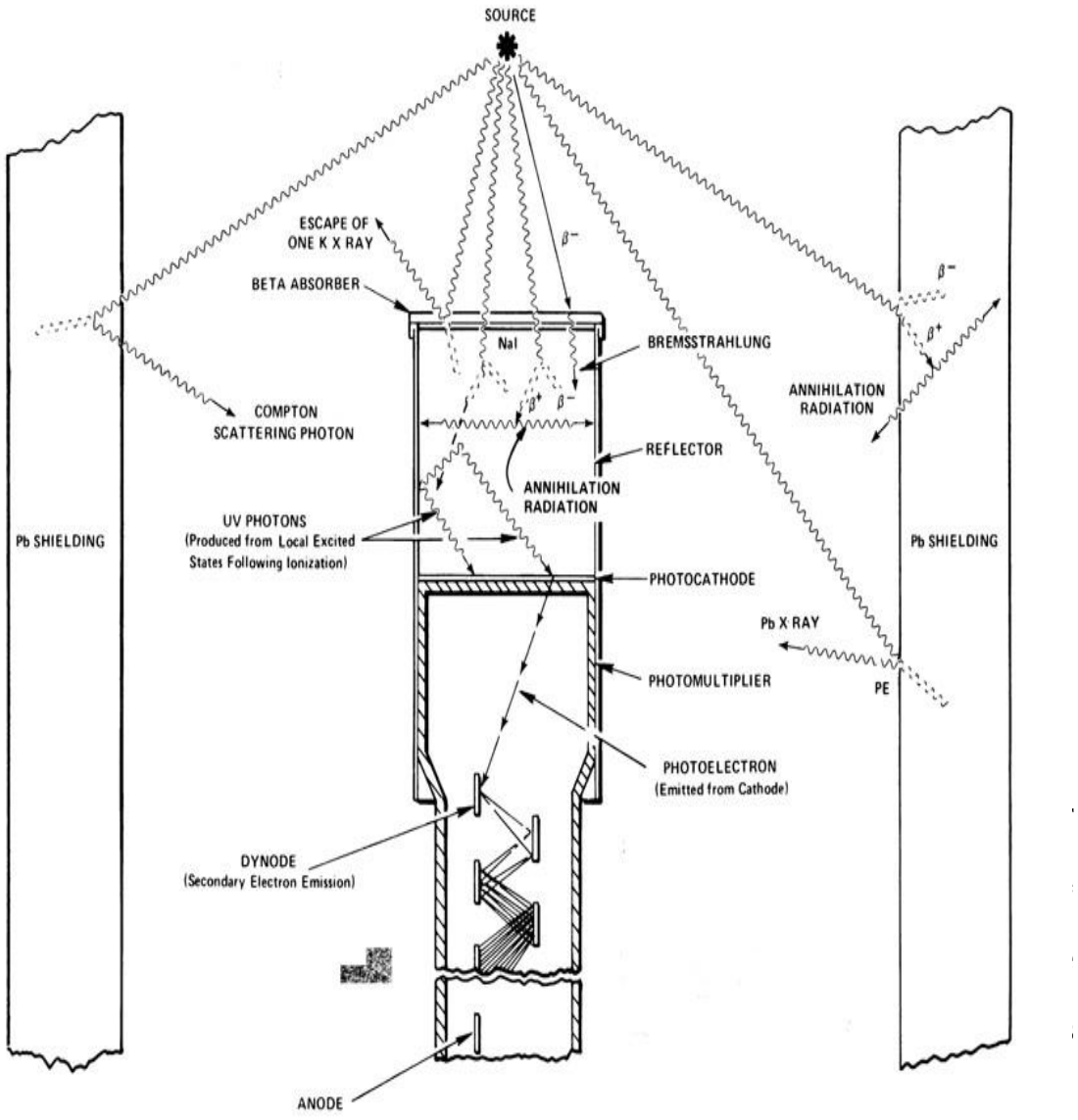


**Figure 3.1: Set up for a gamma ray spectroscopy**

produced in the semiconductor. The created electrons get transmitted from the valence band to the conduction band resulting in an equal number of holes remaining in the band. The electric field is applied to the detector volume, in which the electrons in the conduction band get attracted to the positive contact creating the electrical field resulting in an

electrical signal transmitted to the preamplifier, then a multichannel analyzer and the following subsequent system for complete analysis. The electrical signal is directly proportional to the gamma-ray source radionuclide, which is then used to identify and quantify the radionuclide.

The detector operates under cryogenic temperature, which is provided through liquid nitrogen cooling. The detector uses a semiconductor with a narrow band gap between valence and conduction; as a result, it does not work well at room temperature, resulting in a high amount of leakage current. Therefore, the detector has to be cooled to reduce the thermal excitation noise during its operation. The detector is also placed in a vacuum to limit thermal conductivity between the surrounding air and the crystal.

Semiconductors generally have inherent impurities that reduce the energy needed to create electron-hole pairs. This defect is corrected by a reversed biased p-i-n (i-intrinsic region which is sensitive to the ionizing gamma rays) junction diode is used, resulting in an increased width of the depletion layer due to increased potential difference; thus, no current flow when there is no gamma radiation. This greatly improves the detector's performance. High purity germanium (HPGe) detector has the best energy resolution but poor efficiency compared to the Thallium activated sodium iodide NaI(Tl) detector.

### 3.1.2 Alpha radiation detectors

Alpha radiation detectors are categorized into three based on the measurement method and sensitive material used, i.e., gaseous ionization detectors, scintillation detectors, and semiconductor detectors. The gaseous ionization chambers have a very thin window

through which the alpha particles can penetrate, such as the smoke detector. Scintillation counters are relatively cheap and efficient even though they are not ideal for alpha particles, as alpha particles do not cause sufficient scintillation compared to gamma rays and beta particles. Examples of scintillation materials are CsI (Tl) and NaI (Tl). Semiconductor detectors are based on silicon strips which are very good in charged particle tracking. The commonly used detectors for the measurement of $^{222}$Rn, $^{220}$Rn, and $^{220}$Rn progeny based on these techniques are the RAD7 alpha detector and CR-39 alpha detector.

#### 3.1.2.1 RAD7 Alpha detector

RAD7 alpha detector has a hemispherical chamber coated with silicon semiconductor with a voltage range of 2000-2500 V applied, as shown in figure 3.2. There is a silicon alpha detector at its center and a built-in pump. The decayed isotopes of $^{222}$Rn and $^{220}$Rn nuclei get accelerated by the electric field to the alpha detector at the center and stick to it. $^{222}$Rn and $^{220}$Rn progeny decays on the detector releasing alpha particles that produce electrical signals proportional to the energy, which is then used to quantify and identify the particle. $^{218}$Po and $^{214}$Po at alpha energies 6 MeV & 7.69 MeV used for $^{222}$Rn and $^{216}$Po at an alpha energy of 6.78 MeV used for $^{220}$Rn. Detector is purged after every measurement to remove the already measured $^{222}$Rn and $^{220}$Rn nuclei.

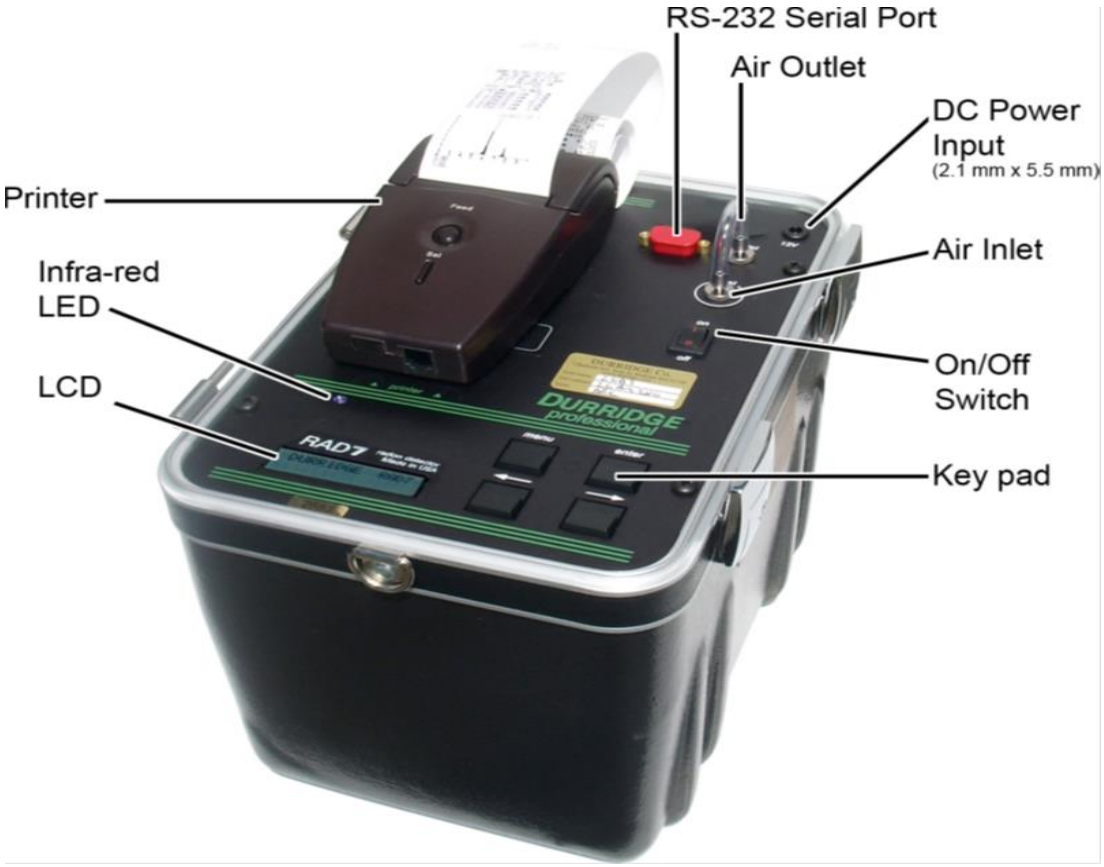


**Figure 3.2: RAD7 alpha detector (Durrigde RAD7 user manual, 2015)**

### 3.1.2.2 Solid State Nuclear Track Detector (CR - 39)

Colombia Resin number 39 (CR – 39) is a solid-state nuclear track detector (SSNTD) made of poly allyl di-glycol carbonate, which creates damage tracks upon interaction with alpha particles at the point of impact. It's a highly sensitive charged particle detector with a refractive index of 1.50 and a density of 1.32 g/cm$^3$. In recent years they have been used to achieve great success in numerous fields such as personal neutron dosimetry, radon isotopes level determination in different materials, alpha particle autoradiography, observation of high energy particles in cosmic rays, heavy nuclear-charged particles identification, and biological sciences.

When an energy-charged particle penetrates CR-39, it produces an ionization spike around its path in the form of a trail. The ionization spike then dissipates into heat and coulomb explosion, moving the target atoms away from their equilibrium positions in the spike. The so-formed spike consists of a broken or altered geometric or molecular structure of atoms in the CR-39 and is a damaged solid. This damaged solid cylinder shows preferential etching when immersed into an etching solution, a hot alkaline solution for CR-39. Etching solution dissolves the damaged material to form a shallow or deep narrow pit in the CR-39 depending upon its energy deposition rate and range in the target. During etching, CR-39 swells due to soaking and heating. The formed tracks are counted with an automatic reading system.

### 3.2 Measurement of Heavy metals using Atomic Absorption Spectroscopy (AAS)

Atomic absorption spectroscopy involves the determination of quantities of heavy metals through the absorption of light radiated from their gaseous state-free atoms. The process applies the sample's atomic absorption spectrum to determine its analyte concentration. It, therefore, needs standards of already known analyte concentration to evaluate the relation between the measured absorbance and that of the analytes. The sample is first atomized using flame atomizers, then optically irradiated using the metal-specific line source, then through a monochromator for element radiation separation then measured by a detector. Flame atomizers use an air-acetylene flame with a temperature of about 2300 °C. Samples dissolved are then used alongside. A pneumatic analytical nebulizer is then used to aspirate the sample and sprayed to mix with the flame gases in the spray chamber.

Flame is passed through a radiation beam to determine its concentration of free atoms in the nebulizer. During sample aspiration, the flame metal in it absorbs some of the light resulting in reduced intensity which is then measured and converted to absorbance. This process is summarized in figure 3.3.

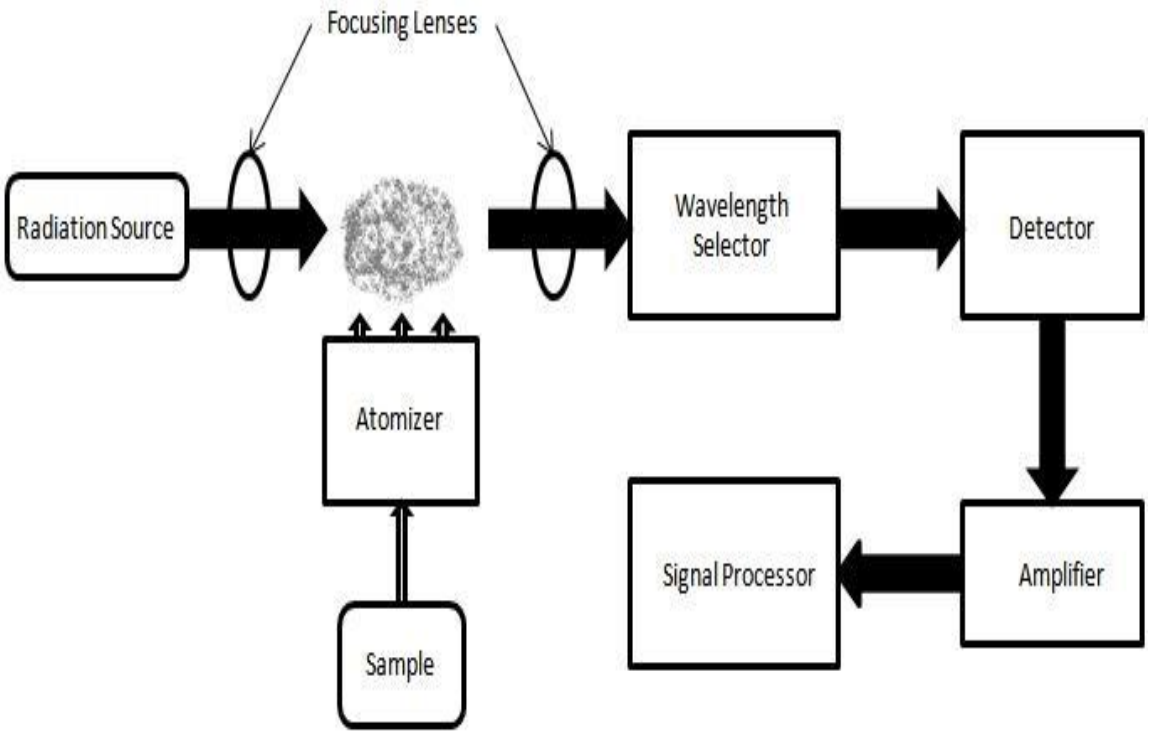


**Figure 3.3: Schematic presentation of the atomic absorption spectrometry process**

### 3.3 Modelling indoor gamma radiation dose due to $^{220}$Rn release

The experimental determination of the activity concentration of $^{232}$Th requires that the samples be sealed tightly to prevent the release of $^{220}$Rn and its progenies for them to attain secular equilibrium with its parent radionuclide $^{232}$Th. Highly porous building materials like earthen materials are not tightly sealed to prevent the release of $^{220}$Rn; therefore, a non-secular equilibrium exists in the $^{232}$Th decay series. The gamma radiation in the $^{232}$Th decay series majorly arises from $^{220}$Rn and its short-lived daughters. Release of $^{220}$Rn from the

earthen walls reduces its concentration alongside its progenies in the walls, consequently reducing the absorbed gamma dose from some of the gamma lines in the $^{232}$Th decay chain. To correct the reduction in absorbed gamma dose, $^{220}$Rn activity concentration inside the walls is used instead of $^{232}$Th to avoid its overestimation. The total $^{220}$Rn activity concentration in the wall consists of the $^{220}$Rn in the pore spaces of the wall and the ones in the solid part of the building material.

The determination of the effect of $^{220}$Rn release on indoor gamma absorbed dose is divided into the following processes:

(i) $^{220}$Rn generation and emanation within the wall.

(ii) Its transportation by diffusion.

(iii) Effect of $^{220}$Rn release from the wall on indoor absorbed gamma dose.

### 3.3.1 $^{220}$Rn generation and emanation

To mathematically express the rate at which $^{220}$Rn is generated, we assume a secular equilibrium state between $^{232}$Th and its daughter atoms $^{224}$Ra. Considering $N_o$ as the number of $^{224}$Ra atoms in a piece of building material at a time, t = 0. $^{224}$Ra decays directly to $^{220}$Rn; thus, the number of its atoms ($N_c$) created at a time t equals the number of $^{224}$Ra atoms that have decayed in that time which by decay law can be expressed as equation 3.1.

$$N_c = N_0(1 - e^{-\lambda_R t}) \quad (3.1)$$

Where $\lambda_R$ is the decay constant of $^{224}$Ra.

The generated $^{220}$Rn atom within the building material experiences any of the following three scenarios; it gets displaced within the building material grain but remains attached in

it, travels through the interstitial space and gets attached in another grain, or gets into the interstitial pore spaces between the grains.

The latter is referred to as the emanation process represented by the emanation coefficient η, which is defined as the ratio of the number of $^{220}$Rn atoms in the pore spaces to the ones created as expressed by equation 3.2.

$$\eta = \frac{N_d}{N_c} \tag{3.2}$$

Which can be rewritten as equation 3.3

$$N_d = \eta N_c \tag{3.3}$$

where $N_d$ is the number of $^{220}$Rn atoms in the pore spaces.

Considering the fact that only $^{220}$Rn atoms in the pore spaces $N_d$ as the ones which will be diffused out of the building material piece, then substituting for $N_c$ from equation 3.1 into equation 3.3 gives the number of $^{220}$Rn atoms available for diffusion as presented by equation 3.4.

$$N_d = \eta N_0(1 - e^{-\lambda_R t}) \tag{3.4}$$

Given the fact that $^{220}$Rn is a radioactive gas hence its activity varies with time, as given by equation 3.5

$$\frac{dN_d}{dt} = \lambda_T N_d \tag{3.5}$$

Where $\lambda_T$ is the decay constant of $^{220}$Rn.

Substituting for $N_d$ from equation 3.4 gives equation 3.6

$$\frac{dN_d}{dt} = \lambda_T \eta N_0 (1 - e^{-\lambda_R t}) \quad (3.6)$$

Considering a time t far much greater than the half-life of $^{224}$Ra, then the term $e^{-\lambda_R t}$ reduces to zero; thus, equation 3.6 becomes 3.7

$$\frac{dN_d}{dt} = \lambda_T \eta N_0 \quad (3.7)$$

Assuming that $N_o$ atoms of $^{224}$Ra are homogeneously distributed within the wall and considering $C_R$ (Bq/kg) as the activity concentration of the $^{224}$Ra, then $N_o$ is given as $N_o = \rho C_R dV$ where $\rho$ is the density of the building material of the wall and $dV$ is the volume of the piece of the building material in $m^3$. Substituting for $N_o$ in equation 3.7 results in equation 3.8.

$$\frac{dN_d}{dt} = \lambda_T \eta \rho C_R dV \quad (3.8)$$

Equation 3.8 can be rearranged into equation 3.9

$$\frac{1}{\rho dV}\frac{dN_d}{dt} = \lambda_T \eta C_R \quad (3.9)$$

But

$$\rho dV = dm \quad (3.10)$$

Equation 3.10 represents the mass of element dV, which on substitution into equation 3.9 results in equation 3.11

$$\frac{dN_d}{\rho dV dt} = \frac{dN_d}{dm dt} = R \quad (3.11)$$

Hence;

$$R = \lambda_T \eta C_R \quad (3.12)$$

Equation 3.12 represents the generation rate of $^{220}$Rn R in Bq/kg of the building material of the wall.

### 3.3.2 $^{220}$Rn diffusion

This is the process through which the emanated $^{220}$Rn transits through the interstitial spaces of the building material to the outer space described by Fick's second law. Assuming a homogeneous earthen wall where $^{220}$Rn atoms move towards the living space taken as *x*-direction. The change in concentration of the emanated $^{220}$Rn atoms with time is expressed as equation 3.13.

$$\frac{\partial C\ (x,t)}{\partial t} = D\frac{\partial^2 C\ (x,t)}{\partial x^2} - \lambda_T C(x,t) + R \qquad (3.13)$$

Where C (*x*, t) is the concentration of $^{220}$Rn in the pore space (Bq/m$^3$), D is the effective pore diffusion coefficient (m$^2$/s), $\lambda_T$ is $^{220}$Rn decay constant (s$^{-1}$), and R is the $^{220}$Rn pore space generation rate as determined by equation 3.12. The first term on the right-hand side of equation 3.13 represents the change in $^{220}$Rn concentration with distance *x* from the centre of the wall, and the second term represents the loss of $^{220}$Rn due to its decay. At steady state conditions, the concentration of $^{220}$Rn in the pore space does not depend on time but on distance *x*. Thus, the left-hand side of equation 3.13 reduces to zero and, upon its rearrangement, gives equation 3.14.

$$\frac{\partial^2 C\ (x,t)}{\partial x^2} - \frac{\lambda_T C(x,t)}{D} = -\frac{R}{D} \qquad (3.14)$$

To solve equation 3.14, it is broken into two parts, i.e., the complementary function and particular integral, and their solutions are added up. The complementary function is solved by equating the left-hand side of equation 3.14 to zero, as given by equation 3.15.

$$\frac{\partial^2 C\,(x)}{\partial x^2} - \frac{\lambda_T C(x)}{D} = 0 \qquad (3.15)$$

Let the complementary solution of equation 3.15 be as given by equation 3.16

$$\mathrm{C(x)} = \mathrm{A}e^{kx} \qquad (3.16)$$

Where A is an arbitrary constant and k is the root of the function.

The second derivative of equation 3.16 with respect to *x* results in equation 3.17

$$\frac{\partial^2 C\,(x)}{\partial x^2} = k^2 C(x) \qquad (3.17)$$

Substituting equation 3.17 into equation 3.15 gives equation 3.18

$$\{k^2 - \frac{\lambda_T}{D}\}C(x) = 0 \qquad (3.18)$$

The concentration C(*x*) cannot be zero, therefore,

$$k^2 - \frac{\lambda_T}{D} = 0$$

$$k = \pm\sqrt{\frac{\lambda_T}{D}} \qquad (3.19)$$

Given that $^{220}$Rn diffusion length $l = \sqrt{\frac{D}{\lambda_T}}$

Then $k = \pm \frac{1}{l}$ (3.20)

Writing equation 3.16 in terms of the roots and substituting for k as given by equation 3.20 gives equation 3.21,

$$C(x) = A_1 e^{\frac{x}{l}} + A_2 e^{-\frac{x}{l}} \qquad (3.21)$$

The particular integral part is solved by taking *C(x) = B* such that differentiating it two times results in equation 3.22

$$\frac{\partial^2 C\,(x)}{\partial x^2} = 0 \qquad (3.22)$$

Substituting equation 3.22 and *C(x)* = *B* into equation 3.14 gives the value of $B = \frac{R}{\lambda_T}$

Which, on summation with equation 3.21, gives equation 3.23

$$C(x) = A_1 e^{\frac{x}{l}} + A_2 e^{-\frac{x}{l}} + \frac{R}{\lambda_T} \qquad (3.23)$$

To determine the values of $A_1$ and $A_2$, we consider a wall with a uniform thickness of 2h measured along the x-axis with the middle of the wall as the origin. We consider the horizontal distance *x* across the wall directed towards the house's living space, with the middle of the wall being *x* = 0 and half the wall thickness as *x* = *h*, as shown in figure 3.4.

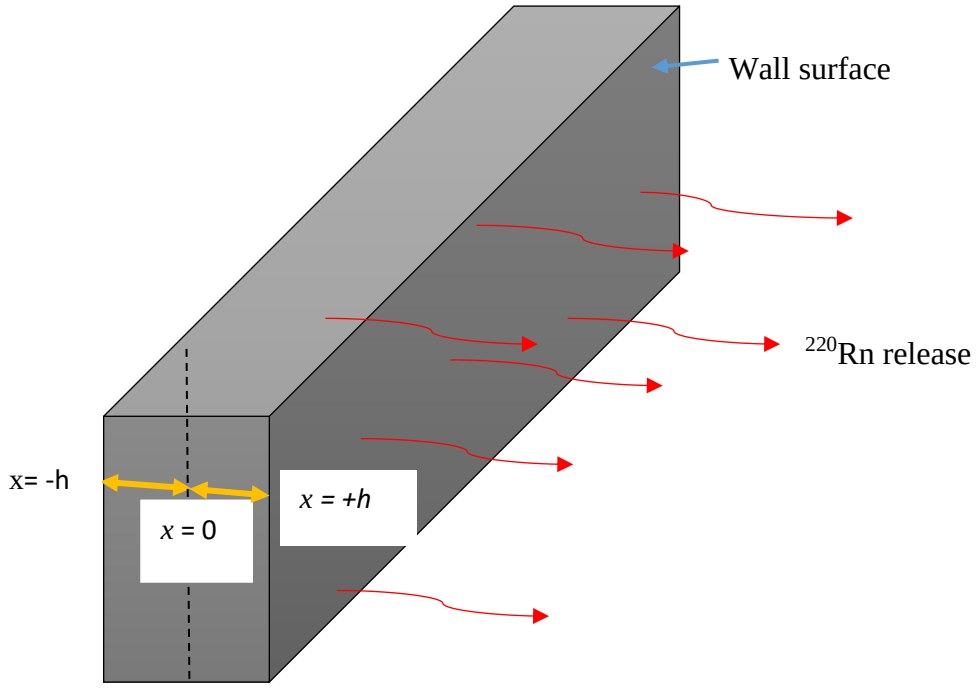


**Figure 3.4: Schematic presentation of $^{220}$Rn release from the wall surface**

Assuming that C ($x$ = - $h$) = C ($x$ = $h$) = C($x$) = 0 hence equation 3.23 is written as equation 3.24.

$$0 = A_1 e^{\frac{x}{l}} + A_2 e^{-\frac{x}{l}} + \frac{R}{\lambda_T}$$

$$A_1 e^{\frac{x}{l}} + A_2 e^{-\frac{x}{l}} = -\frac{R}{\lambda_T} \quad (3.24)$$

The constants $A_1 = A_2 = A$ is calculated as given by equation 3.25

$$A\left(e^{\frac{h}{l}} + e^{-\frac{h}{l}}\right) = -\frac{R}{\lambda_T} \quad (3.25)$$

Rearranged to equation 3.26

$$A = -\frac{R}{\lambda_T} / \left(e^{\frac{h}{l}} + e^{-\frac{h}{l}}\right) \quad (3.26)$$

Substituting for $A_1$ and $A_2$ as given by equation 3.26 into 3.24 results in equation 3.27,

$$C(x) = -\frac{R}{\lambda_T}\left(\frac{e^{\frac{x}{l}} + e^{-\frac{x}{l}}}{e^{\frac{h}{l}} + e^{-\frac{h}{l}}}\right) + \frac{R}{\lambda_T} \quad (3.27)$$

Using the hyperbolic trigonometric identity of $e^{x} + e^{-x} = 2Cosh\, x$ whereby as given by equation 3.28

$$e^{\frac{x}{l}} + e^{-\frac{x}{l}} = 2Cosh\ x/l \quad (3.28)$$

On substitution of equation 3.28 into equation 3.27 and rearranging, it gives the concentration of $^{220}$Rn per unit volume of the pore space C($x$) (Bq m$^{-3}$) as equation 3.29

$$C(x) = \frac{R}{\lambda_T}\left(1 - \frac{Cosh\, x/l}{\mathrm{Cosh}\, h/l}\right) \quad (3.29)$$

Where $\lambda_T$ is $^{220}$Rn decay constant, $l$ is $^{220}$Rn diffusion length, h is the half wall thickness, and R is $^{220}$Rn generation rate as given by equation 3.12.

Substituting equation 3.12 into equation 3.29 results in equation 3.30.

$$C(x) = \frac{\lambda_T \eta C_R}{\lambda_T} \left( 1 - \frac{Cosh\ x/l}{\text{Cosh}\ h/l} \right) \quad (3.30)$$

Which is further simplified to equation 3.31

$$C(x) = \eta C_R \left( 1 - \frac{\cosh x/l}{\cosh h/l} \right) \quad (3.31)$$

Equation 3.31 represents the $^{220}$Rn activity concentration in Bq kg$^{-1}$ of the building material per unit volume of the pore space.

### 3.3.3 Effect of $^{220}$Rn release from the wall on indoor absorbed gamma dose

The influence of $^{220}$Rn release on the secular equilibrium of the $^{232}$Th decay series is corrected by using the total $^{220}$Rn activity concentration in the wall instead of that of $^{232}$Th in the determination of absorbed gamma radiation dose from the $^{232}$Th decay series, which majorly originates from $^{220}$Rn and its progenies. The total $^{220}$Rn activity concentration in the wall $C_T(x)$ consists of the $^{220}$Rn in the pore space given by equation 3.31 and the ones in the building material but not emanated. The non-emanated $^{220}$Rn activity concentration is given as $C_R(1-\eta)$ such that the total activity concentration is the summation with equation 3.31 to give 3.32.

$$C_T(x) = \eta C_R \left( 1 - \frac{Cosh\ x/l}{\cosh h/l} \right) + C_R(1-\eta) \quad (3.32)$$

Simplifying equation 3.32 results in equation 3.33.

$$C_T(x) = C_R[\, \eta \left( 1 - \frac{Cosh\ x/l}{\cosh h/l} \right) + (1-\eta\,)] \quad (3.33)$$

Simplified to equation 3.34

$$C_T(x) = C_R \left( 1 - \eta \frac{Cosh\ x/l}{\cosh h/l} \right) \quad (3.34)$$

The activity concentration of $^{220}$Rn in the wall depends on its release factor $F_T$ (Bq kg$^{-1}$ s$^{-1}$), defined as the ratio between the mass exhalation rate $^{220}$Rn and the amount produced within the wall per unit time. The mass exhalation rate of $^{220}$Rn is obtained as the exhalation rate $E_T$ (Bq m$^{-2}$ s$^{-1}$) per unit density $p$ (kg m$^{-3}$) of the building material and the half wall thickness h (m). The total amount of $^{220}$Rn produced within the wall is the product of its decay constant $\lambda_T$ and $C_R$ the activity concentration $^{232}$Th of in the building material. Therefore, $F_T$ is given as equation 3.35.

$$F_T = \frac{E_T}{ph}\frac{1}{\lambda_T C_R} \tag{3.35}$$

Substituting for $^{220}$Rn exhalation rate, as given by equation 3.36, into equation 3.35 results in the release factor $F_T$ (Bq kg$^{-1}$ s$^{-1}$) as given by equation 3.37.

$$E_T = l\,\lambda_T \eta p C_R \tanh(h/l) \tag{3.36}$$

$$F_T = \frac{l\eta}{h}\tanh\,(h/l) \tag{3.37}$$

To incorporate the $^{220}$Rn release factor $F_T$ effect into the total activity concentration of $^{220}$Rn as given by equation 3.34, the expression for emanation factor η is first obtained by rearranging equation 3.37 as equation 3.38.

$$F_T = \frac{l\eta}{h}\frac{\mathrm{Sinh}\,h/l}{\mathrm{Cosh}\,h/l} \tag{3.38}$$

Equation 3.38 is further rearranged as equation 3.39,

$$\eta = \frac{F_T h}{l}\frac{\cosh h/l}{\sinh h/l} \tag{3.39}$$

Substituting equation 3.39 into equation 3.34 results in the expression for activity concentration of $^{220}$Rn at steady state condition as given by equation 3.40.

$$C_T(x) = C_R\left(1 - \frac{F_T h}{l}\frac{Cosh\, x/l}{\text{Sinh}\, h/l}\right) \quad (3.40)$$

Due to the short half-life of $^{220}$Rn of 55.6 s, only atoms close to the wall surface will be released from the building material; thus, considering the maximum possible wall surface point of its release at $x = h$, then, equation 3.40 becomes equation 3.41

$$C_T(x) = C_R\left(1 - \frac{F_T h}{l}\frac{Cosh\, h/l}{\text{Sinh}\, h/l}\right)$$

$$C_T(x) = C_R\left(1 - \frac{F_T h}{l\tanh h/l}\right) \quad (3.41)$$

The diffusion length of $^{220}$Rn is much smaller than half wall thickness for most building materials $h >> l$ therefore, $\tan h\frac{h}{l} \approx 1$ and equation 3.41 reduces to equation 3.42.

$$C_T(x) = C_R\left(1 - F_T\frac{h}{l}\right) \quad (3.42)$$

Equation 3.42 represents the total $^{220}$Rn activity concentration influenced by its release from the wall. Consequently, the gamma absorbed dose from the $^{232}$Th decay series is achieved by replacing the activity concentration of $^{232}$Th as given in equation 2.1 given by UNSCEAR, 1993, with the corrected one given by equation 3.42. The corrected absorbed gamma dose is therefore given as equation 3.43.

$$D = k_1 C_{Ra} + k_2 C_R\left(1 - F_T\frac{h}{l}\right) + k_3 C_k \quad (3.43)$$

Where $C_{Ra}, C_R$ and $C_k$ are the activity concentration of $^{226}$Ra, $^{232}$Th and $^{40}$K respectively and $k_1$, $k_2$ and $k_3$ are the dose conversion factor of $^{226}$Ra, $^{232}$Th and $^{40}$K respectively. If $^{220}$Rn

is not released, then the release factor is zero; hence both $^{220}$Rn and $^{232}$Th are in secular equilibrium thus, their activity concentration is equal.

# CHAPTER FOUR: MATERIALS AND METHODS

## 4.1 Research design

This research applied the experimental design in the determination of radiation exposure from indoor air as a result of radon and thoron, terrestrial radionuclides in building materials and crops in HBRAs of Homa and Ruri areas as well as radon and heavy metal concentration in Lake Victoria around these regions. The purposive sampling method was applied in the identification of the sampling dwellings based on their position on the hills, i.e., top or bottom, windward or leeward, for the terrestrial radionuclides $^{226}$Ra, $^{232}$Th and $^{40}$K), as well as $^{222}$Rn and $^{220}$Rn surface exhalation rate and their indoor concentration measurements. $^{222}$Rn and $^{220}$Rn exhalation measurements, the activity concentration of $^{226}$Ra, $^{232}$Th, and $^{40}$K in earthen building materials and crops alongside the lake water heavy metals were done in the Kenyatta university research laboratories. Analysis of the measured indoor $^{222}$Rn, $^{220}$Rn, and $^{220}$Rn progeny was done in Hirosaki university research laboratories in Japan. Mathematical modeling was also integrated alongside the descriptive, experimental design for the indoor gamma radiation dose assessment.

## 4.2 Sampling region

The samples were taken from high background radiation areas of Homa and Ruri hills, and a third region not an HBRA, known as Asego hill was considered a control research area. The three regions are all along Lake Victoria in Homa Bay county Kenya. These sample dwellings are shown in figure 4.1, as marked by dots around each hill.

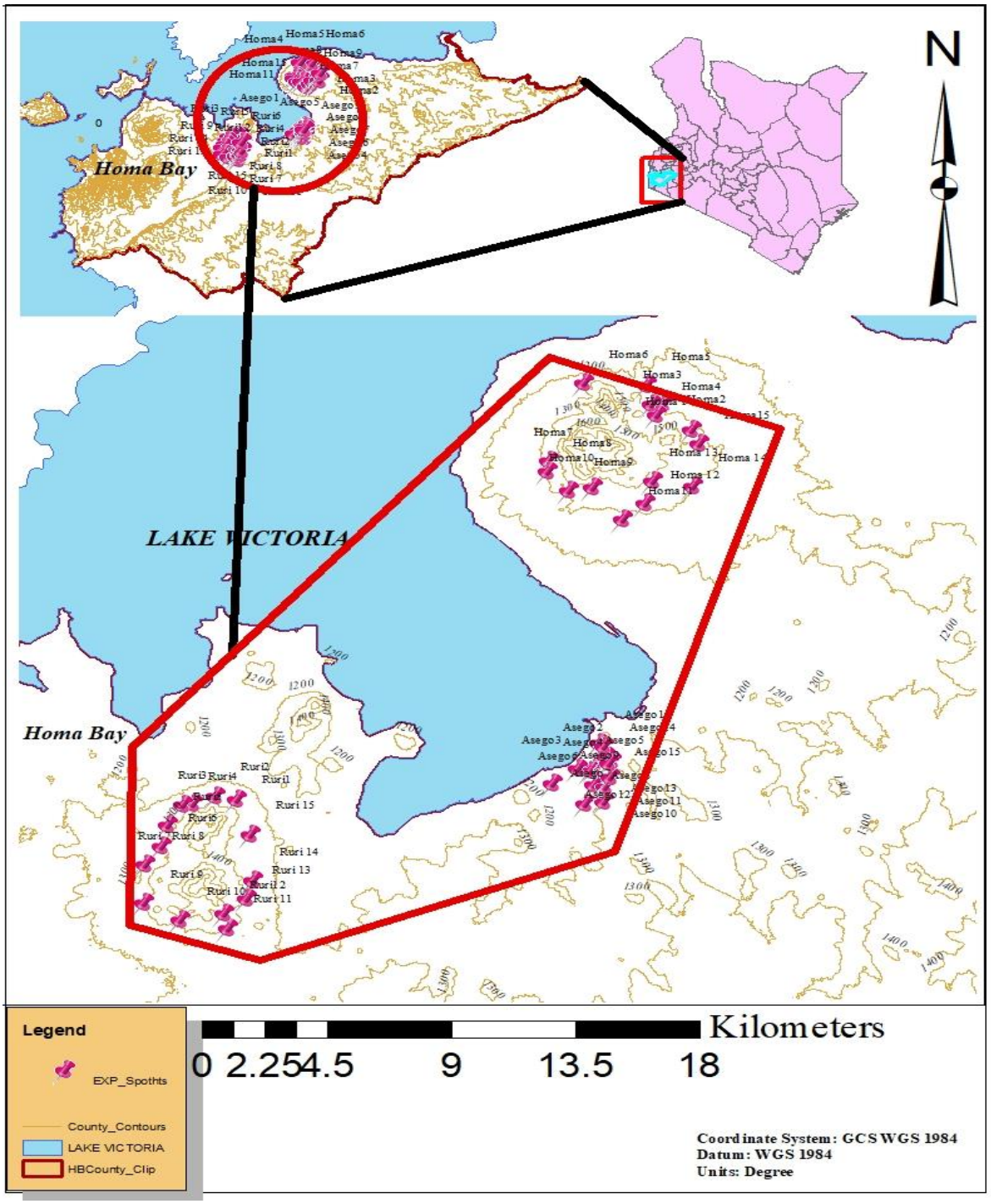


**Figure 4.1: A map of Homa Bay County showing the study regions**

On the other hand, the sample points taken in Lake Victoria for measurements of $^{222}Rn$ and heavy metals in the lake water are shown in figure 4.2.

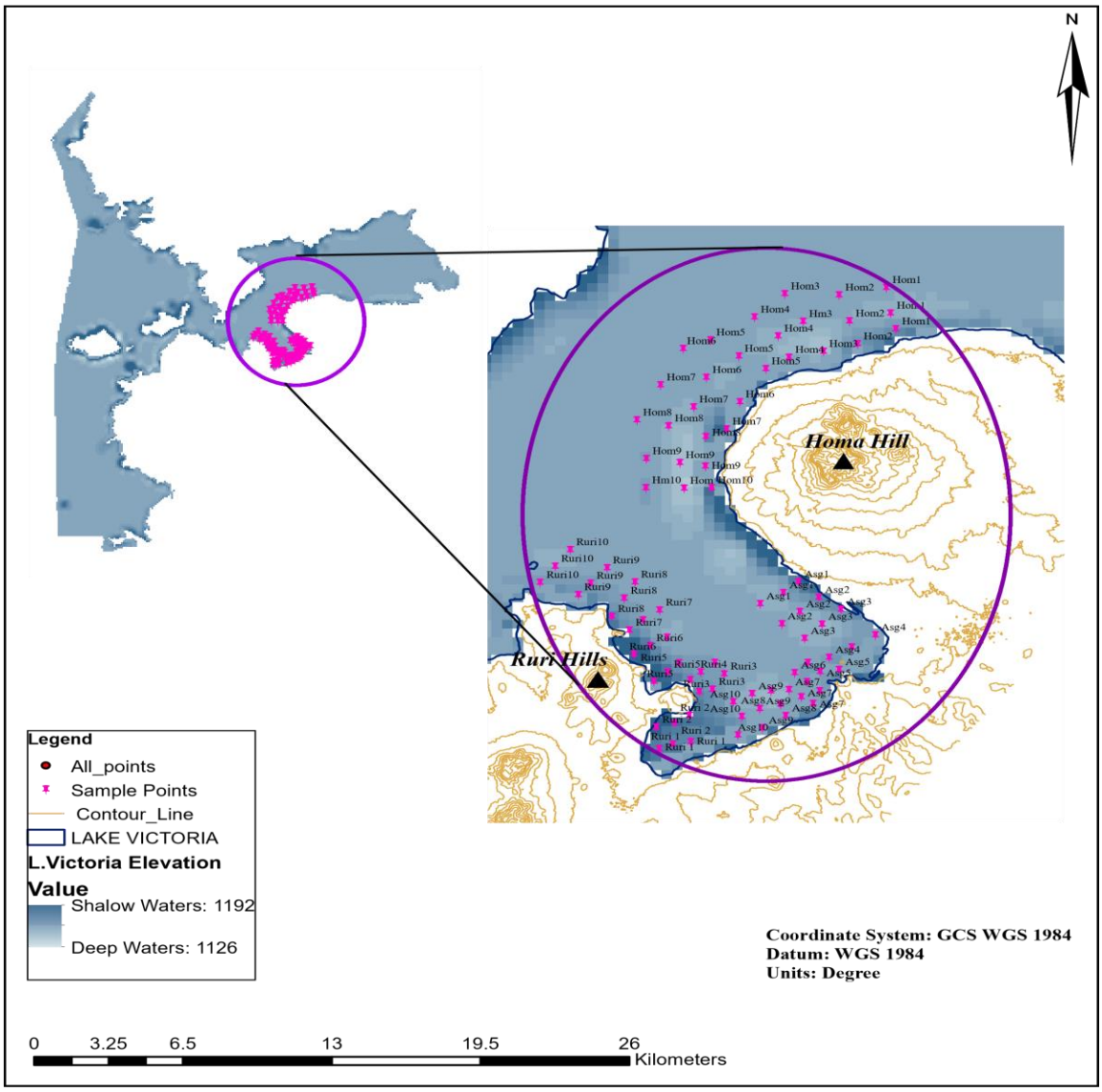


**Figure 4.2: A map of Homa Bay County showing the sampling points in Lake Victoria around study areas of Homa, Ruri, and Asego**

### 4.3 Radioactivity in building materials and crops (maize)

#### 4.3.1 Sampling procedure and sample preparation

The soil lumps used for the $^{222}$Rn and $^{20}$Rn exhalation measurements in section 4.5.1 in this work were the same once used to determine the activity concentration of $^{226}$Ra, $^{232}$Th and $^{40}$K in building materials. The cling film covering the soil lumps was carefully removed in

the laboratory, and each lump was then crushed to a fine powder before drying in an oven at a temperature of 110 $^{o}$C for 24 hours. 250 g mass of each soil sample was then sealed in a plastic container, labelled, and stored for about four weeks to attain radioactive secular equilibrium between $^{226}$Ra, $^{232}$Th and their progenies (Tzortzis *et al.*, 2002). The spectral analysis of the earthen building material samples was done in the Physics Laboratory of Kenyatta University using thallium activated sodium iodide detector.

Fifteen dry white maize samples were collected from farms of the same homes where the soil lumps were picked for the building material measurements in each region during the harvesting period and sun-dried. The sampling points are shown in figure 4.1. Each maize sample was crushed, sieved through a 1 mm sieve then dried in an oven at 70 $^{o}$C for 24h. 250g of each weighed, packed in hermetically sealed plastic containers and then labelled. These samples were then kept for four weeks to allow $^{226}$Ra and $^{232}$Th to attain secular equilibrium with their daughters.

### 4.3.2 Analysis

#### 4.3.2.1 Activity concentration of terrestrial radionuclides

The gamma-ray spectrometer used in this work comprises a 76 mm × 76 mm thallium-activated sodium iodide [NaI (Tl)] single crystal detector, an Oxford PCA-P multichannel analyzer which is a PC-based plug-in PCI card. It consists of an 80MHz Wilkinson analogue-to-digital converter for spectral data acquisition. The energy calibration of the detector was done using Cs-137 at an energy peak of 662 keV and Co-60 at energy peaks of 1170 keV and 1330 keV. The energy calibration spectrum of the intensity (c/s) against energy (keV) is shown in figure 4.3.

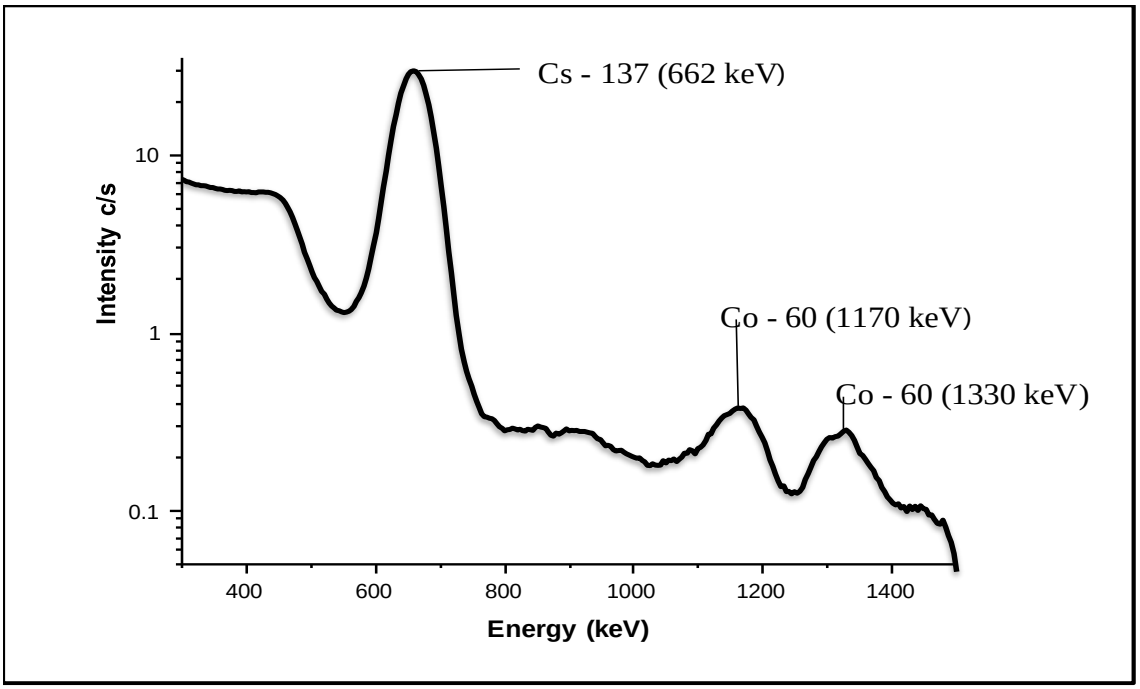


**Figure 4.3: Gamma-ray spectrum of cobalt -60 (1170 keV and 1330 keV) and cesium -137 (662 keV) used for energy calibration of the spectrometer**

The detector efficiency was calibrated using International Atomic Energy Agency (IAEA) standard certified reference materials RGU-1, RGTh-1, and RGK-1 having the same geometry as the samples. $^{226}$Ra and $^{232}$Th activity concentrations were determined based on $^{214}$Bi gamma energy peak of 609 keV and $^{208}$Tl at an energy peak of 2615 keV, respectively, while for $^{40}$K, an energy peak of 1460 keV was used from the spectrum of the background counting using equation 4.1 (UNSCEAR, 2000).

$$A_i = \frac{N}{\gamma m \varepsilon t} \qquad (4.1)$$

where $A_i$ is the activity concentration of radionuclide i (Bq/kg), N is the residual net counts at a peak energy of interest obtained by subtracting the background counts from the total

sample counts, γ is the emission probability of gamma-ray of interest, m is the mass of the sample in kg, ε is the detection efficiency of the gamma-ray of interest and t is the acquisition time in seconds.

The minimum detectable activity (MDA) was determined by first doing a background count using an empty bottle used to hold the samples for 30,000s on the NaI (Tl) detector. Using the spectrum of the background counting, the following isotopes and their corresponding energy peaks $^{214}$Bi (1764.49 keV) and $^{208}$Tl (2614.5 keV) and for $^{238}$U and $^{232}$Th respectively, and energy peak of 1460.83 KeV for $^{40}$K were used to determine their lower limit of detection (LLD) then MDA respectively.

The background counts were then used to correct the net peak area of gamma rays of the measured standard isotopes. The LLD and MDA were calculated using equations 4.2 and 4.3, respectively (Currie, 1968; Carrer, 2006).

$$LLD = 4.66\sigma_b + 3 \qquad (4.2)$$

$$MDA = \frac{LLD}{\varepsilon Y t} \qquad (4.3)$$

where $\sigma_b$ is the standard deviation of the background in the region of interest, $\varepsilon$ is the absolute efficiency of the detector, $Y$ is the absolute gamma emission probability of the gamma decay, and t is the counting time in seconds. The minimum detectable activity (MDA) for $^{40}$K, $^{232}$Th, and $^{226}$Ra was determined as 1.4 Bq/kg, 0.196 Bq/kg, and 0.401 Bq/kg, respectively.

#### 4.3.2.2 Radium equivalent activity ($Ra_{eq}$)

It is defined as the activity concentration of a radionuclide equivalent to 1 Bq/kg of $^{226}Ra$ such that 1 Bq/kg of $^{232}Th$ is equivalent to 1.429 Bq/kg of $^{226}Ra$ and 1 Bq/kg of $^{40}K$ is equivalent to 0.0769 Bq/kg of $^{226}Ra$. Therefore, $^{226}Ra$ is considered relatively radiotoxic compared to $^{232}Th$, with $^{40}K$ being the least radiotoxic. It was determined by equation 4.4 (Beretka *et al.,* 1985).

$$Ra_{eq} = A_{Ra} + 1.429A_{Th} + 0.0769A_k \quad (4.4)$$

where $A_{Ra}$, $A_{Th,}$ and $A_K$ are the activity concentrations of $^{226}Ra$, $^{232}Th$, and $^{40}K$, respectively. The 1.429 and 0.0769 are $^{226}Ra$ equivalent conversion factors for $^{232}Th$ and $^{40}K$, respectively.

### 4.4 External gamma radiation dose rate in the air inside the dwellings

The ambient absorbed gamma dose rate in the air inside the dwellings was measured 1m above the floor, approximately at the centre of the dwellings. The measurements were carried out in the same houses mapped in figure 4.1 using a hand-held multi-purpose survey meter Geiger Muller Counter Data Logger (GQ GMC-320 Plus). This meter determines radiation in an area by measuring gamma dose rates in μSv/h with a measurement range of 0.0 to 327.99 μSv/h. Its gamma sensitivity is between 0.1 to 1 MeV and a background of 0.2 pulses/s. The values from the instrument were recorded against each sampled house.

## 4.5 Radon ($^{222}$Rn) and Thoron ($^{220}$Rn) exhalation measurements

### 4.5.1 Sampling and sample preparation

Fifteen soil lumps were chopped off the walls using kitchen knife of the randomly selected houses, as shown in figure 4.1, around each of the hills and labelled. The location for each sampled house was determined using hand-held Garmin GPS and then recorded. The dimensions and volume of each sample were determined by applying the approximation method since they had irregular shapes. They were then dried in an oven at a temperature of 110 $^{o}$C for 24 hours to remove the moisture, which would otherwise reduce the sensitivity of the RAD7 detector. Three sides of each sample were then covered using several rolls of cling film, as shown in figure 4.4, to effectively reduce thoron and radon exhalation to nearly zero on those sides and allow exhalation from just one side typical representation of a wall (Chege *et al.*, 2015).

**Figure 4.4: A snapshot showing pre-covered soil lump sample for the $^{222}$Rn and 20Rn exhalation measurement**

Each sample was then enclosed in an accumulation chamber connected to a solid-state alpha detector (RAD7, Durridge Co. Inc., USA) for 8 hours to measure $^{222}$Rn and $^{220}$Rn exhalation rates.

### 4.5.2 Accumulation chamber technique

The accumulation chamber technique coupled with the RAD7 detector was used in radon surface exhalation rate measurements. The accumulation chamber was made of a 3-litre stainless steel barrel with a tight air lid, inlet, and outlet ports to the RAD7 detector via silicone hoses, as shown in figure 4.5.

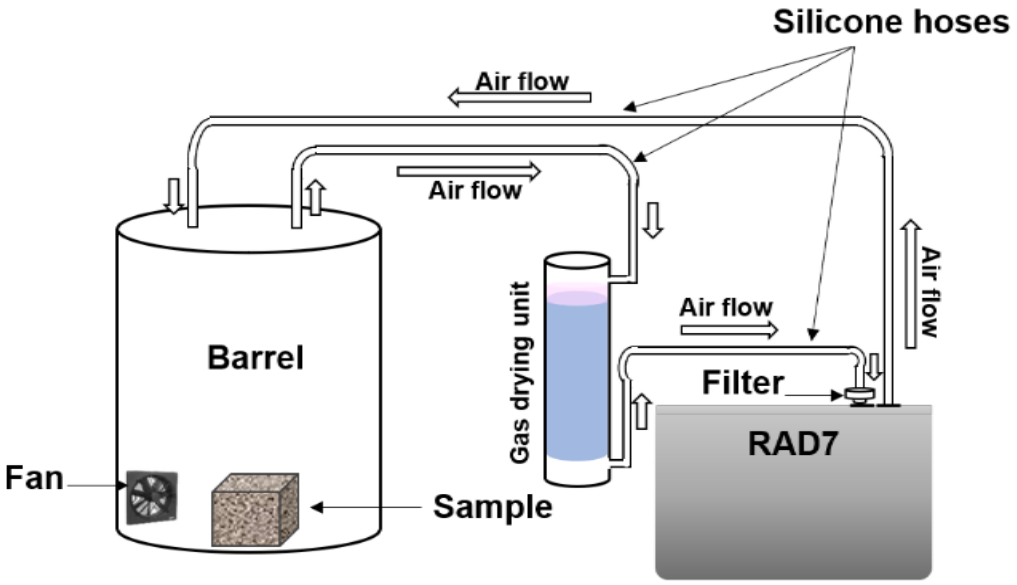


**Figure 4.5: A schematic representation of the experimental arrangement**

The inlet was connected to a gas drying unit with desiccant ($CaSO_4$ with 3% $CoCl_2$ as an indicator) to maintain the relative humidity of the measuring system to less than 10%. The inlet was also connected to a filter to suppress isotope progeny, thus allowing only $^{222}Rn$ and $^{220}Rn$ gases into the RAD7 as well as free air movement. A small fan was fixed at the lower part of the accumulation chamber to keep the air inside the chamber well mixed. The outdoor air was used to purge the detector for 10 minutes after every measurement to clear out the $^{222}Rn$ and $^{220}Rn$ and their progeny previously measured. The RAD7 was set on Auto mode with a cycle time of one hour and recycling of eight hours (Chege *et al.*, 2015). The RAD7 detector used was calibrated in Durridge company Billerica laboratories USA with the normal mode sensitivity of 0.013 CPM/(Bq/$m^3$) and sniff mode sensitivity of 0.0619 CPM/(Bq/$m^3$), a negligible background of 0.2 Bq/$m^3$and detection limit of 4 Bq/$m^3$for both $^{222}Rn$ and $^{220}Rn$.

The accumulation chamber technique has two limitations which are leakage and back diffusion. To stop gas leakage from the system, the barrel lid was tightly sealed with special gaskets and silicone (Xiaofeng *et al.,* 2011). The back-diffusion effect was minimized by ensuring that the effective air volume of the system was at least ten times more than that of the sample pore space. This enables the activity concentration of $^{220}$Rn and $^{222}$Rn inside the accumulation chamber to be less than that in the sample pore space volume; therefore, the back-diffusion effect can be neglected (Hassan et al., 2011).

The isotope surface exhalation rate is the amount of radon released into the air per unit time per unit area from the surface of a building material. Taking the initial $^{222}$Rn and $^{220}$Rn concentration inside the chamber to be zero, the isotope surface exhalation rate $E_i$ (Bq/m$^2$ /s) was determined by equation 4.5 (Iwaoka *et al.,* 2012).

$$E_i = \frac{C_o V_e \lambda}{A_s} \qquad (4.5)$$

Where $C_o$ is the measured equilibrium concentration of isotope i (Bq/m$^3$), $\lambda$ is isotope decay constant ($\lambda_{thoron}$ = 0.0125 s$^{-1}$ and $\lambda_{radon}$ = 2.111 x 10$^{-6}$ s$^{-1}$), $V_e$ is effective air volume (m$^3$) (sum of accumulation chamber residual volume, silicone pipes volume and detector chamber volume (approximately 0.00395 m$^3$) and $A_S$ is sample's exposed side surface area (approximately 0.0025 m$^2$) and a thickness of about 0.03 m.

### 4.6 $^{222}$Rn, $^{220}$Rn and $^{220}$Rn progeny concentration measurements

#### 4.6.1 Sampling procedure and sample preparation

A total of forty-five earthen dwellings, fifteen around each of the three sampling regions (Homa, Ruri, and Asego), were selected for the $^{222}$Rn, $^{220}$Rn, and $^{220}$Rn progeny

concentration measurements, as shown in figure 4.1. Passive integrating radon–thoron discriminative monitor (RADUET) for $^{222}$Rn and $^{220}$Rn measurements and equilibrium equivalent thoron concentration (EETC) monitors for $^{220}$Rn progeny measurements were simultaneously installed in each house for three months (Tokonami *et al.,* 2005). Each monitor (RADUET and EETC) was packed in an air-tight polythene sachet and only unpacked at the sampling site during the installation. They were tied using a string at an approximate horizontal distance of 0.5 m from the wall and an approximate vertical height of 1.8 m from the floor surface, which is the breathable air space in any dwelling, as indicated in appendix 3. $^{222}$Rn and $^{220}$Rn concentration measurements were done in the dry season (December - February) and the rainy season (August - October). After three months, the monitors were collected from the dwellings, each packed in airtight zip lock bags to prevent contamination, and transported to Hirosaki University, Japan, for analysis.

### 4.6.2 Data analysis of radiation concentration

#### 4.6.2.1 Indoor $^{222}$Rn, $^{220}$Rn and $^{220}$Rn progeny concentration

The RADUETs were used for the measurement of indoor $^{222}$Rn and $^{220}$Rn. They are made of 30 $cm^3$ pairs of cylindrical diffusion chambers, which are passive integrated $^{222}$Rn and $^{220}$Rn discriminating. $^{220}$Rn is measured by the high diffusion rate chamber ($C_H$), which has six holes of 6mm with an electroconductive sponge allowing both $^{222}$Rn & $^{220}$Rn into it. $^{222}$Rn is measured by the low diffusion rate chamber ($C_L$) with an invisible air gap between its lid and bottom part, as shown in figure 4.6 and figure 4.7.

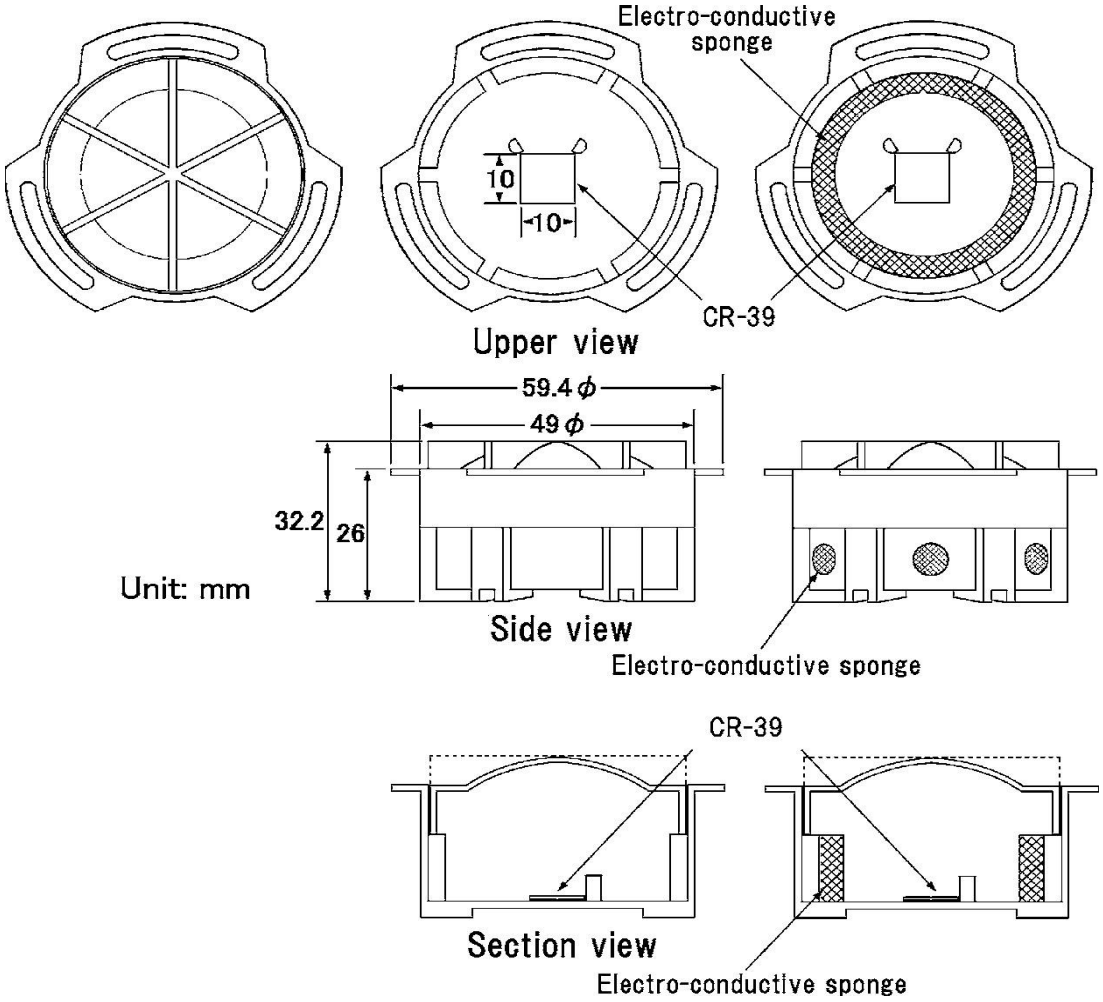


**Figure 4.6: Schematic presentation of RADUET monitor pair (Tokonami et al., 2005)**


**Figure 4.7: RADUET monitor pair used in this study for $^{222}$Rn & $^{220}$Rn concentration measurement**

An electroconductive sponge/plastic prevents $^{222}$Rn and $^{20}$Rn progenies entry. A solid-state nuclear track detector (CR-39 chip) is placed at the bottom of each chamber. $C_L$ & $C_H$ air exchange rates differ by two order magnitude, and track density in CR-39 discriminate $^{222}$Rn and $^{220}$Rn (Kranrod *et al.*, 2020).

CR-39 is chemically etched in 6M NaOH solution at 60$^o$ C for 24 hours to identify alpha tracks in CR-39 chips as indicated in figures 4.8 and 4.9 for high and low chambers, respectively.

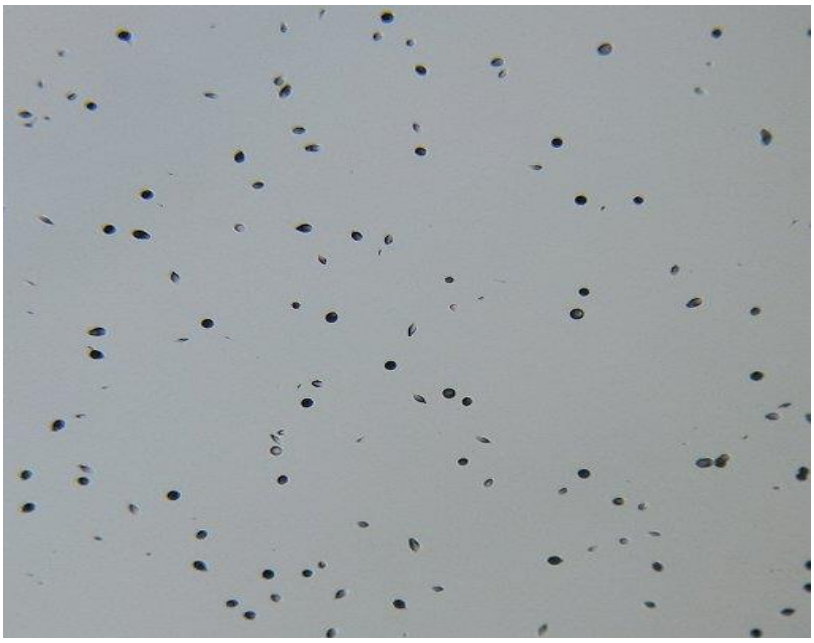

**Figure 4.8: Damage track from CR-39 from high diffusion chamber in this study**

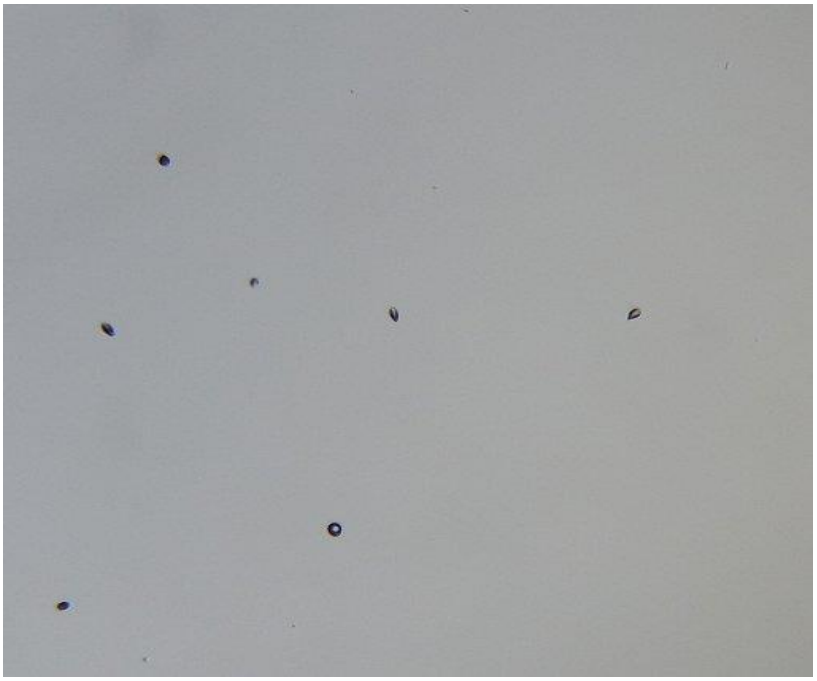

**Figure 4.9: Damage track from CR-39 from low diffusion chamber in this study**

The CR-39 chips were then washed in distilled water then dried. Track density was counted by the software Image-J based on the image from an optical microscope. The spatial resolution of read out track size was 12 – 200 pixels, and circularity of 0.4 – 1.

The concentration of $^{222}Rn$ ($C_{Rn}$) and that of $^{220}Rn$ ($C_T$) in $Bq/m^3$ were determined by equations 4.6 and 4.7 (Tokonami *et al.*, 2005).

$$N_L = C_{Rn}F_{1R}t + C_TF_{1T}t + B \quad (4.6)$$

$$N_H = C_{Rn}F_{2R}t + C_TF_{2T}t + B \quad (4.7)$$

Where $N_H$ and $N_L$ is the track densities in $C_H$ & $C_L$ chambers, B is background track density, $F_{1R}$ & $F_{2R}$ are conversion factors for $C_L$ & $C_H$ $^{222}Rn$, $F_{1T}$ & $F_{2T}$ are conversion factors for $C_L$ & $C_H$ for $^{220}Rn$, t is the exposure time 90 days.

The EETC monitors were used to measure $^{220}Rn$ progeny concentration in the dwellings. The monitors only detect alpha energy 8.8 MeV of $^{212}Po$, the highest alpha energy as shown in figure 4.10.

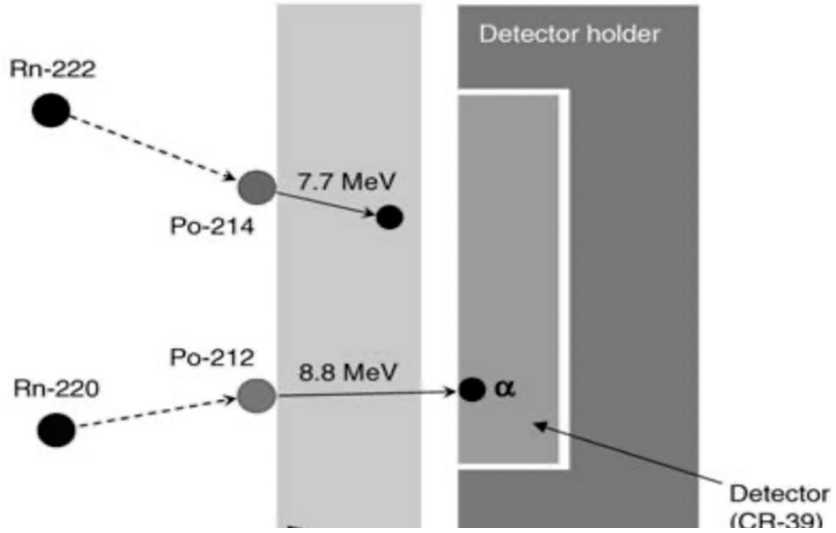


**Figure 4.10: Schematic presentation of an EETC Monitor (Tokonami et al., 2005)**

Aluminium vaporized Mylar film of 71mm thickness separates the alpha energies and only allows the detection of 8.8 MeV alpha. Four CR-39 chips are installed inside the where tracks of alpha particles are recorded, as shown in figure 4.11 and figure 4.12.

**Figure 4.11: Picture of EETC Monitor used in this study for the $^{220}$Rn progeny measurements**

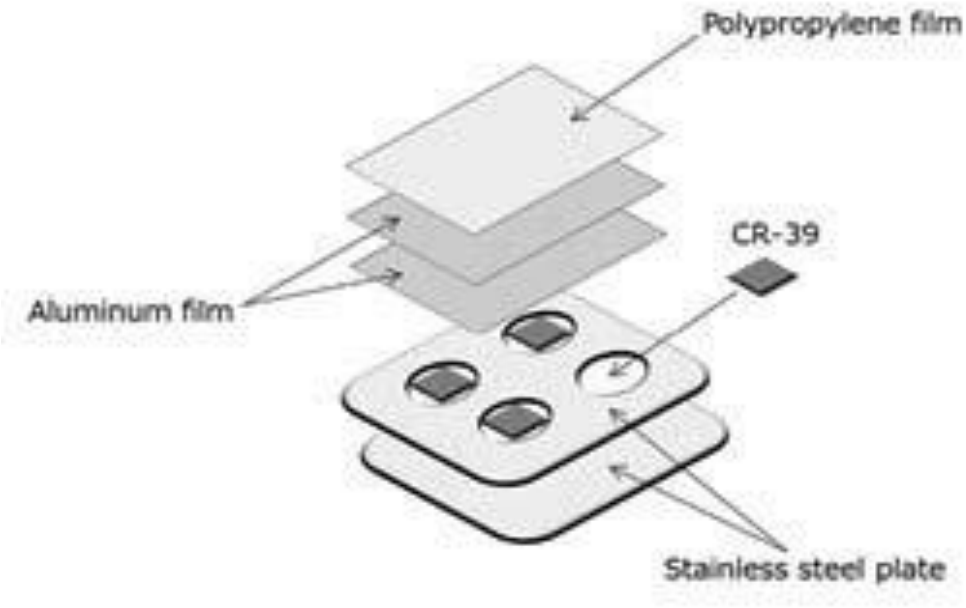


**Figure 4.12: Schematic representation of EETC Monitor with the 4 CR-39 chips**

$^{220}$Rn progeny concentration in the dwellings EETC (Bq m$^{-3}$) was determined by equation 4.8 (Tokonami, 2020).

$$D = EETC \text{ (Bq m}^{-3}) \times C + B \quad (4.8)$$

D is the track density (tracks/mm$^2$), C is the conversion factor which was experimentally obtained as 0.017 tracks mm$^{-2}$ (Bq/m$^3$/day)$^{-1}$.

## 4.7 Radon ($^{222}$Rn) concentration in Lake Victoria

### 4.7.1 Sampling procedure and sample preparation

A total of 90 water samples were collected, 30 from each of the three regions (Homa, Ruri, and Asego) from the point shown in figure 4.2. Ten randomly identified sampling points (mostly beaches) were identified from each sampling region from which three samples

were collected at different depths from the lake surface; the first sample was collected from the water surface at the shoreline, the second one at a depth of 5 m from the water surface to the floor of the lake and the third one was collected from a depth of 10 m from the water surface to the floor of the lake making a total of 30 samples per region. The depths were chosen based on the Lake Victoria depth profiling by (Okungu et al., 2005), as shown in figure 4.13. The surface samples were collected using a two-litre plastic soda bottle which was submerged in an upside-down position and then inverted while inside water so that the air inside was displaced by water and filled from about 0.1 m from the water surface and capped under water to ensure no contact of water with air as per the big bottle system manual (Durridge RAD7,2015).

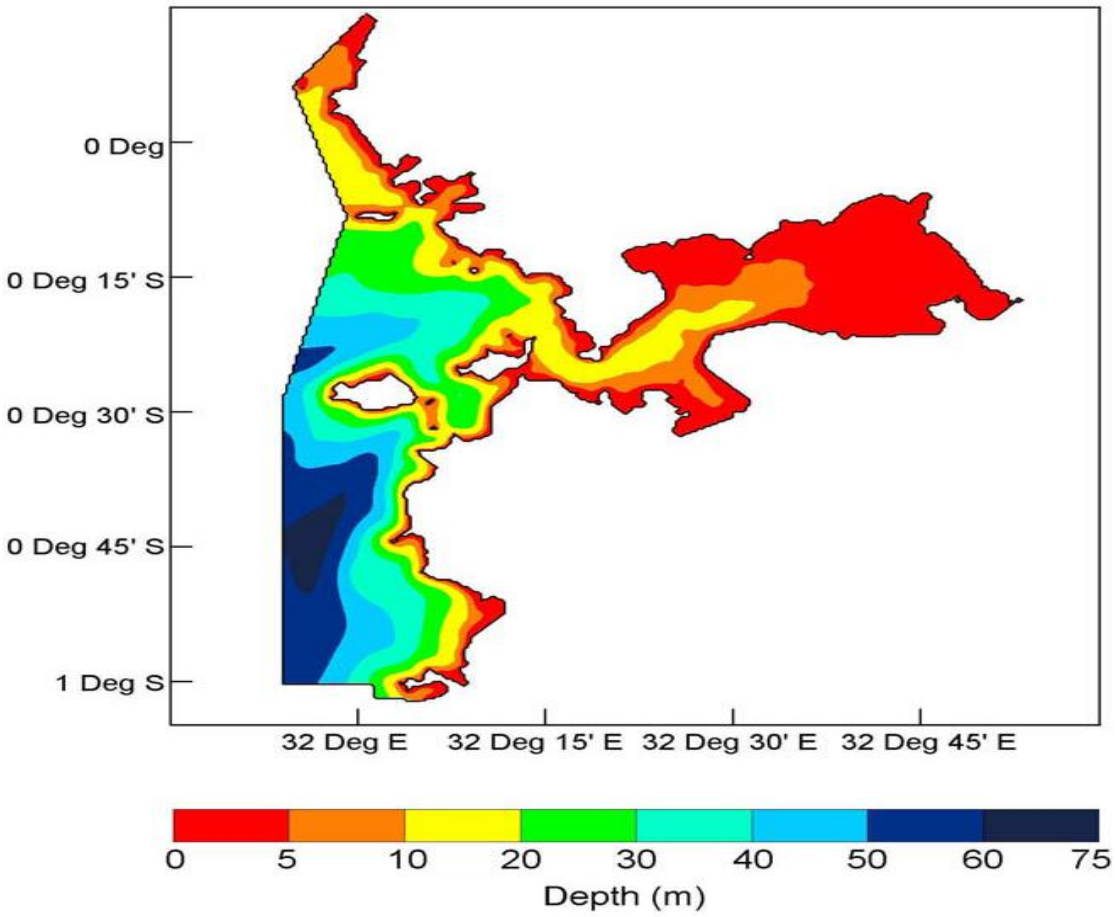


**Figure 4.13: Variation by the depth of the Kenyan part of Lake Victoria (Okungu et al., 2005)**

The water at 5 m and 10 m depths were collected using a deep-water sampler from which water was transferred to the 2-litre soda bottle using the air-tight tubing from the sampler under the water surface and capped underwater surface to avoid air contact with the sampled water. The plastic soda bottles were filled to avoid the head space between the water and the bottle top, which might trap air which might degas $^{222}Rn$ before it is measured as per the Durridge RAD 7 Big bottle system manual as illustrated by appendix IV (Durridge RAD7, 2015). The time and location of the sampling were then noted using a

hand-held GPS, and the samples were labelled accordingly. The depth, temperature, and pH were determined using the hand-held YSI Pro DSS (Digital sampling system) multiparameter meter shown in figure 4.14. The YSI Pro Digital Sampling System (Pro DSS) is the most advanced portable handheld water quality spot sampling and profiling multiparameter field instrument. It measures a wide range of parameters such as dissolved oxygen, total algae, turbidity, pH, ORP, conductivity, specific conductance, salinity, TDS, resistivity, TSS, ammonium, ammonia, chloride, nitrate, depth, and temperature. It has a handheld cable of different lengths as well as depth sensors. Radon concentration was then measured from each water sample using the RAD 7 coupled with the big bottle system.


**Figure 4.14: Picture of YSI Pro DSS multiparameter meter used in this study**

### 4.7.2 Analysis

#### 4.7.2.1 $^{222}$Rn concentration in water

The big Bottle System schematic representation is shown in figure 4.15, and the snap shot of the physical setup used in this study is illustrated in figure 4.16.

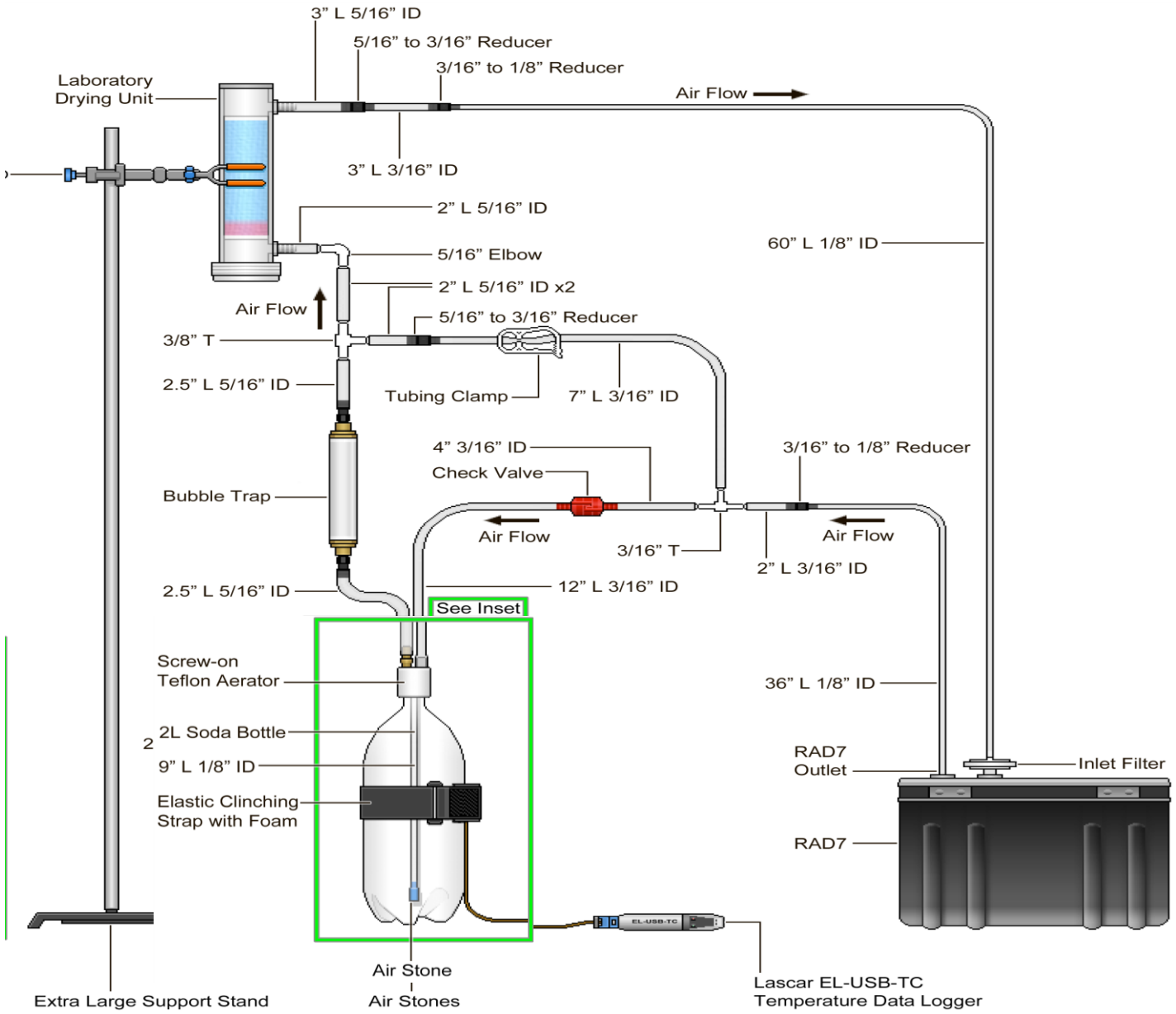


**Figure 4.15: Schematic representation of the big bottle experimental setup. (Durridge RAD7,2015)**

**Figure 4.16: A photograph showing the big bottle technique assembly experimental setup used in this study**

It uses a closed-loop aeration scheme whereby the air and water volumes are constant and independent of the flow rate. The air recirculates through the water and extracts the radon until a state of equilibrium develops. Aerating the water in the Big Bottle System moves the bulk of the radon from the water into the air loop taking around 45 minutes, after which the aeration process is complete, and the radon in the air loop is at equilibrium with the remaining radon in the water. The system reaches this state of equilibrium after aeration, with the extraction efficiency being temperature dependent; thus, the temperature is monitored using the temperature logger kit. The clip between the T-connectors is then opened to allow the airflow to bypass the bottle. The desiccant in a big laboratory drying

unit was used at all times to dry the air stream before it entered the RAD7. RAD7 was used in Sniff mode three recycles with each cycle time of 15 minutes to measure the radon concentration in the air loop whose extraction efficiency from water depends on the temperature of the water; thus, a temperature logger was attached directly to the bottle with the elastic strap as per the Durridge RAD 7 big bottle system manual (Durridge RAD7,2015) as indicated in figure 4.16.

A conversion factor is used to convert the measured radon concentration in the air loop to radon concentration in water which is automatically done by Durridge's CAPTURE software for windows (*RAD7 CAPTURE software manual version*, 2015). The physical configuration of the experiment was specified, e.g., the volume of the bottle and tubing apparatus, the type of drying unit used, and the temperature of the water at the time of aeration to the software. The measurements were corrected for the delay time from the time the sample was collected to the time it was counted by use of the decay correction factor ($D_{CF}$) on the measured values, using equation 4.9 (Ali *et al.*, 2010).

$$D_{CF} = e^{\lambda T} \qquad (4.9)$$

Where T is the time difference between sample collection and counting, λ is the decay constant of $^{222}$Rn.

## 4.8 Heavy metal analysis in Lake Victoria

### 4.8.1 Sampling procedure and sample preparation

Thirty water samples were collected at the lake surface using a one-litre plastic soda bottle from the same points as where the samples for measurement of $^{222}Rn$ in water were collected on the first points of the depth of 0.1m, as shown in figure 4.2. The soda bottles used for collecting the samples were first cleaned, rinsed with 10% nitric acid, then double distilled water, and finally using, the sample water was at the collection point. The sampling location was noted using a hand-held GPS, and the samples were labelled accordingly. The water samples' pH and electrical conductivity were measured in situ using a portable digital multiparameter. The water samples were then transported to the laboratory, where they were preserved using nitric acid to a pH of less than two to enable the release of metals that might have been adsorbed onto the bottle surface. The water samples were left for three days before analysis was done using the Atomic Absorption Flame Emission Spectrophotometer. (Chege *et al.,* 2013). The elements considered in this study were cadmium (Cd), lead (Pb), chromium (Cr), Manganese (Mn), and Nickel (Ni).

### 4.8.2 Analysis

#### 4.8.2.1 Heavy metal concentration in water measurement

The water samples were analyzed for heavy metals using the Atomic Absorption Flame Emission Spectro-photometer (AA-6200) at Kenyatta University, as illustrated in figure 4.17 and appendix V.

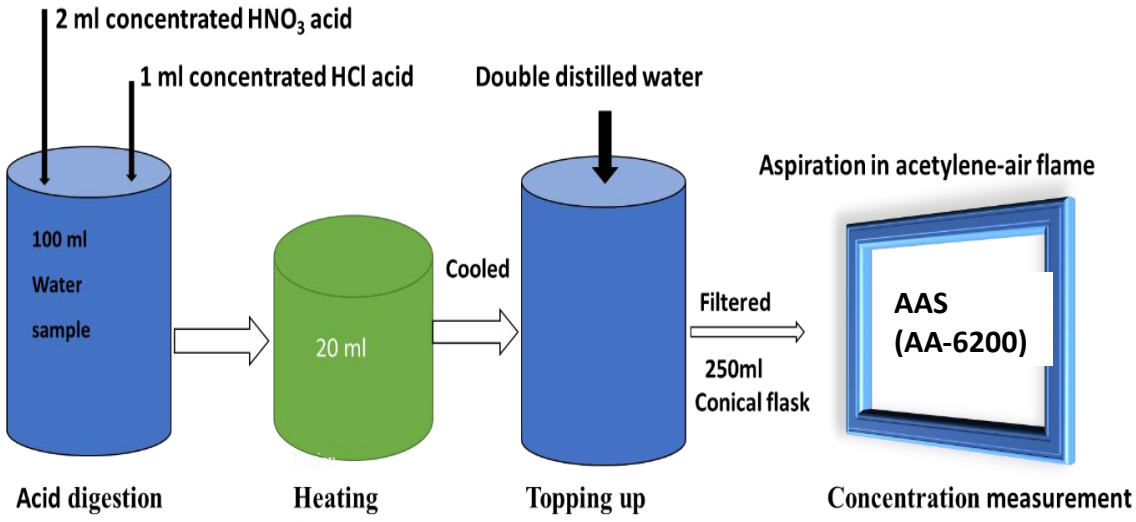


**Figure 4.17: Schematic representation of Atomic Absorption Flame Emission Spectro-photometer for heavy metal analysis**

Stock solution of heavy metal of interest was diluted to a known concentration in range in which Lambert-Beer's law hold. The resulting different concentrations were then aspirated into acetylene–air flame. A cathode lamp of each element of interest is used as a source of light where the absorbance of light is measured for different concentrations of the stock solution then a calibration curve of absorbance versus concentration is generated. The generated curve was then used as the standard of reference against which the concentration of the particular heavy metal in the sample was determined for each element. The water samples were prepared for analysis by acid digestion by adding 2 ml concentrated nitric acid and 1 ml concentrated hydrochloric acid to 100 ml of each sample. The resulting solution was heated at a solution temperature of $95^0$ C until the volume was reduced to 20 ml, then left to cool and topped up to 100 ml using double distilled water. The resulting

solution was then filtered in a 0.45µm filter into 100 ml plastic bottles. A blank solution was prepared in the same way as the samples using double distilled water to correct for the acids used in the digestion process. The blank and the digested samples were measured together, and the concentration of each metal was determined by subtracting the metal concentration of the blank (Chege *et al.*, 2013).

# CHAPTER FIVE: RESULT AND DISCUSSION

## 5.1 Natural radioactivity measurements results and analysis

### 5.1.1 Building materials

Table 5.1 summarizes the determined activity concentration results of $^{226}Ra$, $^{232}Th$, and $^{40}K$ in building materials from Homa and Ruri sampling areas, respectively.

**Table 5.1: Activity concentration of $^{40}K$, $^{226}Ra$ and $^{232}Th$ and associated $Ra_{eq}$ in earthen building materials**

| Region | $^{226}Ra$ (Bq/kg) | $^{226}RaRa_{eq}$ ($A_{Ra}$) (Bq/kg) | $^{232}Th$ (Bq/kg) | $^{232}Th$ $Ra_{eq}$ ($1.429A_{Th}$) (Bq/kg) | $^{40}K$ (Bq/kg) | $^{40}K$ $Ra_{eq}$ ($0.0769A_k$) (Bq/kg) | Total $Ra_{eq}$ (Bq/kg) |
|---|---|---|---|---|---|---|---|
| Homa | 129±10 | 129 ± 10 | 399±20 | 570 ± 46 | 894±45 | 69 ± 5 | 768± 61 |
| Ruri | 111±6 | 111±6 | 1094±55 | 1564±125 | 489±24 | 38 ± 3 | 1713±137 |
| Asego | 68 ± 8 | 68 ± 8 | 95 ± 10 | 135 ± 13 | 107±11 | 8 ± 1 | 211±19 |

The average activity concentration of $^{226}Ra$ was not significantly different as per the one-way analysis of variance (ANOVA) at $\alpha = 0.05$ level of significance between the two regions, as indicated by appendix VI. These averages were, however, higher than the world $^{226}Ra$ average (in soil) of 35 Bq/kg by about a factor of 3, with Homa having an average of 129 ± 10 Bq/kg and Ruri 111 ± 6 Bq/kg. Homa had an average activity concentration of 399 ± 20 Bq/kg for $^{232}Th$, which was approximately 60% lower than the average determined activity concentration in Ruri, probably due to the presence of monazite and

pyrochlore minerals in Ruri, which tend to harbour relatively higher thorium concentration (McCall, 1958).

Homa had an average activity concentration of 399 ± 20 Bq/kg for $^{232}$Th, which was approximately 60% lower than the average determined activity concentration in Ruri, probably due to the presence of monazite and pyrochlore minerals in Ruri, which tend to harbour relatively higher thorium concentration (McCall, 1958).

$^{232}$Th was 13 and 36 times higher than the world average of 30 Bq/kg in Homa and Ruri, respectively. On the other hand, the average activity concentration of $^{40}$K in Homa was 894 ± 45 Bq/kg which was about 40% higher than that of Ruri, attributed to the alkaline igneous rocks in Homa associated with higher potassium levels (Mayaka *et al.,* 2015). $^{40}$K was about twice the world average of 400 Bq/kg (UNSCEAR, 2000) in Homa but about 20% less than the Ruri average of 489 Bq/kg.

Figure 5.1 presents the distribution of the three natural radionuclides $^{226}$Ra, $^{232}$Th, and $^{40}$K across all the sampling points in both Homa and Ruri, with $^{226}$Ra showing the least activity concentration levels.

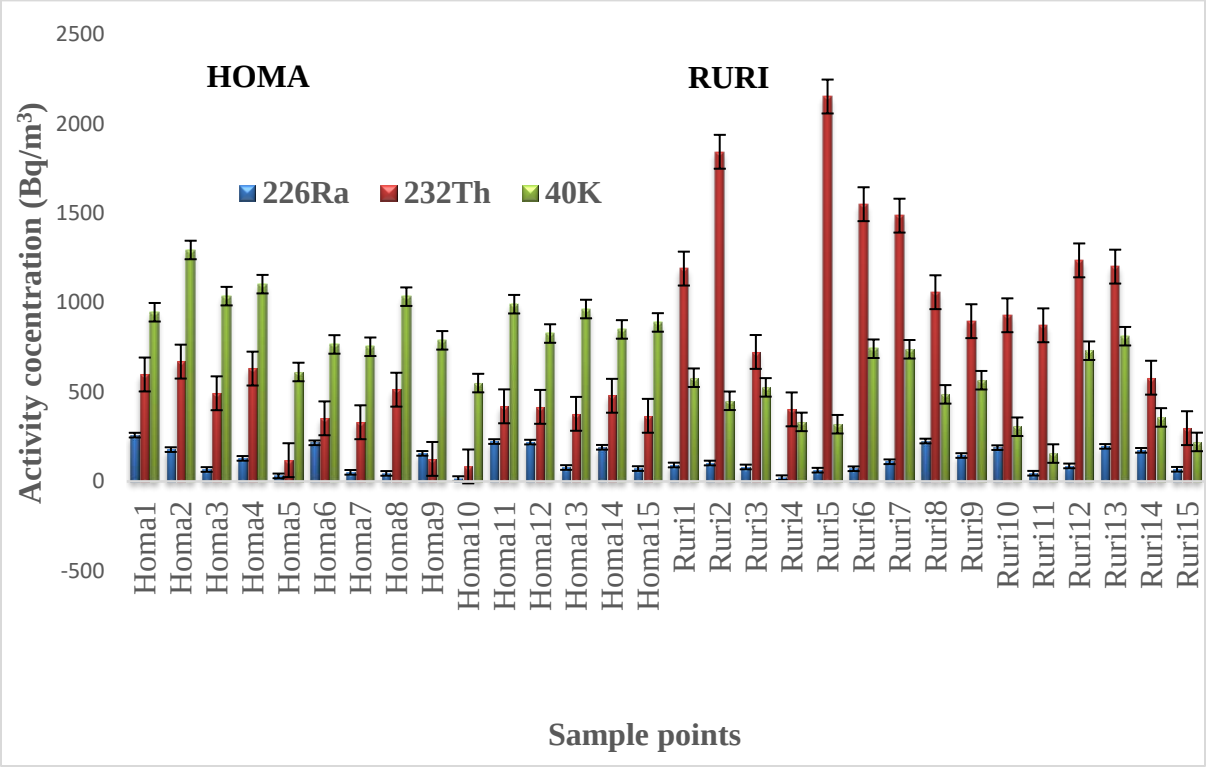


**Figure 5.1: Distribution pattern of activity concentration of the natural radionuclides $^{226}$Ra, $^{232}$Th, and $^{40}$K in both Homa and Ruri hill**

At the same time, $^{232}$Th depicted very high activity concentration levels across the sampled points. The average measured activity concentration of $^{226}$Ra in Asego was approximately half the ones obtained in both Homa and Ruri, $^{232}$Th average in Asego was about 4 and 10 times lower than the ones obtained in Homa and Ruri respectively, while $^{40}$K in Asego was 4 and 8 times lower than the average values in Homa and Ruri respectively attributed to the fact that Asego is a low radiation background area thus, its rocks does not have high concentration $^{226}$Ra, $^{232}$Th and $^{40}$K.

The results obtained in this work have been compared to the one reported in building materials in other high background radiation areas in Kenya known as Mrima hill (Chege

*et al.*, 2015). $^{40}$K was 70% and 50% higher in Homa and Ruri, respectively, compared to Mrima, which reported an activity concentration of 249 Bq/kg. Similarly, $^{226}$Ra in Mrima was 134 Bq/kg which was 5% and 20% higher than Homa and Ruri, respectively, attributed to Mrima hill's carbonatite intruded by igneous deposits with relatively higher $^{226}$Ra. On the other hand, $^{232}$Th was 60% higher in Ruri than Mrima, attributed to monazite and pyrochlore minerals in Ruri, which contain higher thorium levels. There was no significant difference in the value at Homa, which was 399 Bq/kg.

The calculated average values of radium equivalents ($Ra_{eq}$) for $^{226}$Ra, $^{232}$Th, and $^{40}$K and the total average radium equivalent in Homa and Ruri are presented in table 5.1. Figures 5.2 and 5.3 show a pie chart representing the contribution of $^{226}$Ra, $^{232}$Th and $^{40}$K to the total $Ra_{eq}$ in Ruri and Homa, respectively.

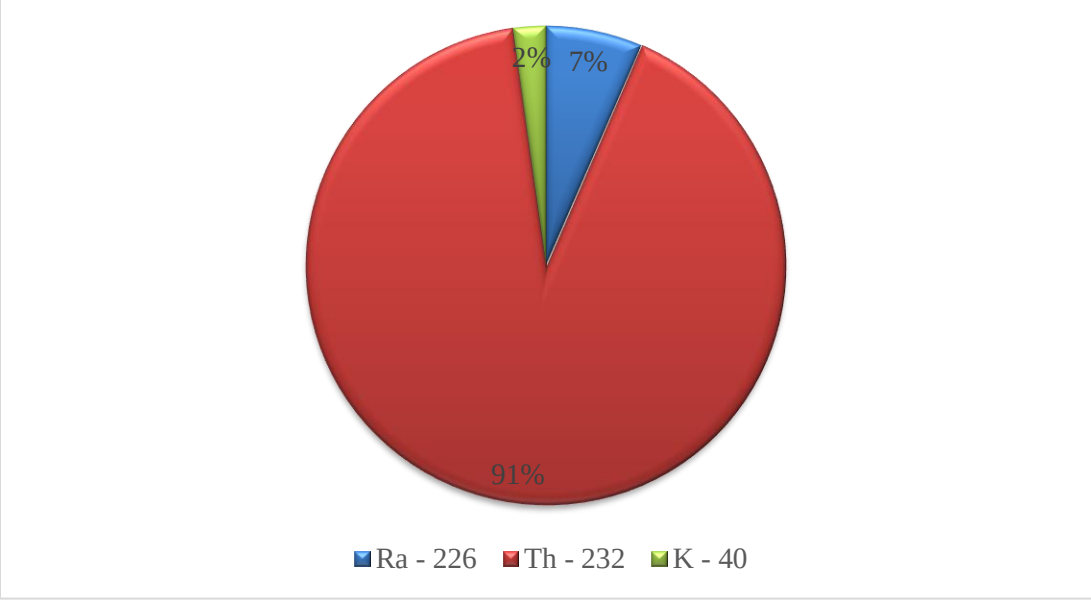


**Figure 5.2: Percentage contributions of $^{226}$Ra, $^{232}$Th, and $^{40}$K to the total $Ra_{eq}$ in the 15 samples from the Ruri as analyzed in this work**

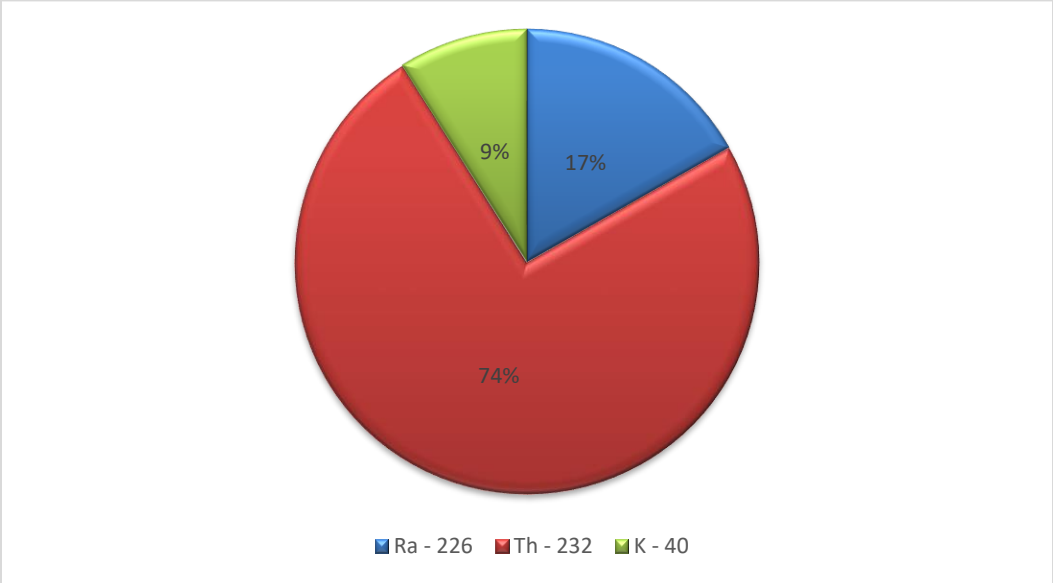


**Figure 5.3: Percentage contributions of $^{226}$Ra, $^{232}$Th, and $^{40}$K to the total $Ra_{eq}$ in the 15 samples from the Homa area analyzed in this work**

In Homa hill, $^{232}$Th contributed 74% as $^{40}$K contributed 9% to the total $Ra_{eq}$ despite $^{40}$K having the highest activity concentration, while in Ruri, $^{232}$Th contributed 91% to the total $Ra_{eq,}$ and the lowest contributor still was $^{40}$K at just 2% of the total $Ra_{eq}$. $^{232}$Th was, therefore, the highest contributor to total radium equivalent in both regions; thus, other factors held constant would be the highest contributor to radiation exposure in the study region. The calculated average total radium equivalent in Homa was 767 ± 61 Bq/kg which was just 40% of the total radium equivalent in Ruri, attributed to the high activity concentration of $^{232}$Th, which had the greatest contribution to radium equivalent in both regions.

#### 5.1.1.1 Absorbed gamma radiation dose rate (D) and Indoor Annual effective absorbed gamma dose rate (AEDR)

The absorbed gamma dose is simply the measure of deposited energy by ionizing radiation in matter per unit mass. It depends on the concentration of the terrestrial radionuclides in the building materials and the absorbing medium's density. It is measured at 1m above the ground surface, a height considered as a typical reference point for the dose to an inhabitant staying in a room. The absorbed gamma dose rate D (nGy/h) was determined using equation 5.1 (UNSCEAR, 1993), and the calculated values are summarized in table 5.2.

$$D = 0.462A_{Ra} + 0.604A_{Th} + 0.0417A_k \quad (5.1)$$

Where 0.462, 0.604, and 0.0417 $nGyh^{-1}/Bqkg^{-1}$ are dose conversion factors for $^{226}Ra$, $^{232}Th$ and $^{40}K$ respectively. $A_{Ra}$, $A_{Th}$ and $A_K$ are the activity concentrations of $^{226}Ra$, $^{232}Th$ and $^{40}K$ in Bq/kg respectively assuming a radioactive secular equilibrium condition in $^{226}Ra$ and $^{232}Th$ decay series.

The indoor annual effective absorbed dose rate, which measures the biological effect of radiation on humans inside a dwelling made of soil, was determined by equation 5.2 (UNSCEAR, 2000; Colgan *et al.*, 2008) and the statistics summarized in table 5.2.

$$AEDR = D(nGy/h) \text{ x } 8{,}760h \text{ x } O_f \text{ x } 0.7\ (Sv/Gy) \text{ x } 10^{-6} \text{ x } 1.4 \quad (5.2)$$

Where AEDR is the indoor annual effective absorbed dose rate in mSv/y, D is the absorbed dose rate in nGy/h, 8760 is time in hours for a whole normal year of 365 days, $O_f$ is the indoor occupancy factor which is 0.6 for the rural Kenya residence (Kebwaro *et al.,* 2011) and 0.7 Sv/Gy is the gamma dose conversion factor, 1.4 is a

factor that accounts for the indoor environment given that gamma dose rates indoor is about 1.4 times higher than outdoors ((UNSCEAR, 1993; Colgan *et al.*, 2008).

**Table 5.2: Statistical summary of Absorbed dose rate D (nGy/h) and Indoor annual effective dose rate AEDR (mSv/y) from the earthen building materials**

| Region | D (nGy/h) | Indoor AEDR (mSv/y) |
|---|---|---|
| **Homa** | 338 ± 30 | 1.74 ± 0.14 |
| **Ruri** | 733 ± 66 | 3.78 ± 0.30 |
| **Asego** | 108 ± 12 | 0.51 ± 0.04 |

$^{232}$Th contributed 65% and 85% to the indoor annual effective dose rates in Homa and Ruri, respectively, as $^{40}$K contributed the least to the effective dose in both regions despite having a high activity concentration as shown in figure 5.4.

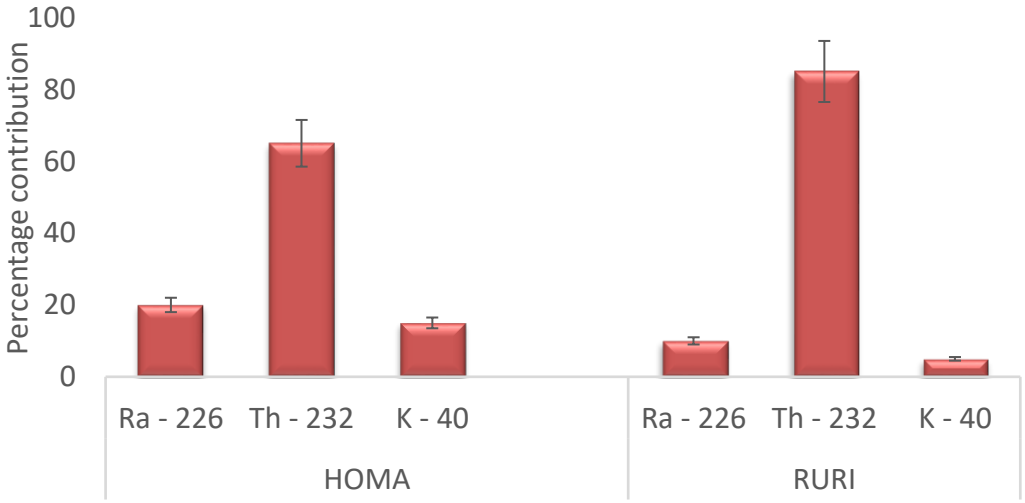


**Figure 5. 4: Percentage contribution of $^{226}$Ra, $^{232}$Th, and $^{40}$K to the indoor annual effective dose rate estimated in the samples analyzed in this work**

Approximately 80% of the sampled points in Homa had indoor AEDR above the recommended safe limit of 1 mSv/y (ICRP, 2005), while all the sampled points in Ruri were above this limit. The average annual effective dose rate in Asego was 3 and 7 times lower than the average values in Homa and Ruri, respectively, attributed to the low activity concentration of the terrestrial radionuclides $^{226}$Ra, $^{232}$Th and $^{40}$K being a low radiation background area. The comparison of the effective indoor dose in Mrima with the ones calculated in both Homa and Ruri indicates that the effective dose in Mrima, which was 1.8 mSv/y, was 8% more than Homa one but 40% less than the one of Ruri attributed to higher $^{232}$Th levels in Ruri (Chege *et al.*, 2015).

### 5.1.2 Crops (maize)

Table 5.3 summarizes the activity concentration of terrestrial radionuclides of $^{226}$Ra, $^{232}$Th and $^{40}$K (Bq/kg) as measured in maize samples from Homa and Ruri. The average $^{232}$Th levels in maize from Homa was three times lower than that from Ruri, which was attributed to the elevated $^{232}$Th levels in the soil. On the other hand, the average $^{40}$K in maize samples from Homa region was twice as higher as that from Ruri area due to the high $^{40}$K in soil.

**Table 5.3: Activity concentration of $^{226}$Ra, $^{232}$Th & $^{40}$K (Bq/kg) in maize samples measured in this work**

| Region | $^{226}$Ra (Bq/Kg) | $^{232}$Th (Bq/Kg) | $^{40}$K (Bq/Kg) |
|---|---|---|---|
| **Homa** | 53 ± 7 | 102 ± 11 | 611 ± 32 |
| **Ruri** | 46 ± 5 | 381 ± 22 | 366 ± 17 |
| **Asego** | 20 ± 2 | 15 ± 2 | 316± 14 |

### 5.1.2.1 The Daily intake of radioactive material ($D_i$), Committed Effective dose ($D_e$) and Excess lifetime cancer risk from maize intake (ELCR)

The accumulation of the radionuclides $^{226}$Ra, $^{232}$Th and $^{40}$K in the human body as a result of consumption of maize depends on the rate of its intake alongside the level concentration of the natural radionuclides in it. The daily intake of radioactivity $D_i$ (Bq per day) as a result of maize consumption by an adult human was determined using equation 5.3 (Patra *et al.*, 2013; Khandaker *et al.*, 2013).

$$D_i(\text{Bq per day}) = \sum(A_i \times C_d) \quad (5.3)$$

Where $A_i$ is the concentration of $^{226}$Ra, $^{232}$Th and $^{40}$K in the maize, $C_d$ is the average daily maize consumption grown in the region, which is an average of 0.11 kg per day from the maize grown in the studied region.

The committed effective dose from accumulating these radionuclides in the human body from maize consumption was determined using equation 5.4 (Khandaker *et al.*, 2013).

$$D_e(\text{mSv } y^{-1}) = \sum_i(D_i \times q_i \times n) \quad (5.4)$$

Where $q_i$ is the dose conversion factor which is 2.8 x $10^{-4}$, 2.3 x $10^{-4}$, and 0.062 x $10^{-4}$ mSv $Bq^{-1}$ for $^{226}$Ra, $^{232}$Th and $^{40}$K, respectively and n is the number of days in a normal year.

The excess lifetime cancer risk (ELCR) due to the consumption of maize was estimated using equation 5.5 (Patra *et al.,* 2013).

$$ELRC = D_i \times R \times L \times n \quad (5.5)$$

Where L is the Kenyan life expectancy which is averagely 66.7 years, R is the ingestion

mortality cancer risk coefficients given as $9.56 \times 10^{-9}$, $2.45 \times 10^{-9}$ and $5.89 \times 10^{-10}$ $Bq^{-1}$ for $^{226}Ra$, $^{232}Th$ and $^{40}K$ respectively and n are the number of days in a normal year (USEPA,1991).

Table 5.4 summarizes the average committed effective dose $D_e$ (mSv/y) and the total excess lifetime cancer risk (ELCR) from maize consumption.

**Table 5.4: Committed effective dose De and Total ELCR from maize samples**

| **Region** | **$D_e$ (mSv/y)** | **Total ELCR x $10^{-3}$** |
|---|---|---|
| **Homa** | 1.54 ± 0.23 | 3.1 ± 0.3 |
| **Ruri** | 4.11 ± 0.56 | 4.3 ± 0.7 |
| **Asego** | 0.28 ± 0.03 | 1.1 ± 0.3 |

The average committed effective dose in Ruri maize was twice that from Homa due to high $^{232}Th$. It was 5 and 13 times higher than the safe limit of 0.29 mSv/y (UNSCEAR, 2000) in Homa & Ruri, respectively. Total excess lifetime cancer risk was 40% higher in Ruri compared to Homa. It was also 20% and 40% higher than the safe limit of $2.5 \times 10^{-3}$ (ICRP, 1991) in Homa and Ruri respectively, as shown in figure 5.5.

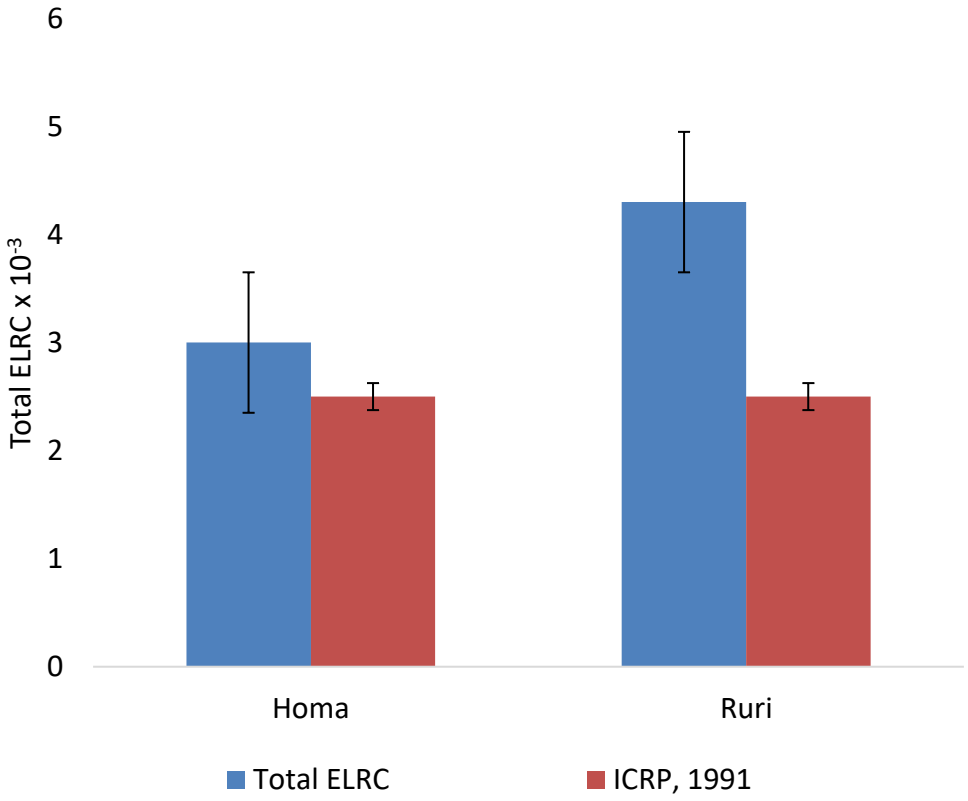


**Figure 5.5: Comparison of the total ELRC with ICRP world limit in maize samples from Homa and Ruri as analyzed in this work**

### 5.2 Modelling indoor gamma absorbed dose rate

The modelled absorbed gamma dose rate as a result of non-secular equilibrium in $^{232}$Th decay series as derived in section 3.4 combined with the correction previously derived by Orabi et al., 2019 on non-secular equilibrium in $^{226}$Ra decay series as presented by equation 5.6 in relation to the UNSCEAR, 1993 formulation was used in the determination of the modelled absorbed gamma dose rate.

$$D = 0.462A_{Ra}(1 - F_R) + 0.604\,A_{Th}(1 - F_T\frac{h}{l}) + 0.0417\,A_k \qquad (5.6)$$

Where 0.462, 0.604 and 0.0417 nGyh$^{-1}$/Bqkg$^{-1}$ are dose conversion factors for $^{226}$Ra, $^{232}$Th and $^{40}$K, respectively. $A_{Ra}$, $A_{Th}$ and $A_K$ are the activity concentrations of $^{226}$Ra, $^{232}$Th and $^{40}$K in Bq/kg respectively. $F_R$ and $F_T$ are the release factors for $^{222}$Rn and $^{220}$Rn, respectively.

$^{220}$Rn release factor $F_T$ was determined using equation 3.35 in section 3.4 by considering the $^{220}$Rn exhalation rate $E_T$ reported in section 5.3.1 and the activity concentration of $^{232}$Th as reported in section 5.1.1. $^{220}$Rn decay constant $\lambda_T$ given as 0.0125 s$^{-1}$, half thickness of the earthen building material sample h, taken as 0.015 m. The study region (Homa and Ruri) is characterized by sandy loam soil therefore, the density p is 1,440 kg/m$^{3,}$ and the $^{220}$Rn diffusion length is 0.011 m (Meisenberg *et al.,* 2011; Chege *et al.,* 2015). Table 5.5 shows the summary of the determined $^{220}$Rn release factor $F_T$ and absorbed gamma dose rate D due to the non-secular equilibrium in the $^{232}$Th decay series due to the release of $^{220}$Rn from the earthen building material. Similarly,$^{222}$Rn release factor $F_R$ was determined using equation 3.35 in section 3.4 by considering the $^{222}$Rn exhalation rate $E_R$ reported in section 5.3.1 in this work, and the activity concentration of $^{226}$Ra was also reported in section 5.1.1. $^{222}$Rn decay constant $\lambda_R$ given as 2.11 × 10$^{-6}$ s$^{-1}$.

The modelled indoor absorbed dose rate as determined with non-secular equilibrium conditions in $^{226}$Ra and $^{232}$Th decay series in Homa and Ruri is presented in table 5.5. The non-secular equilibrium in the $^{232}$Th decay series due to $^{220}$Rn release having an average reduction in the absorbed gamma dose rate of about 15% in both regions.

**Table 5.5: Summary of $^{222}$Rn and $^{220}$Rn release factors, the resulting modelled, and net absorbed gamma dose rate from the earthen building materials**

| Region | $^{222}$Rn Release factor ($F_R$) | $^{220}$Rn Release factor ($F_T$) | Modelled D (nGy/h) | Net Measured D (nGy/h) |
|---|---|---|---|---|
| Home | 0.16 ± 0.02 | 0.15 ± 0.02 | 274 ± 13 | 300 ± 14 |
| Ruri | 0.17 ± 0.02 | 0.08 ± 0.01 | 658 ± 30 | 704 ± 35 |
| Asego | 0.08 ± 0.01 | 0.06 ± 0.01 | 97 ± 4 | 101 ± 5 |

The gamma absorbed dose rate was less reduced in dwellings with the high indoor concentration of the $^{222}$Rn and $^{220}$Rn, as observed in Homa, which had a lower concentration of the radon isotopes. This is attributed to the fact that part of the radon isotopes that do not get out of the house through ventilation emit gamma radiation alongside their decay series inside the house, adding to the ones emitted from the wall.

A validation measurement carried out by the portable survey meters gave an average of 358 nGy/h and 756 nGy/h in Homa and Ruri, respectively. These directly measured values were higher than the modelled and experimental results attributed to the contribution of absorbed dose rate from the cosmic rays in the two hills.

The absorbed dose rate from cosmic rays $E_z$ (nGy/h) depends on the altitude as given by equation 5.7 (UNSCEAR, 2000)

$$D_z = D_o(0.21e^{-1.649z} + 0.79e^{0.4528z}) \quad (5.7)$$

Where $D_o$ is the absorbed dose rate at sea level given as 32 nGy/h and z is the altitude in kilometers. Homa is at an average altitude of 1,751 m, while Ruri is at an average altitude

of 1,545 m above sea level. Using equation 5.7, the absorbed dose rate from the cosmic rays averagely becomes 55 nGy/h and 52 nGy/h in Homa and Ruri, respectively. Subtracting these values from the directly measured absorbed dose rate results in net absorbed dose rate values below the experimental ones averagely as 300 nGy/h and 704 nGy/h in Homa and Ruri, respectively, as listed in Table 5.5. The comparison between the modelled, experimental, and net measured results is as plotted in figure 5.6. and they indicate a strong agreement that supports the fact that the release of $^{220}$Rn affects the absorbed gamma dose rate.

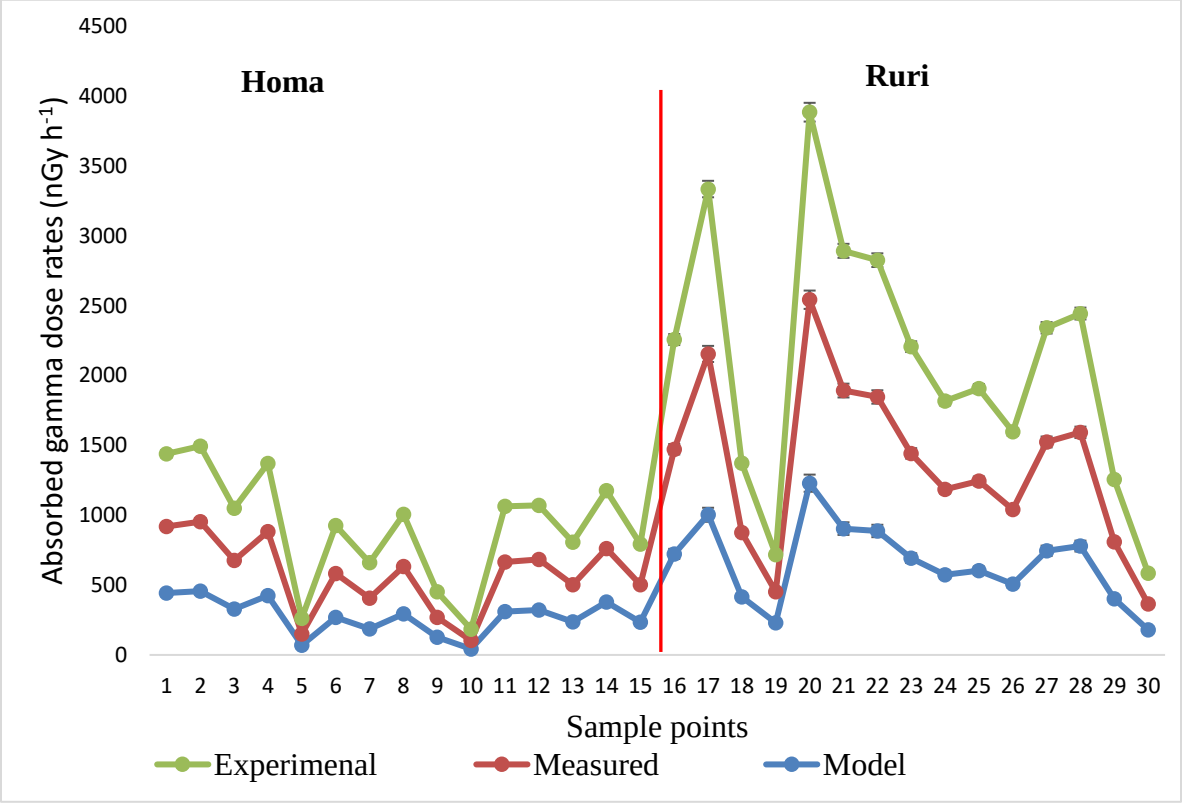


**Figure 5.6: Comparison between the modeled, experimental, and measured absorbed dose in dwellings of Homa and Ruri**

The reduction in absorbed gamma dose rate in this research work is comparable to the study by Orabi, 2017, which reported a reduction in the absorbed gamma dose due to the correction of $^{226}$Ra non-secular equilibrium condition as a result of $^{222}$Rn release exceeding 25% of the uncorrected one. De Jong et al. 2008 model reported a corrected non-equilibrium in the $^{226}$Ra decay series reduced the absorbed gamma dose rate by an average of 4% on all considered materials, with gypsum recording the highest reduction of 9%. These results are also in good agreement with Stranden, 1979 studies which assessed that a strong radon isotope emanation could cause an overestimation of the absorbed gamma dose of up to 20%.

### 5.3 Radon ($^{222}$Rn) and Thoron ($^{220}$Rn) measurements

#### 5.3.1 $^{222}$Rn and $^{220}$Rn exhalation rate

Table 5.6 summarizes the surface exhalation rates of $^{222}$Rn and $^{220}$Rn from the samples in Homa and Ruri, respectively.

**Table 5.6: Statistical summary of $^{222}$Rn (mBq/m$^2$/s) and $^{220}$Rn (Bq/m$^2$/s) surface exhalation rate from the earthen building materials**

| Region | Surface exhalation rate | | | | | |
|---|---|---|---|---|---|---|
| | $^{222}$Rn (mBq/m$^2$/s) | | | $^{220}$Rn (Bqm$^2$/s) | | |
| | Minimum | Maximum | Average | Minimum | Maximum | Average |
| **Homa** | 0.2 ± 0.1 | 1.9 ± 0.3 | 1 ± 0.1 | 3 ± 1 | 35 ± 5 | 18 ± 2 |
| **Ruri** | 0.2 ± 0.1 | 1.5 ± 0.2 | 0.9 ± 0.1 | 5 ± 1 | 43 ± 6 | 25 ± 3 |
| **Asego** | 0.1 ± 0.0 | 1.2 ± 0.2 | 0.5 ± 0.1 | 1 ± 0.5 | 8 ± 2 | 4 ± 1 |

The average value of $^{220}Rn$ was approximately $10^4$ times more than $^{222}Rn$. This was attributed to a higher parent radionuclide activity concentration of $^{232}Th$ compared to $^{226}Ra$ as measured in this work average as 399 Bq/kg for $^{232}Th$ and 129 Bq/kg for $^{226}Ra$. Similarly, for Ruri, the measured activity concentration in this work was 1094 Bq/kg for $^{232}Th$ and 111 Bq/kg for $^{226}Ra$, in addition to the fact that $^{220}Rn$ generally has a higher decay rate compared to $^{222}Rn$.

$^{222}Rn$ was 26 times lower than the world average of 26.2 $mBq/m^2/s$, which is attributed to a low concentration of $^{226}Ra$ and high ventilation rate of the dwellings in the study region coupled with the longer diffusion length of $^{222}Rn$. $^{220}Rn$ was 21 times higher than the world average of 1 $Bq/m^2/s$ (UNSCEAR, 2008), attributed to the high measured concentration of $^{232}Th$ on the study region and the many cracks on the earthen wall and floor studied. Figure 5.7 shows a comparative bar graph representing the average surface exhalation rates in Homa and Ruri hill for both $^{222}Rn$ and $^{220}Rn$.

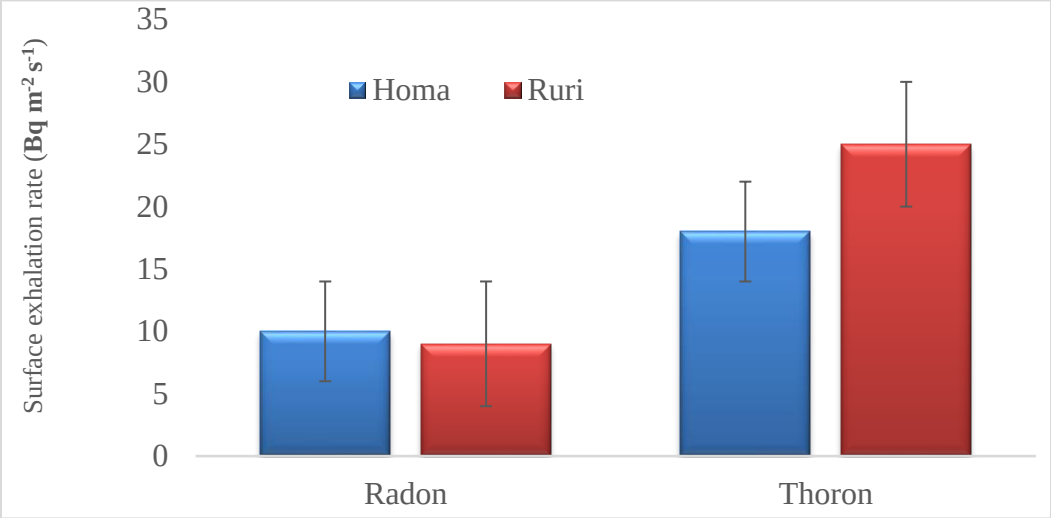


**Figure 5.7: Comparative bar graph of the average surface exhalation rates in Homa and Ruri hills for $^{222}$Rn and $^{220}$Rn**

The exhalation rate of $^{220}$Rn was 38% higher in Ruri compared to Homa hill, attributed to a nearly 70% higher concentration of mother radionuclide $^{232}$Th in Ruri as measured in this work. On the other hand, the exhalation rate of $^{222}$Rn in Homa hill was 8% higher than Ruri, which is again attributed to the nearly 14% higher concentration of $^{226}$Ra in Homa based on the measured activity concentration in this work.

### 5.3.2 Indoor concentration of $^{222}$Rn, $^{220}$Rn and $^{220}$Rn progeny

Table 5.7 presents the statistical summary of measured values of indoor $^{222}$Rn, $^{220}$Rn and $^{220}$Rn progeny concentration in the dwellings sampled from Homa, Ruri and Asego hill, which was used as a control. The determined average concentration $^{222}$Rn in Homa was about 20% higher than Ruri, attributed to the 8% higher $^{226}$Ra activity concentration and $^{222}$Rn exhalation rate in Homa as determined in this work. However, the average concentration of $^{220}$Rn was approximately 45% higher in Ruri than in Homa, attributed to

the 60% higher activity concentration of $^{232}$Th and $^{220}$Rn exhalation rate in Ruri, as determined in this work.

The measured average concentration of $^{222}$Rn was 36 ± 9 Bq/m$^3$ and 30 ± 7 Bq/m$^3$ for Homa and Ruri, respectively, all of which were below the (WHO, 2009) indoor reference level of 100 Bq/m$^3$.

This is attributed to the low activity concentration of $^{226}$Ra as well as the very low surface exhalation rate of $^{222}$Rn determined in this research work. The $^{222}$Rn concentration indoors is also greatly affected by its emanation as well as environmental factors such as humidity, temperature, the inflow of soil gas, and ventilation of the house (Ramola *et al.*, 2016).

**Table 5.7: Statistical summary of concentration of $^{222}$Rn, $^{220}$Rn (Bq/m$^3$) and $^{220}$Rn progeny (Bq/m$^3$) in sampled dwellings**

| Region | | Dry period | | Rainy period | | |
|---|---|---|---|---|---|---|
| | | $^{222}$Rn (Bq/m$^3$) | $^{220}$Rn (Bq/m$^3$) | $^{222}$Rn (Bq/m$^3$) | $^{220}$Rn (Bq/m$^3$) | EETC (Bq/m$^3$) |
| **Homa** | Minimum | 12±5 | 110±45 | 21±9 | 104±23 | 2.9±0.6 |
| | Maximum | 73±13 | 976±45 | 89±17 | 1359±61 | 50.5±8.1 |
| | Average | 36±9 | 372±28 | 44±7 | 412±31 | 21.5±2.2 |
| **Ruri** | Minimum | LOD | 211±21 | LOD | 261±18 | 12.6±1.6 |
| | Maximum | 59±12 | 2513±123 | 66±11 | 1550±51 | 86.2±9.9 |
| | Average | 30±7 | 579±39 | 35±6 | 635±32 | 33.6±5.4 |
| **Asego** | Minimum | LOD | LOD | LOD | 33±16 | 0.4±0.1 |
| | Maximum | 54±6 | 138±14 | 51±12 | 216±24 | 18.6±3.2 |
| | Average | 20±4 | 84±17 | 26±5 | 93±11 | 10.7±1.1 |

**LOD** is the limit of detection $^{222}$Rn = 6 Bq/m$^3$,$^{220}$Rn = 21 Bq/m$^3$ and EETC = 0.005 Bq/m$^3$.

Homa and Ruri are both closer to Lake Victoria; therefore, they experience a humid breeze from the lake. This greatly reduces the concentration of $^{222}$Rn indoors alongside the well-ventilated type of houses that aids the free air circulation indoors; therefore, $^{222}$Rn may not easily build up indoors due to its relatively long half-life of 3.8 days compared to $^{220}$Rn [55.6s] (Frutos-Puerto *et al.*, 2020).

The concentration of $^{220}$Rn was 4 and 6 times higher than the WHO $^{222}$Rn reference level of 100 Bq $m^{-3}$ in Homa and Ruri, respectively. This was attributed to highly porous earthen walls, higher $^{232}$Th activity concentration and very high $^{220}$Rn surface exhalation rate as measured in this work. Therefore, $^{220}$Rn is the major source of indoor radioactivity from the two sampled regions, as was already observed by the higher activity concentration of its parent radionuclide $^{232}$Th as measured in this work.

The determined average indoor concentration of $^{220}$Rn in Asego was 84 ± 17 Bq/$m^{3,}$ four times higher than that of $^{222}$Rn, but both were lower than the WHO $^{222}$Rn reference level of 100 Bq/$m^3$ (WHO, 2009). The average measured concentration of $^{220}$Rn in Asego was 5 and 7 times lower than the average values in Homa and Ruri, respectively. The average determined value of $^{222}$Rn in Asego was about 35% and 45% lower than those of Homa and Ruri, respectively. This was attributed to the fact that Asego is not a high-radiation background area. Therefore, it does not have a high concentration of the parent radionuclides $^{226}$Ra and $^{232}$Th for $^{222}$Rn and $^{220}$Rn respectively.

Figures 5.8 and 5.9 represents the frequency distribution of the determined concentration of $^{222}$Rn and $^{220}$Rn (Bq/$m^3$), respectively, in all the thirty sampled houses in Homa and Ruri. Both of which were skewed to the left. 80% of the sampled houses had a $^{222}$Rn

concentration of less than 50 Bq/$m^{3,}$ even though all were below the safe WHO reference level of 100 Bq/$m^3$.

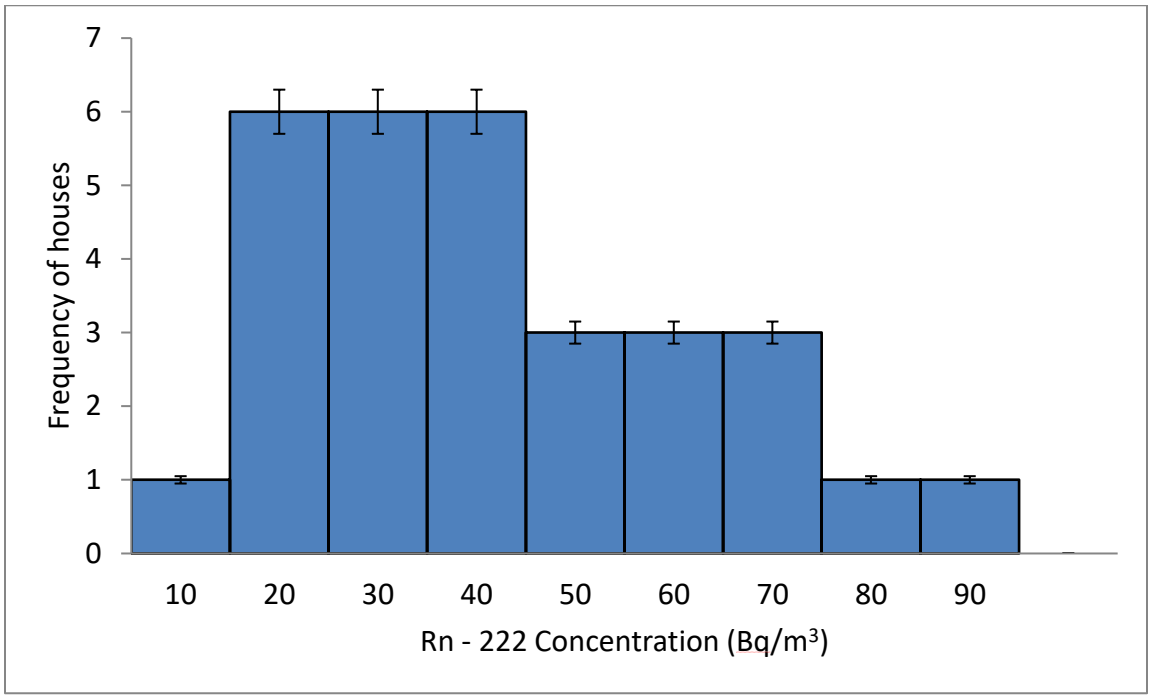

**Figure 5.8: The frequency distribution of concentration of $^{222}$Rn (Bq/m$^3$) from the study samples**

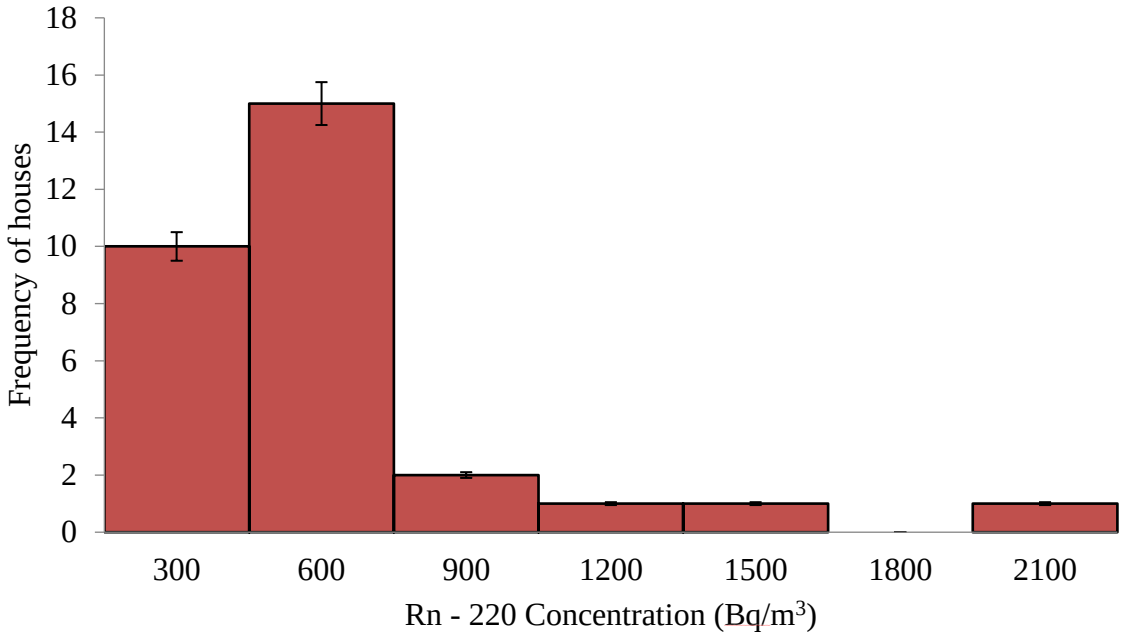


**Figure 5.9: The frequency distribution of concentration of $^{220}$Rn (Bq/m$^3$) from the study samples**

The observed variation from one sample point to the other was attributed to variation in the parent radionuclide activity concentration of $^{232}$Th ($^{220}$Rn) and $^{226}$Ra ($^{222}$Rn), ventilation of the house, exhalation rate of $^{222}$Rn and $^{220}$Rn, porosity, the side of the hill and density of soil making up the wall all of which affects the indoor concentration of $^{222}$Rn and $^{220}$Rn (Ramola *et al.*, 2016).

The average $^{220}$Rn progeny concentration (EETC) in Ruri was 55% higher than in Homa, which was attributed to a higher $^{232}$Th concentration in the building materials. The frequency distribution plot of $^{220}$Rn progeny is shown in figure 5.10, skewed to the left and below $^{222}$Rn WHO, 2009 reference level of 100 Bq/m$^3$ in all the sampled houses.

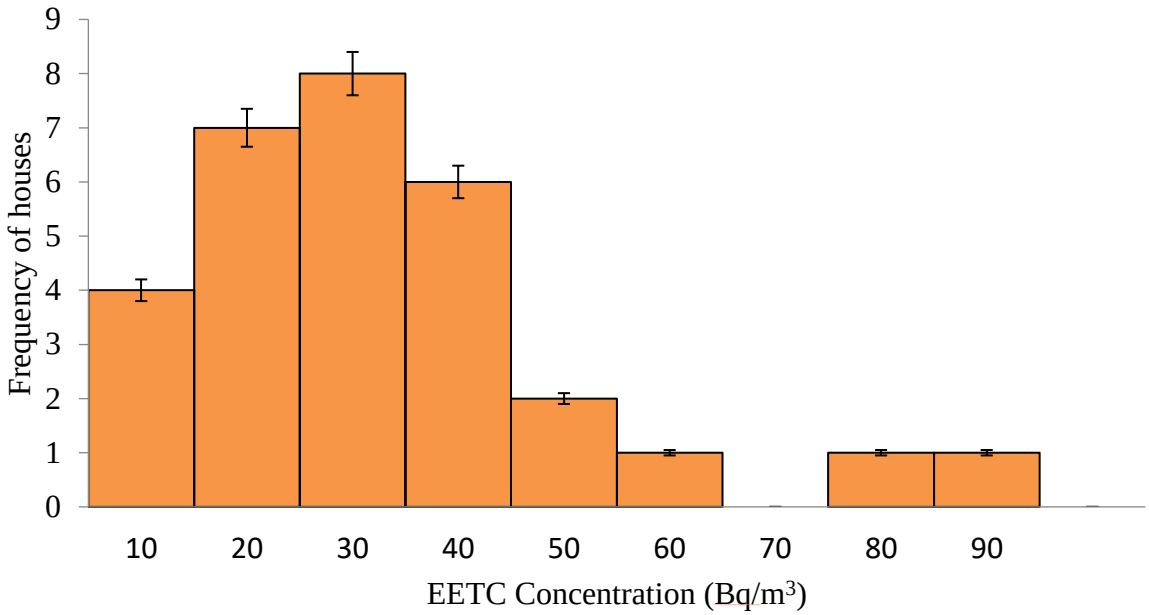


**Figure 5.10: The frequency distribution of concentration of EETC (Bq/m$^3$) from the study samples**

There was no correlation between the concentration of $^{222}$Rn with that of $^{220}$Rn, as shown in figure 5.11 attributed to the fact that $^{222}$Rn concentration indoors is affected by environmental factors such as humidity, temperature, and ventilation of the house (Ramola *et al.,* 2016) all of which were varied in Homa and Ruri.

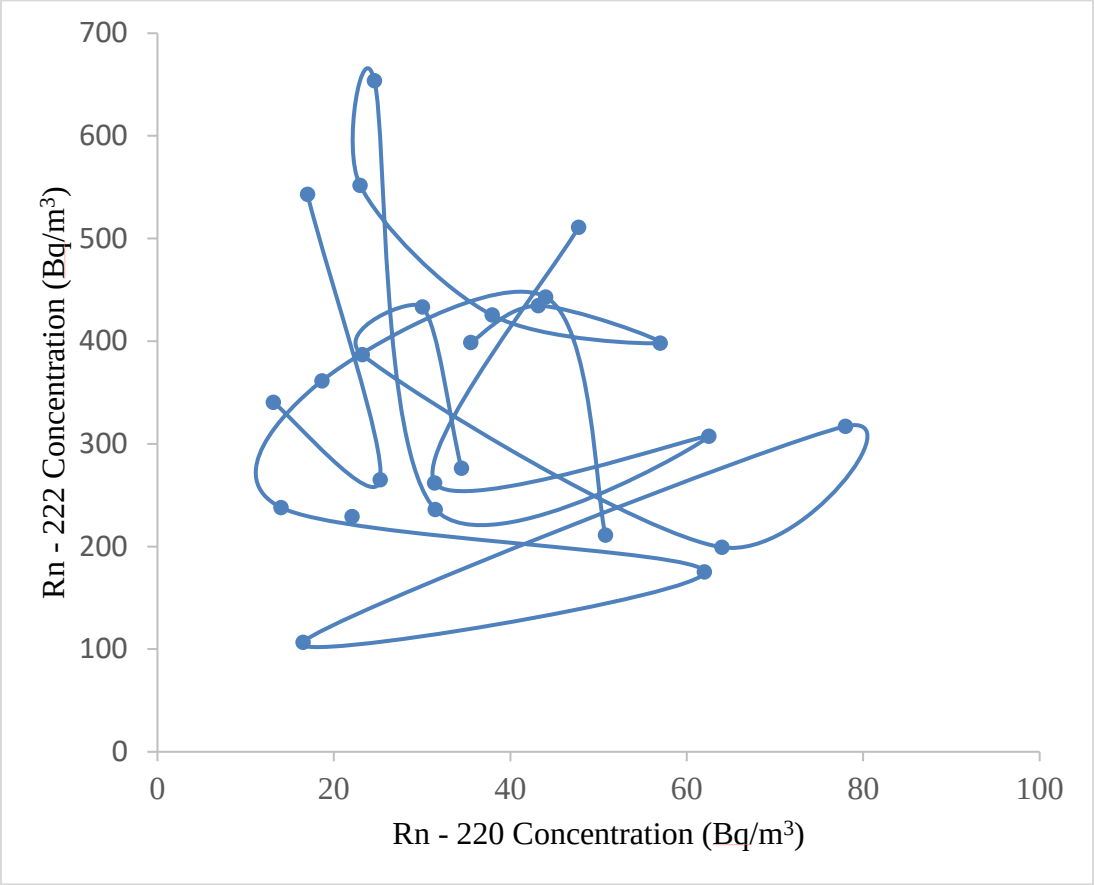


**Figure 5.11: Relation plots between $^{222}$Rn and $^{220}$Rn (Bq/m$^3$) in the study area**

The proximity of Lake Victoria to the two hills exposes them to the humid breeze from the lake, which greatly reduces the concentration of $^{222}$Rn indoors without necessarily affecting that of $^{220}$Rn. In addition to that, the houses in the two regions were well-ventilated using the gap between the wall and the roof *(reru)*, which enabled free air circulation indoors, limiting $^{222}$Rn from easily building up indoors due to its relatively longer half-life [3.8 days] compared to $^{220}$Rn [55.6s] (Frutos-Puerto *et al.*, 2020). There was a low correlation between $^{220}$Rn and its progeny EETC as shown in figure 5.12 this was attributed to the non-uniform distribution of indoor $^{220}$Rn.

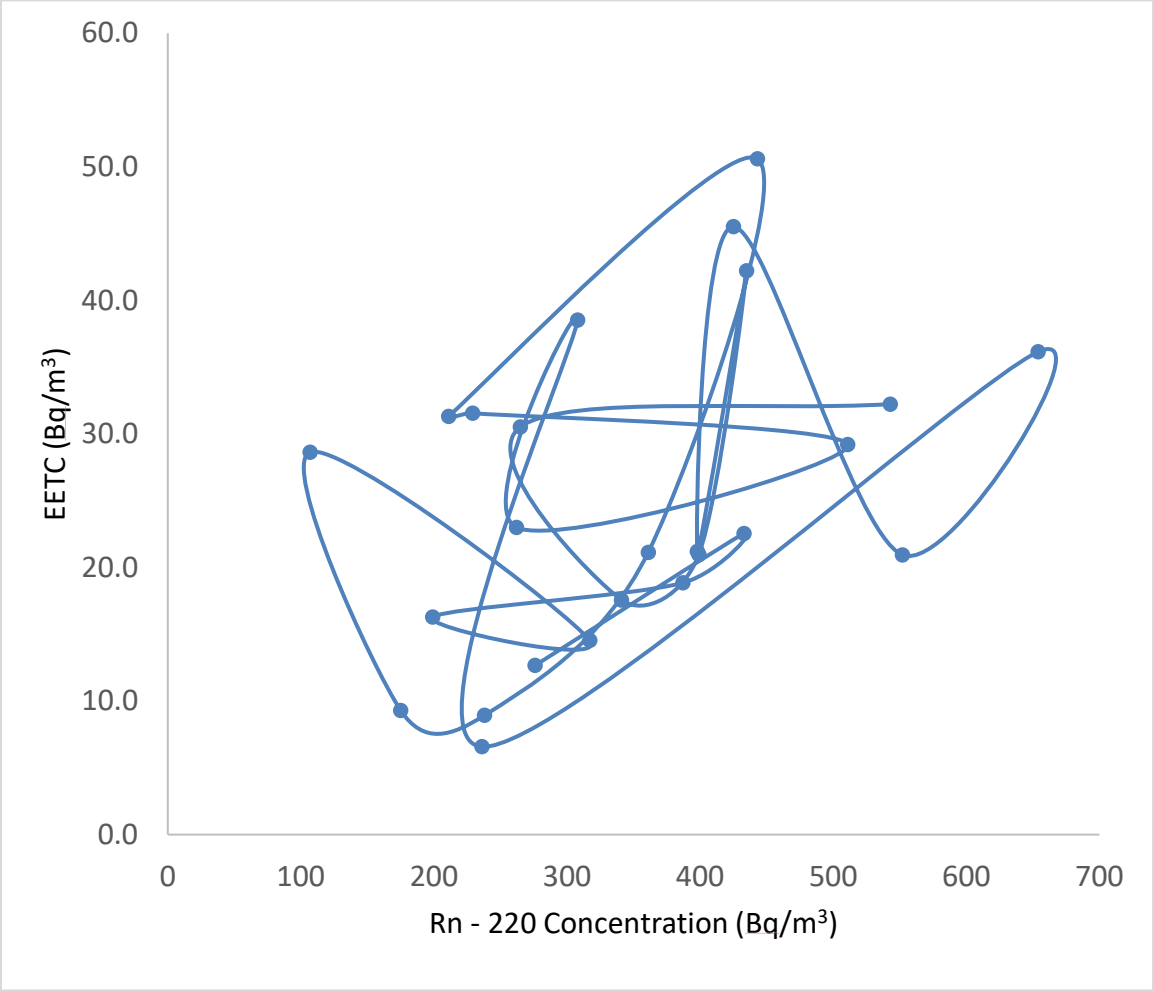


**Figure 5.12: Relation plots between $^{220}$Rn and EETC (Bq/m$^3$)**

The determined indoor concentration of $^{222}$Rn and $^{220}$Rn were 20% and 10% higher during the rainy season than in the dry season, as shown in figure 5.13. This was attributed to the low ventilation rate during the rainy season, as doors remain closed when it is raining, and the low air exchange rate with the outside of the house.

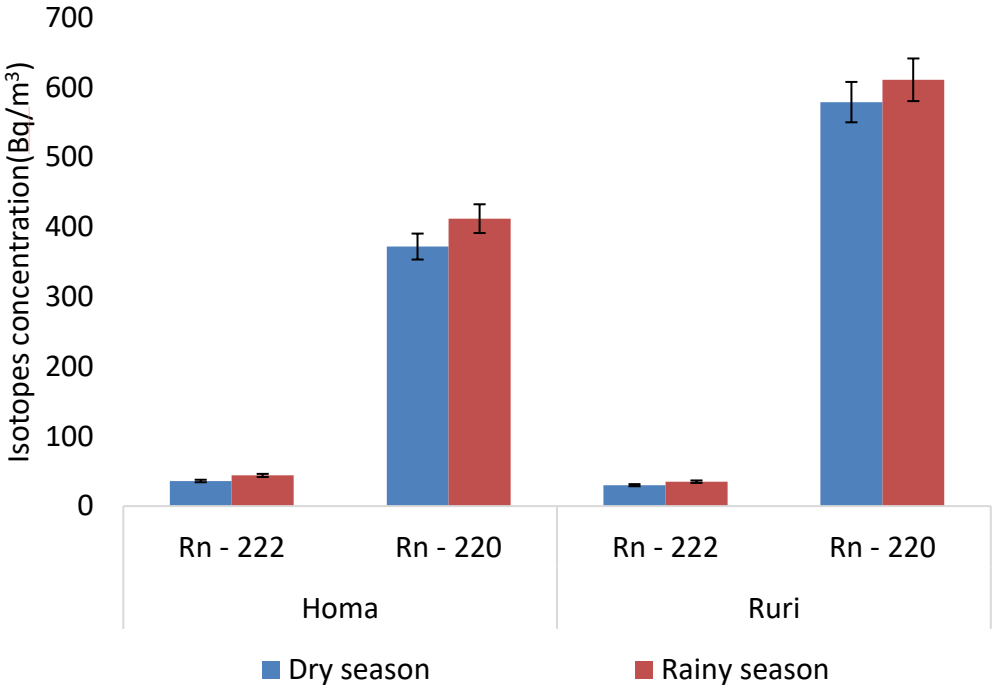


**Figure 5.13: Seasonal comparison of the concentration of $^{222}$Rn and $^{220}$Rn (Bq/m$^3$)**

Secondly, during the rainy season, water gets to the earthen walls making them moist; this increases the radon emanation rate, which linearly depends on increases in moisture content to a maximum of 60% (Cozmuta *et al.*, 2003). Lastly, there are low outdoor and high indoor temperatures during the rainy season, as the doors are closed when it rains. Air flows from outside towards the house, which reduces the outward air flow, thus less radon and lower radon outflow.

The Shapiro-Wilk test showed $^{222}$Rn (W = 0.802) and $^{220}$Rn (0.591) hence not normally distributed. In addition to that, the Kruskal Wallis test was used to test data in the two seasons at 0.05 level of significance, 1 degree of freedom & critical chi-square value of

3.841, H statistic was $^{222}$Rn (H = 1.764) and $^{220}$Rn (H = 0.8688) thus no significant difference in data of the two seasons. This could be attributed to the fact that there were no extreme weather changes during the seasons.

#### 5.3.2.1 Annual Effective Dose due to indoor $^{222}$Rn ($E_R$) and $^{220}$Rn ($E_T$)

$^{220}$Rn concentration inside a room is not uniformly distributed as it varies widely within a space and exponentially decreases with the distance from its source due to its very short half-life of (55.6 s) as opposed to $^{222}$Rn, which is evenly distributed in space. Therefore, $^{220}$Rn concentration in space is not used for effective dose assessment. Still, its progenies concentrations which are evenly distributed in space, are used as a combination expressed in Equivalent Equilibrium Thoron Progeny Concentration (EETC) as measured in this study (De With *et al.,* 2018). The annual effective dose as a result of inhalation of $^{222}$Rn ($E_R$) and $^{220}$Rn ($E_T$) was determined using equations 5.8 and 5.9, respectively (Tokonami, 2005).

$$E_R(mSv\ y^{-1}) = C_{Rn} \text{ x } F_R \text{ x } Q_i \text{ x } O_f \text{ x } t \quad (5.8)$$

$$E_T(mSv\ y^{-1}) = EETC \text{ x } Q_i \text{ x } O_f \text{ x } t \quad (5.9)$$

Where $C_{Rn}$ is the concentration of $^{222}$Rn in the dwellings in Bq m$^{-3}$, $F_R$ is the equivalent factor for $^{222}$Rn, which is 0.4, $Q_i$ is the dose conversion factor for isotope i (i is $^{222}$Rn, $^{220}$Rn) which is 9 and 40 nSv (Bq/m$^3$/h)$^{-1}$ for $^{222}$Rn and $^{220}$Rn respectively, $O_f$ is the indoor occupancy factor which is 0.6 for rural Kenya because rural Kenyans spend more time outdoors in their farms or fishing in the lake (Kebwaro *et al.,* 2011) and t is the time in hours for the whole normal year which is 8,760 h. EETC is the equilibrium equivalent of thoron concentration.

The inhaled annual effective dose resulting from the inhalation of the gases in the sampled dwellings was summarized in table 5.8. The average determined effective dose of $^{222}Rn$ ($E_R$) was three times lower WHO minimum action level of 3 mSv $y^{-1}$ (WHO, 2009), attributed to high ventilation rate in both studied regions.

**Table 5.8: Annual inhaled effective dose rate as a result of $^{222}Rn$ ($E_R$) and $^{220}Rn$ progeny ($E_T$) (mSv/y)**

| Region | | $E_R$ (mSv/y) | $E_T$ (mS/y) |
|---|---|---|---|
| **Homa** | Minimum | 0.4±0.1 | 0.5±0.1 |
| | Maximum | 1.7±0.4 | 6.4±1.1 |
| | Average | 0.8±0.2 | 2.7±0.5 |
| **Ruri** | Minimum | 0 | 1.6±0.3 |
| | Maximum | 1.2±0.3 | 11±2 |
| | Average | 0.7±0.1 | 4.2±0.6 |
| **Asego** | Minimum | 0 | 0.1±0 |
| | Maximum | 1±0.2 | 2.3±0.4 |
| | Average | 0.5±0.1 | 1.4±0.3 |

On the other hand, the average determined effective dose from $^{220}Rn$ progeny ($E_T$) in Ruri was 40% above the WHO, $^{222}Rn$ action level of 3 mSv/y due to high $^{232}Th$ levels, the average effective dose from Homa was 10% below this level. The average total annual inhaled effective dose due to both $^{222}Rn$ and $^{220}Rn$ progeny ($E_R$ and $E_T$) in Ruri was 40%

higher than in Homa. These values were 16% and 30% higher than $^{222}$Rn WHO action level of 3 mSv/y in Homa & Ruri. From these results, $^{220}$Rn progeny contributed 90% to the total annual inhaled effective dose attributed to high $^{232}$Th. $^{220}$Rn major contributor to inhaled radiation exposure similar to Mrima (HBRA) in Kenya, as shown in figure 5.14.

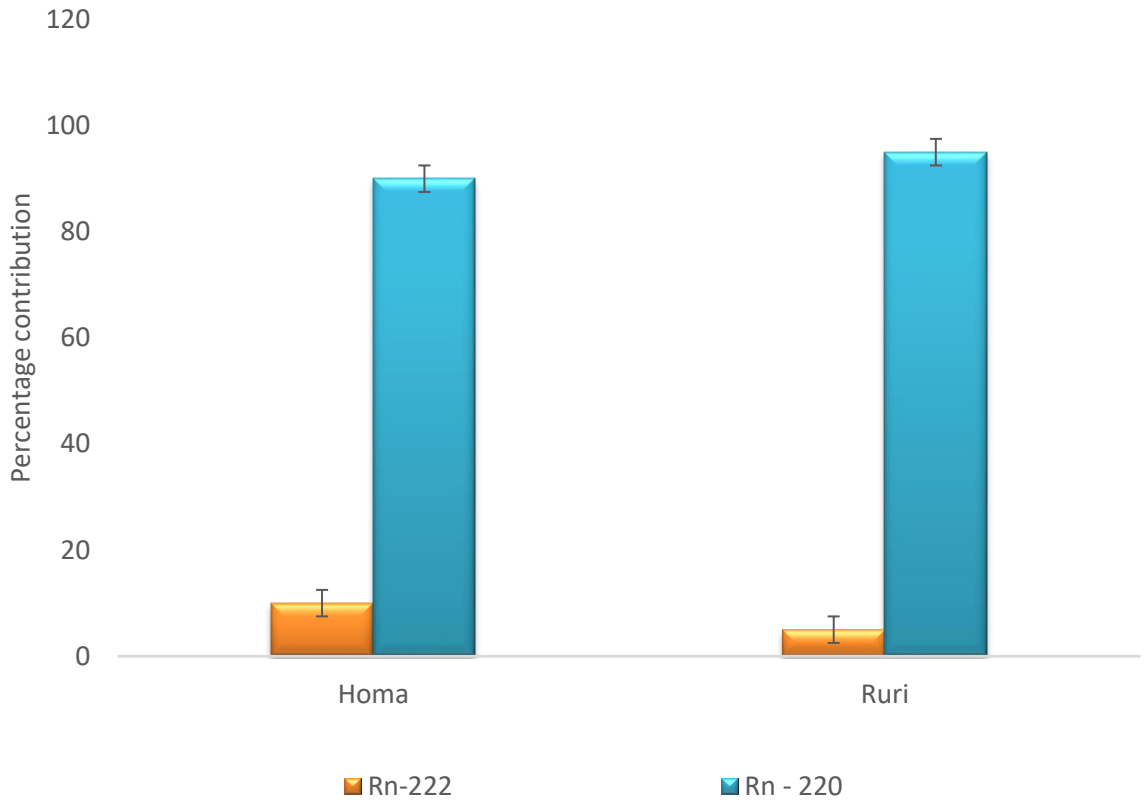


**Figure 5.14: Contribution of $^{222}$Rn and $^{220}$Rn to total annual inhaled effective dose**

Results obtained in this work for the indoor concentration of $^{222}$Rn, $^{220}$Rn and $^{220}$Rn progeny have been compared with other parts of the world, as summarized in table 5.9 (Yamada *et al.*, 2006; Chege *et al.*, 2015; Omori *et al.*, 2016; Nyambura *et al.*, 2019).

**Table 5.9: Comparison of the concentration of $^{222}$Rn (Bq/m$^3$), $^{220}$Rn (Bq/m$^3$), EETC (Bq/m$^3$) and total annual effective dose rate (mSv/y) in these work and other regions**

| Region | Country | $^{222}$Rn | $^{220}$Rn | EETC | Total effective dose | Reference |
|---|---|---|---|---|---|---|
| Homa | Kenya | 40 | 392 | 20 | 3.5 | This work |
| Ruri | Kenya | 33 | 595 | 33 | 4.9 | This work |
| Mrima | Kenya | 35 | 652 | - | 14 | Chege *et al.*, 2015 |
| Kilimambogo | Kenya | 67 | 195 | 12 | 3.7 | Nyambura *et al.*, 2019 |
| Gansu caves | China | 91 | 351 | | 12.1 | Yamada *et al.*, 2006 |
| Kerala | India | 5 | 2.15 | | 0.54 | Omori *et al.*, 2016 |

The indoor concentration $^{222}$Rn in Mrima hill which is an HBRA in Kenya was nearly the same with those of Homa and Ruri. However, $^{220}$Rn indoor concentration was approximately 40% and 10% higher than Ruri and Homa, respectively, attributed to their *ongoro* smeared walls and highly ventilated houses. The studies in Mrima also reported $^{220}$Rn as the major contributor to the inhaled annual effective dose rate, just as in the case of Homa and Ruri. Kilimambogo in central Kenya which is not an HBRA had the average indoor concentration of $^{220}$Rn two and three times lower than Homa and Ruri respectively.

### 5.3.3 $^{222}$Rn in Lake Victoria water

Table 5.10 summarizes the concentration of $^{222}$Rn in Lake Victoria water from Homa, Ruri and Asego sampling regions at the three different sampling depths of 0.1 m, 5 m and 10 m below the water surface.

**Table 5.10: Summary of concentration of $^{222}$Rn in Lake Victoria around Homa, Ruri, and Asego at depths of the water temperature and pH**

| Depth | | | Home | Ruri | Asego |
|---|---|---|---|---|---|
| **0.1 m** | $^{222}$Rn concentration (Bq/L) | Minimum | 8.9±1.3 | 9.4±1.4 | 6.7±1.0 |
| | | Maximum | 23.4±3.9 | 17.8±3.0 | 21.6±3.6 |
| | | Average | 14.8±1.9 | 12.9±1.6 | 13.2±1.7 |
| | Temperature ($^{o}$C) | | 25.3±1.1 | 26.1±1.5 | 26.9±1.6 |
| | Ph | | 8.0±0.5 | 7.7±0.3 | 7.9±0.3 |
| **5 m** | $^{222}$Rn concentration (Bq/L) | Minimum | 18.5±2.7 | 15.6±2.3 | 11.3±1.6 |
| | | Maximum | 36.1±6.1 | 28.3±4.8 | 29.6±5.0 |
| | | Average | 25.9±3.3 | 21.1±2.7 | 22.1±2.8 |
| | Temperature ($^{o}$C) | | 24.5±1.0 | 25.4±1.3 | 26.0±1.4 |
| | pH | | 8.1±0.5 | 7.9±0.3 | 8.0±0.4 |
| **10 m** | $^{222}$Rn concentration (Bq/L) | Minimum | 16.2±2.4 | 13.4±2.0 | 9.5±1.4 |
| | | Maximum | 29.4±4.9 | 22.8±3.8 | 26.7±4.5 |
| | | Average | 21.8±2.8 | 17.7±2.3 | 18.6±2.4 |
| | Temperature ($^{o}$C) | | 24.1±1.0 | 24.9±1.3 | 7.8±0.4 |
| | pH | | 8.3±0.6 | 25.5±1.4 | 8.2±0.5 |

The average $^{222}$Rn concentration in the Lake Victoria shoreline of Homa hill was about 10% higher than that at Ruri, which was 12.9 ± 1.6 Bq/L attributed to the difference in rock matrix in Homa carbonatites rocks with slightly higher $^{226}$Ra content (Le Bas, 1977) compared to the ones of Ruri which has more Monazite associated with higher $^{232}$Th (McCall, 1958).

The average $^{222}$Rn concentration in water at a depth of 5 m was approximately 15% higher than at a depth of 10 m across all the sampled regions. This was attributed to the fact that different water depth columns induce a significant change in $^{222}$Rn concentrations inside a water body; the 10 m water column exerts more pressure on the lake floor, reducing the rate of radon emanation recoiling into the lake waters (Kies *et al.,* 2002). Secondly, the change in the rock matrix containing the radium which reduces as one moves further away from the hills into the lake floor. At a depth of 0.1 m (lake surface), the average $^{222}$Rn concentration in water was approximately 40% and 30% lower than the ones at depths of 5 m and 10 m, respectively, across all three sampled regions, as illustrated in figure 5.15.

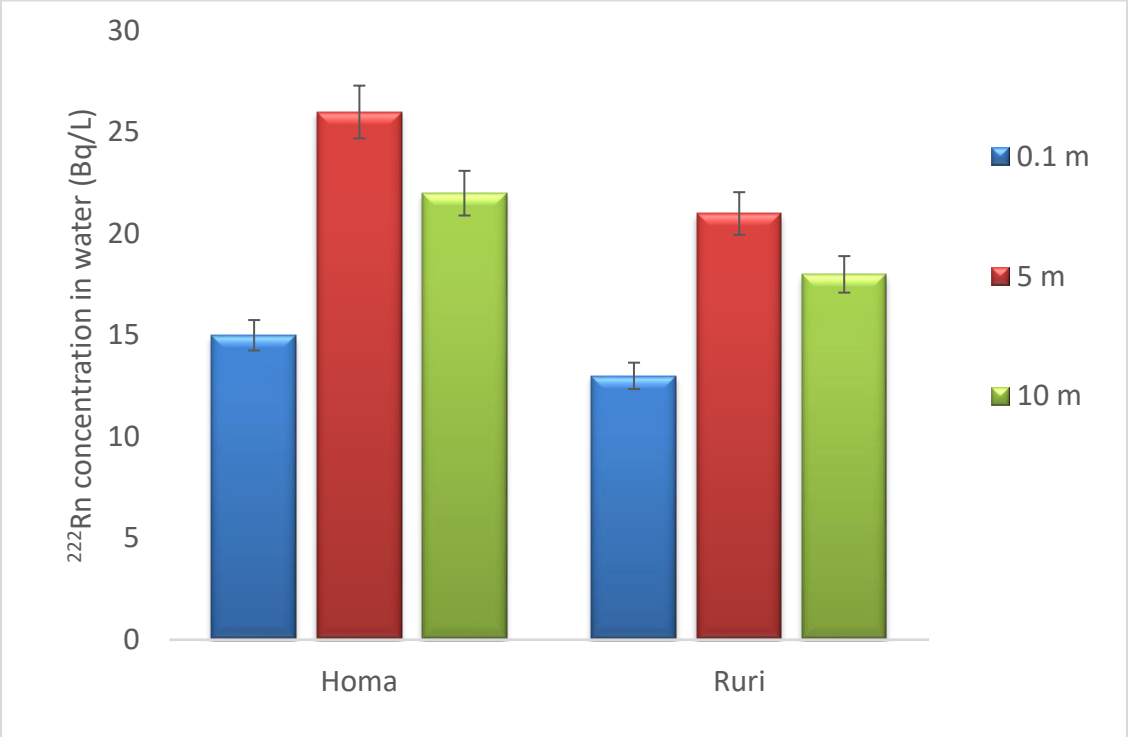


**Figure 5.15: Comparison of average $^{222}$Rn concentration at different Lake Victoria water depths between Homa and Ruri**

Figure 5.16 shows the variation of the concentration of $^{222}$Rn across all the sampled points with depth; the water surface had the least concentration in all the points, with the depth of 5 m having the highest concentration in all the points. This was attributed to the wind blowing on the lake's surface, which induces fast degassing of a large quantity of $^{222}$Rn, reducing its surface concentration compared to deeper water depths.

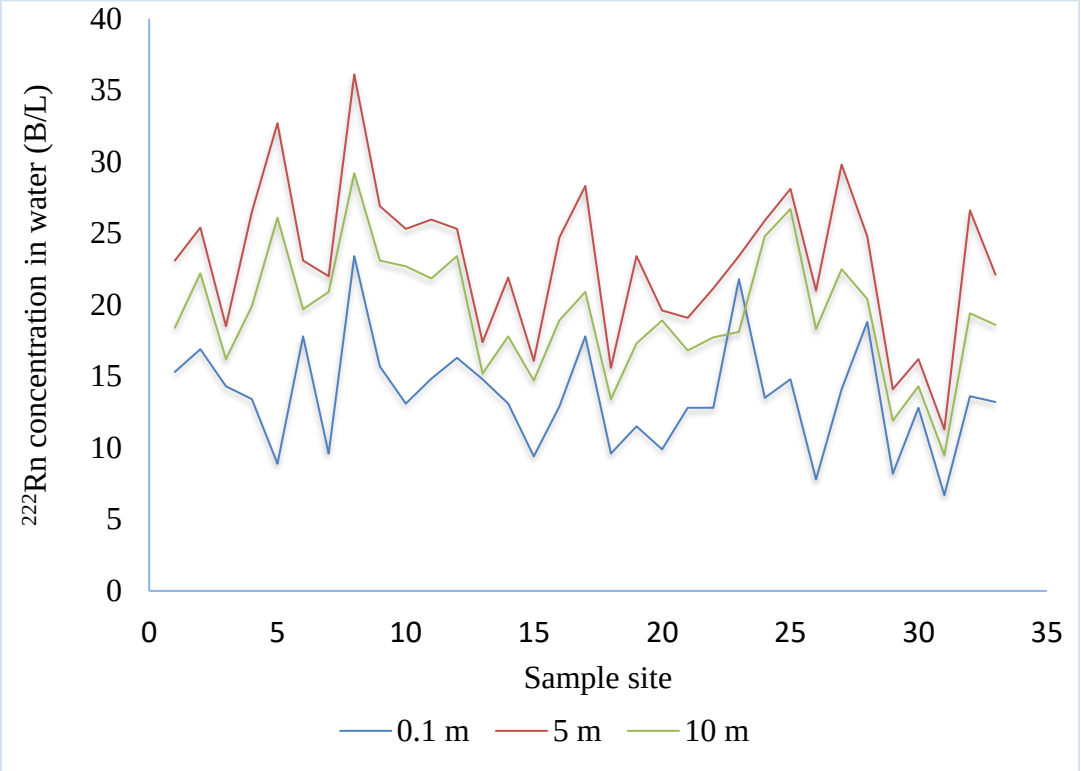


**Figure 5.16: Variation of the concentration of $^{222}$Rn across all the sampled points with depth**

The average $^{222}$Rn concentration in Lake Victoria was approximately 20%, 100% and 90% above the United States Environmental Protection Agency (US EPA, 1991) recommended limit of 11.1 Bq/L at 0.1 m, 5 m, and 10 m depths, respectively for all the samples measured. On the other hand, all the measured values of $^{222}$Rn concentrations in all the samples were below the European Commission and the WHO recommendation limit in drinking water of 100 Bq/L (EU, 2001).

The pH values from the sampled lake waters varied from a minimum of 7.2 – 8.3, with an average of 7.7, 7.9, and 8.0 in Ruri, Asego and Homa, respectively, at the water surface. There was no observed significant variation of pH with depth. The high pH was attributed

to the carbonatite rocks around region. The measured average temperature of Lake Victoria showed a general low decrease from the water surface, with depth with the surface water being approximately 0.9 $^{o}$C and 0.4 $^{o}$C higher than the 5 m and 10 m depths, respectively, which is in agreement with the previous measurements on temperature variation with depth (Sitoki *et al.*, 2010).

#### 5.3.3.1 Annual effective dose from $^{222}$Rn concentration in water

$^{222}$Rn in the water enters the human body through ingestion and inhalation, and it is released from water to indoor air; thus, radon in water becomes a source of radiation dose to both the stomach when water is directly consumed and lungs during inhalation of the water-borne radon. The annual effective dose due to ingestion of water by adults was calculated using equation 5.10 (UNSCEAR, 2000).

$$E_g = C_{RnW}\ x\ C_W\ x\ EDC \qquad (5.10)$$

Where $E_g$ is the $^{222}$Rn ingestion annual effective dose (mSv/y), $C_{RnW}$ is the radon concentration in water (Bq/L), $C_W$ is the weighted estimate of water consumption (2 liters per day for a whole year of 365 days), and EDC is the effective dose coefficient for ingestion which is 3.5 nSv/Bq.

Table 5.11 presents a summary of the ingested annual effective dose ($E_g$) due to ingestion of $^{222}$Rn in Lake Victoria at the different considered depths as measured in this work. $E_g$ was approximately 20% higher in Homa than in Ruri.

**Table 5.11: Statistical summary of ingested ($E_g$) annual effective dose rates from the $^{222}Rn$ in Lake Victoria**

| Depth | $E_g$ (μSv/y) | Homa | Ruri | Asego |
|---|---|---|---|---|
| **0.1 m** | Minimum | 22.7±3.4 | 24.0±3.6 | 17.1±2.6 |
| | Maximum | 59.8±9.5 | 45.5±7.2 | 55.2±8.8 |
| | Average | 37.8±4.5 | 33.0±3.9 | 33.7±4.0 |
| **5 m** | Minimum | 47.3±7.1 | 39.9±6.0 | 28.9±4.3 |
| | Maximum | 92.2±14. | 72.3±11.1 | 75.6±12. |
| | Average | 66.2±7.9 | 53.9±6.4 | 56.5±6.7 |
| **10 m** | Minimum | 41.4±6.2 | 34.2±5.1 | 24.3±3.6 |
| | Maximum | 75.1±12. | 58.3±9.3 | 68.2±10. |
| | Average | 55.7±6.6 | 45.2±5.4 | 47.5±5.7 |

It was 40% and 25% higher at 5 m depth than at 0.1 m and 10 m depths respectively. All its values at 0.1m samples were lower than the WHO safe limit of 100 μSv/y; approximately 30% and 20% of the samples were above WHO safe limit at 5 m and 10 m respectively. These results implies that water on Lake Victoria surface is safe for consumption as illustrated by figure 5.17.

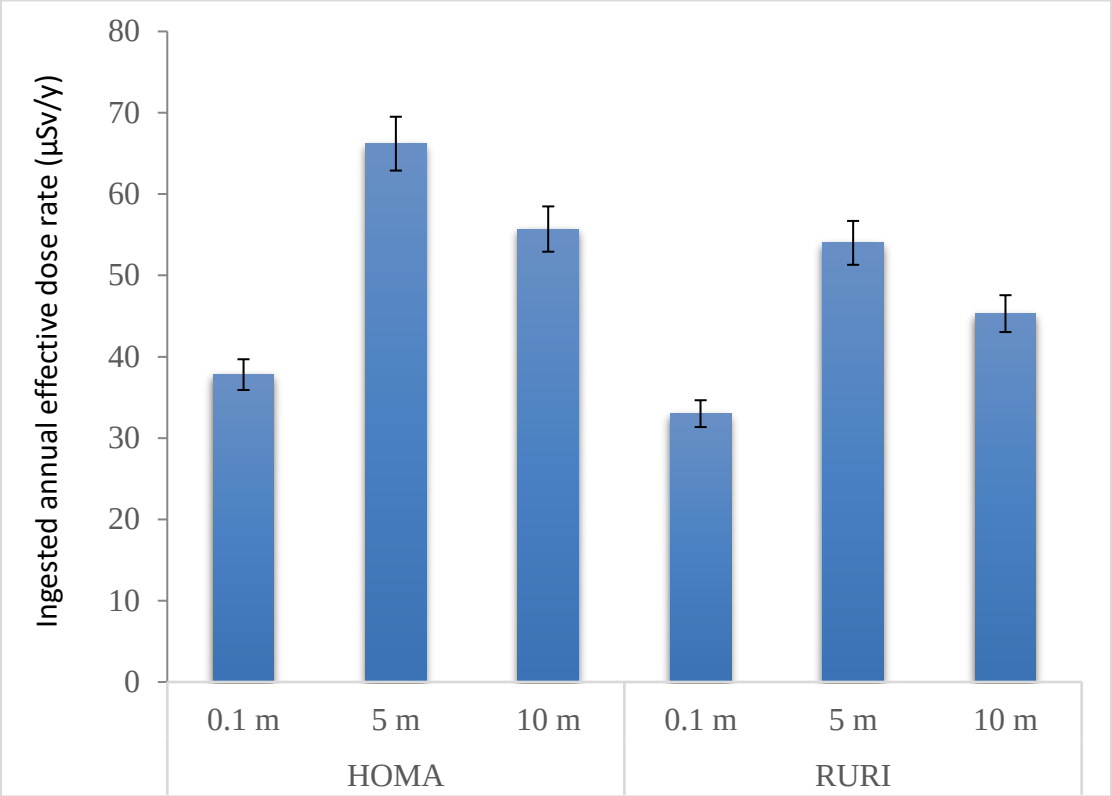


**Figure 5.17: Comparison of total average annual effective dose from $^{222}$Rn in water ingestion**

Results of the Lake Victoria water $^{222}$Rn concentration levels obtained in this work have been compared with others done in Kenya and other parts of the world, as summarized in table 5.12. Measurement of radon concentration done in Homa groundwater (Mayaka *et al.*, 2015) was about three times higher than the ones obtained in Lake Victoria around the same Homa area, as is expected for the basic reason of surface lake water easily loses radon to air due to its exposure.

**Table 5.12: Comparison of the concentration of $^{222}Rn$ and the total annual effective dose in Lake Victoria waters along Homa, Ruri and Asego, and other parts of the world**

| Region | Country | $^{222}Rn$ concentration (Bq/l) | Ingested annual effective dose (µSv/y) | Reference |
|---|---|---|---|---|
| Lake Victoria Homa Bay | Kenya | 13.6 | 34.8 | This work |
| Kenyan groundwater | Kenya | 0.8 – 371.7 | - | Otuoma *et al.*, 1998 |
| Homa hill groundwater | Kenya | 49.4 | - | Mayaka *et al.*, 2015 |
| Sudan surface water | Sudan | 14.2 | - | Elzain *et al.*, 2014 |
| Lake Darbandikhan | Irac | 0.877 | 1.6 | Jafir *et al.*, 2016 |
| Peninsular coast | Malaysia | 21 | 4.5 | Ismail *et al.*, 2021 |

## 5.4 Heavy metal analysis in Lake Victoria

### 5.4.1 Heavy metal concentration

The concentration of cadmium (Cd), lead (Pb), chromium (Cr), manganese (Mn) and nickel (Ni) in Lake Victoria waters around Homa, Ruri and Asego (Homa bay town) have been measured alongside the pH and the electrical conductivity of the water as summarized in table 5.13.

**Table 5.13: Summary of concentration of Cd, Pb, Cr, Mn, and Ni, pH, and electrical conductivity in Lake Victoria waters**

| Region | Average Concentration of heavy metals (µg/L) | | | | | pH | EC (µS/cm) |
|---|---|---|---|---|---|---|---|
| | Cd | Pb | Cr | Mn | Ni | | |
| **Homa** | | | | | | | |
| Minimum | 0.5±0.1 | 3.3±0.5 | 1.7±0.5 | 4±1 | 13.6±1.7 | 7.1±0.9 | 110±24 |
| Maximum | 4.1±0.8 | 13.9±1.8 | 7.9±1.2 | 11.1±5 | 19.9±2.5 | 8.8±1.4 | 183±36 |
| Average | 2.2±0.6 | 5.9±1.3 | 3.0±0.9 | 7.1±3 | 16.6±2.1 | 8.2±1.2 | 158±29 |
| **Ruri** | | | | | | | |
| Minimum | 0.3±0.1 | 1.1±0.3 | 1.1±0.4 | 2.1±0.5 | 13.9±1.8 | 7.0±0.8 | 104±18 |
| Maximum | 3.2±0.6 | 11.1±1.0 | 2.3±0.6 | 9.6±1.7 | 19.1±2.4 | 8.4±1.2 | 161±31 |
| Average | 1.9±0.4 | 4.3±0.8 | 1.6±0.4 | 4.3±1.4 | 17.3±2.2 | 7.9±1.1 | 144±25 |
| **Asego** | | | | | | | |
| Minimum | 0.9±0.3 | 6.0±1.0 | 0.5±0.1 | 2±0.5 | 11.9±1.2 | 6.8±0.7 | 124±22 |
| Maximum | 6.7±1.2 | 22.8±1.3 | 7.9±1.1 | 49±7 | 22.8±2.6 | 8.5±1.5 | 174±38 |
| Average | 2.9±0.7 | 12.2±1.5 | 6.0±0.6 | 14±3 | 17.8±2.2 | 8.0±1.3 | 165±33 |

The average lead concentration in Asego (Homa bay town) was 12.2 ± 1.5 µg/L which was approximately two times higher than in Homa and Ruri, respectively. The mean lead concentration in Asego was 22% higher than the WHO safe limit of 10 µg/L, attributed to leaded fuel spillages and industrial waste discharge into the lake waters along the Homa bay town shoreline. Still, it was approximately 45% lower than this limit in Homa and Ruri. Six, three and one out of the ten samples exceeded the WHO limit in Asego, Homa and Ruri, respectively. The average concentration of nickel in Homa was 16.6 ± 2.1 µg/L which was nearly equal to the concentration in Asego and Ruri but nearly four times lower than the WHO safe limit of 70 µg/L attributed to the fact that it majorly originates from nickel deposits or pollution from nickel metallic materials which are not common in these regions. In Ruri, the average cadmium concentration was 1.9 ± 0.4 µg/L, about 13% and 35% lower than Homa and Asego, respectively. The average cadmium concentration in Asego was just about 5% below the WHO recommended limit of 3 µg/L, with four samples exceeding this limit attributed to pollution from sewerage waste water in Asego; however, it was approximately 25% and 35% lower than this limit and 3 and 2 samples exceeding the limit in Homa and Ruri respectively. The average concentration of chromium in Homa was 3.0 ± 0.9 µg/L which was approximately twice that of Ruri, attributed to the use of fertilizers and herbicides in the many farms along the Homa shoreline but was about half that of Asego attributed to heavy pollution in Asego shoreline. All the measured concentrations in all samples across the three regions were below the WHO-recommended safe limit of 50 µg/L. Lastly, manganese, the only essential element measured in this work, had an average concentration of 14 ± 3 µg/L in Asego, which was about two and three times higher than Homa and Ruri, respectively, attributed to the sewerage discharge in Asego. However, its

concentration in all the samples measured was below the US EPA action levels of 50 µg/L. A comparison of the average heavy metal concentration in each of the three sampling regions and the WHO limits is shown in figure 5.18.

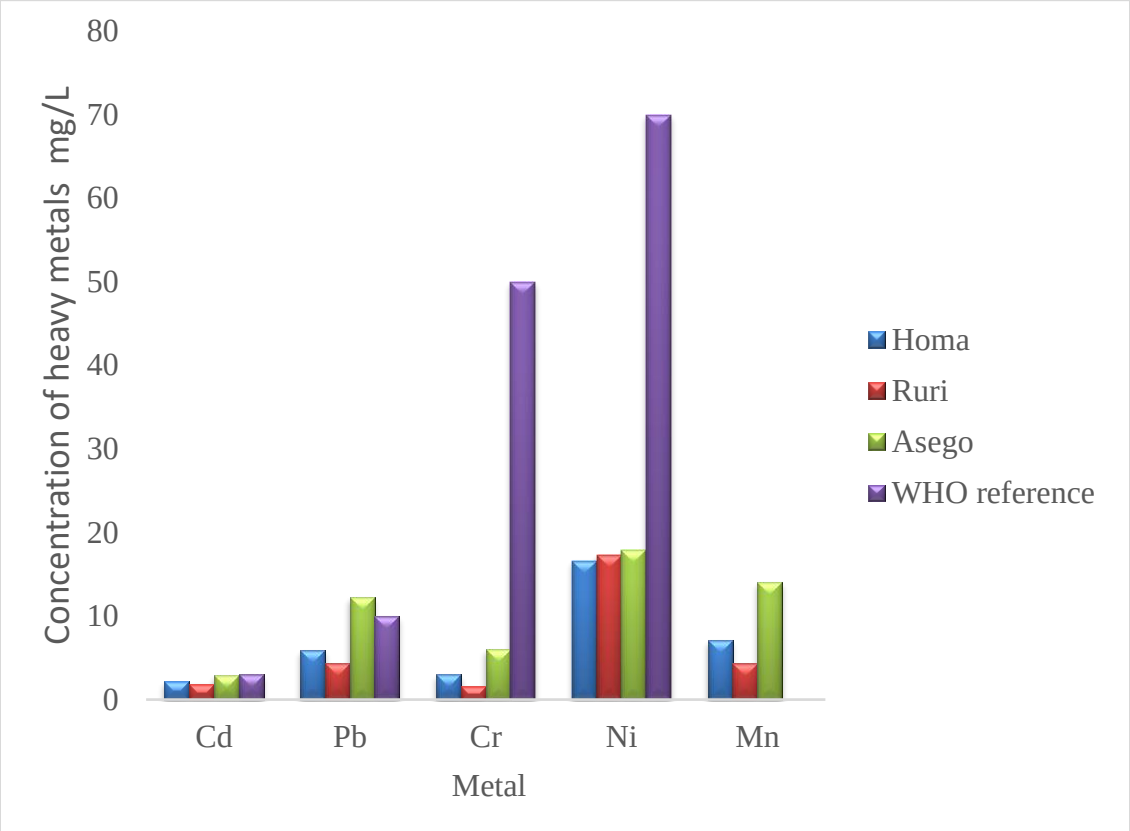


**Figure 5.18: Comparison of the concentration of the measured heavy metals in this work and WHO reference**

The average measured pH of water samples from Lake Victoria around the three sampled regions had no significant difference though slightly alkaline, due to the carbonatite rocks around these regions. The electrical conductivity of Lake Victoria waters is relatively low. It is within the group I, which includes lakes with electrical conductivity less than 600 µS

$cm^{-1}$ as categorized by (Talling *et al.,* 1966). It also generally had no significant difference across the three sampled regions.

### 5.4.2 Human Health Risk Assessment due to Heavy metals in water

The carcinogenic and non-carcinogenic effects of the studied heavy metals in water were determined by first calculating the chronic daily intake CDI (mg/kg/d) in milligrams of the heavy metal intake per kilogram of the body weight in a day by use of equation 5.11 (USEPA, 1991; Wongsasuluk et al., 2014; Nyambura *et al.,* 2020).

$$CDI = \frac{C_m \text{ x } IR \text{ x } EF \text{ x } ED}{BW \text{ x } AT} \quad (5.11)$$

Where $C_m$ is the concentration of the metal in water (mg $L^{-1}$), IR is the ingestion rate per unit time (1 L per day for a child and 2L per day for an adult in the studied region), EF is the exposure frequency (350 days/year), ED is the exposure duration (66.7 years which is the average life expectancy in Kenya) WHO (2017), BW is the body weight in kg (Averagely 70 kg for adults and 15 kg for children) and AT is the average time of exposure (AT = ED x 365 days for carcinogenic in both adults and children. For non-carcinogenic (AT = 365 days x 30 years) for adults and (AT = 365 days × six years) for children, where 30 and 6 years are the average numbers of years of non-carcinogenic exposure from heavy metals in the lifetime of an adult and child respectively (USEPA, 2011a).

The non-carcinogenic effects due to heavy metals in drinking water were determined by the non-cancer hazard quotient (HQ) using equation 5.12 (US EPA, 2011a; Wongsasuluk *et al.,* 2014; Nyambura *et al.*, 2020).

$$HQ = \frac{CDI}{RfD} \quad (5.12)$$

Where HQ is the non-cancer hazard quotient, CDI is the chronic daily intake (mg $kg^{-1}$ $d^{-1}$) $R_fD$ is the Reference dose as provided by (US EPA, 2011a) as listed in table 5.14 which is an estimate of a daily oral exposure level for the human population. The Potential risk to human health was determined by the summation of the HQ for all the heavy metals measured, known as chronic hazard index (HI), which has a safety limit of 1, which also applies to the individual HQs.

The incremental lifetime cancer risk determined the carcinogenic health risk (ILCR) calculated using equation 5.13 (US EPA, 2011a; Nyambura *et al.*, 2020).

$$ILCR = CDI\ x\ CSF \tag{5.13}$$

Where CDI is the chronic daily intake, CSF is the cancer slope factor, simply the risk produced by a lifetime average dose of 1 mg/kg body weight/day of heavy metal, as listed in table 5.14 (US EPA, 2011a). The total cancer risk was determined by the summation of the individual metal incremental risks for all the heavy metals considered. (US EPA, 2011a) considers the allowed cancer risk within a range of $1 \times 10^{-6}$ to $1 \times 10^{-4}$.

**Table 5.14: Oral reference dose ($R_fD$) and Cancer slope factor (SF) (USEPA, 2011a) were used in this work**

| Heavy metal | Oral $R_fD$ (mg/kg/d) | Cancer Slope factor (CSF) $(mg/kg/d)^{-1}$ |
|---|---|---|
| Cd | $5 \times 10^{-4}$ | $6.1 \times 10^{-3}$ |
| Pb | $3.5 \times 10^{-3}$ | $8.5 \times 10^{-3}$ |
| Cr | $3.0 \times 10^{-3}$ | $4.1 \times 10^{-3}$ |
| Ni | $2.0 \times 10^{-2}$ | $8.4 \times 10^{-4}$ |
| Mn | $1.4 \times 10^{-1}$ | Not cancerous |

The non-carcinogenic health risks from consuming heavy metals in water were determined by the non-cancer hazard quotient (HQ) and its summation chronic hazard index (HI), as summarized in table 5.15.

**Table 5.15: Summary of non-cancer hazard quotient (HQ) and chronic hazard index (HI) in Lake Victoria waters for adults and children**

| | HQ | Homa | Ruri | Asego |
|---|---|---|---|---|
| **Adults** | Cd | 0.260 | 0.231 | 0.353 |
| | Pb | 0.898 | 0.655 | 1.886 |
| | Cr | 0.001 | 0.001 | 0.001 |
| | Ni | 0.051 | 0.053 | 0.054 |
| | Mn | 0.003 | 0.002 | 0.006 |
| | HI | 1.222 | 0.901 | 2.301 |
| **Children** | Cd | 0.671 | 0.579 | 0.883 |
| | Pb | 2.250 | 1.640 | 4.650 |
| | Cr | 0.000 | 0.000 | 0.001 |
| | Ni | 0.126 | 0.131 | 0.136 |
| | Mn | 0.008 | 0.005 | 0.015 |
| | HI | 3.100 | 2.400 | 5.700 |

The average hazard quotient for cadmium was below the limit of 1 for adults and children in the three sampled regions, except for four sample points in Asego. Lead had the highest average HQ with nearly two and four times more than the recommended limit of 1 for adults and children, respectively, in Asego, as the Homa and Ruri also had an approximate average of 1.5 and 2 times higher, respectively for the case of children. Chromium, nickel, and manganese-all had values below the recommended safe limit of 1 in all the sampled points for adults and children.

The average chronic index (HI) was 20% and 60% higher than the safe limit of 1 in Homa and Asego, respectively, for adults, while for children, it was approximately 3, 2 and 5 times higher in Homa, Ruri, and Asego respectively. The hazard indices for children were higher than for adults implying that children experience more non-cancer risks than adults as they absorb chemicals four times more than adults (Akkus & Ozdenerol, 2014).

The carcinogenic health risks from consuming heavy metals in water were determined by incremental lifetime cancer risk (ILCR) and its summation for all the considered carcinogenic metals, as summarized in table 5.16.

**Table 5.16: Summary statistics of incremental lifetime cancer risk (ILCR) in Lake Victoria waters along Homa, Ruri, and Asego for adults and children**

| | **ILCR x $10^{-4}$** | **Homa** | **Ruri** | **Asego** |
|---|---|---|---|---|
| **Adults** | Cd | 0.4 | 0.3 | 0.5 |
| | Pb | 1.4 | 1.1 | 2.8 |
| | Cr | 3.3 | 1.8 | 6.7 |
| | Ni | 0.5 | 0.4 | 0.7 |
| | Total ILCR | 5.6 | 3.6 | 10.7 |
| **Children** | Cd | 0.9 | 0.8 | 1.2 |
| | Pb | 3.2 | 2.3 | 6.6 |
| | Cr | 8.1 | 4.2 | 16.1 |
| | Ni | 0.8 | 0.9 | 0.9 |
| | Total ILCR | 13 | 8.2 | 24.8 |

According to US EPA, any heavy metal with an ILCR less than 1 x $10^{-6}$ is considered insignificant to cancer risk, while an ILCR above 1 x $10^{-4}$ is considered a potential cancer risk. From the results, the ILCR for the considered heavy metals had chromium with the

highest chance of cancer risk followed by lead and the least being cadmium for both adults and children in all the three studied regions. The average total ILCR in Asego was the highest at 141 x $10^{-4}$ and 249 x $10^{-4}$ for the case of adults and children, respectively, which were nearly four and two times higher than Ruri and Homa, respectively. The obtained average total ILCR were all above the recommended limit of 1 x $10^{-4}$ by a factor of 5.6, 3.6 and 10.7 for adults and 13, 8.2 and 24.8 for children in Homa, Ruri and Asego respectively, thus posing a potential cancer risk to the residents for both adults and children with children having the greatest risk.

Results obtained in this work have been compared with other previous measurements of heavy metals in Lake Victoria around Homa bay county and generally Winam gulf (gulf of the northeastern corner of Lake Victoria, southwestern Kenya), as summarized in table 5.17.

**Table 5.17: Comparison of the measured concentration of the selected heavy metals in this work and other previous measurements in Lake Victoria**

| **Region** | **Average Concentration of heavy metals (µg/L)** | | | | | **Reference** |
|---|---|---|---|---|---|---|
| | **Cd** | **Pb** | **Cr** | **Mn** | **Ni** | |
| Homa bay (Homa, Ruri & Asego) | 2.3 | 7.5 | 3.5 | 8.5 | 17 | This work |
| Homa bay (Mainuga) | - | 1.1 | 0.4 | - | 2.2 | Outa *et al.*, 2020 |
| Homa bay (Homa farms) | 10 | 35 | - | 89 | - | Akenga *et al.*, 2019 |
| Winam gulf | 0.1 | 1.6 | 0.2 | - | - | Ogoyi *et al.*, 2011 |
| Winam gulf | 10 | 15 | - | - | - | Tole et al., 2003 |
| Winam gulf | | 1 - 9 | BDL - 4 | 10 - 390 | - | Mwamburi *et al.*, 1996 |

The measurements done by Outa et al. 2020 in Mainuga, which is between Homa and Asego showed approximately seven times lower concentrations of Ni, Pb and Cr compared to the ones obtained in this work. This is attributed to the fact that Mainuga is a rural setup with few agricultural activities and, thus, few pollutants. However, measurements done by Akenga et al., 2019 in the irrigation water from Lake Victoria in Homa hill farms had four times higher concentrations of lead and cadmium and nearly ten times higher for manganese compared to the concentrations obtained in this work attributed to the pollution by leaded fuel spillages by the pumps used, fertilizers, herbicides, and other industrial farm inputs applied.

# CHAPTER SIX: CONCLUSION AND RECOMMENDATIONS

## 6.1 Conclusion

The activity concentration levels of $^{226}Ra$, $^{232}Th$ and $^{40}K$ in earthen building materials used in high background radiation areas of Homa and Ruri had all the measured activity concentration values above the world average values of 35 Bq/kg, 30 Bq/kg and 400 Bq/kg respectively (UNSCEAR, 2000). The Radium equivalent absorbed gamma radiation dose rate and indoor annual effective dose rate has also been determined from the measured activity concentrations. $^{232}Th$ was the highest contributor to the total radium equivalent and indoor annual effective dose rates in both Homa and Ruri. Therefore, the radionuclide responsible for the largest radiation exposure in the studied region is $^{232}Th$. It was attributed to high monazite levels. The determined indoor annual effective dose rates due to exposure to indoor gamma radiation was above the recommended safety limit of 1 mSv/y for all the sampled houses in Ruri and 80% of the sampled houses in Homa (ICRP, 2005). The measured values of $^{226}Ra$, $^{232}Th$, and $^{40}K$ in all the maize samples indicated a potential cancer risk as the determined total ELCR was higher than ICRP safe limit.

A model of absorbed gamma dose by considering non-secular equilibrium in $^{232}Th$ decay series due to $^{220}Rn$ release has been developed and validated through direct field measurements, both of which showed a strong agreement. The modeled values of absorbed dose were approximately 15% lower than the ones calculated without considering the effect of non-secular equilibrium in the $^{232}Th$ decay series.

The $^{220}Rn$ surface exhalation rates were higher than $^{222}Rn$. The exhalation rate of $^{220}Rn$ determined from each of the thirty sample points in this research work was higher than the world average of 1 $Bq/m^2/s$ while all the values of $^{222}Rn$ exhalation rate from the 30

sample points in this work were lower than the world average of 26.2 mBq/$m^2$/s (UNSCEAR, 2008).

The concentration of indoor $^{222}$Rn in the sampled houses in Homa and Ruri was all below the WHO $^{222}$Rn reference level of 100 Bq/$m^3$. Similarly, the determined inhaled annual effective dose as a result of $^{222}$Rn was below the ICRP recommended safe limit of 3 mSv/y[1] in all the houses considered; however, the inhaled annual effective dose rate as a result of $^{220}$Rn was above this limit in all the sampled houses for both Homa and Ruri. $^{220}$Rn contributed nearly 85% to the total annual inhaled effective dose in both Homa and Ruri hills, attributed to the high $^{232}$Th activity concentration levels. Therefore, $^{220}$Rn is a major contributor to radiation exposure due to the inhalation of air in this region.

The measured concentration of $^{222}$Rn in Lake Victoria Homa Bay County, Kenya, at different depths from the lake water surface, had significant variations with an increase in the concentration up to 5 m depth and then a decrease downwards. The annual effective dose as a result of the water ingestion in all the considered depths and sampled region were below the safe limit of 100 µSv/y (UNSCEAR, 2008) thus, the lake water has safe radon levels.

The concentration of cadmium, lead, chromium, manganese, and nickel measured along the shoreline of Homa, Ruri, and Asego have shown heavy pollution from partially treated municipal and industrial wastes. This greatly contributes to the levels of heavy metals in Lake Victoria, as observed in Asego (Homa bay town) shoreline, which had the highest concentrations. The results on carcinogenic and non-carcinogenic effects indicate a potential health risk as both the determined HI and HQ in this work were above the safe limit of 1 and 1 x $10^{-4,}$ respectively, for the sampled regions.

Radiation exposure from indoor air, indoor gamma radiation from building materials, terrestrial radionuclides in maize, $^{222}$Rn in Lake Victoria in Homa and Ruri have indicated elevated levels of radiological exposure to the residents. The combined total annual effective dose as a result of building materials, maize, indoor air and Lake Victoria water in Ruri was 12.6 mSv/y which was 45% higher than Homa. Indoor air, building materials, maize and water each contributed 45%, 30, 24% and 1% respectively of the dose in both regions. Therefore, indoor $^{222}$Rn and $^{220}$Rn are the highest contributors to radiation exposure in Homa and Ruri.

## 6.2 Recommendations

1. The earthen building materials in both hills are not safe for the construction of the dwellings; therefore, the residents should source earthen building materials from other surrounding areas like Asego to construct their houses.
2. The residents should reduce the intake of maize grown in the region and mix it with other maize grown from other regions.
3. The non-secular equilibrium in the decay series of $^{232}$Th should be considered when determining the absorbed gamma dose in porous building materials like soil to avoid overestimation.
4. Houses in both regions require proper ventilation and increased smearing of the walls to reduce the cracks on them and the risk of high levels of indoor $^{222}$Rn and $^{220}$Rn.
5. The residents should boil the Lake Victoria water, and the water should also be constantly monitored for $^{222}$Rn levels for safe water use by residents.

6. There is an immediate need to control the influx of heavy metals into Lake Victoria and constantly monitor heavy metal concentration levels.

## REFERENCES

Achola, S. O., Patel, J. P., Mustapha, A. O., and Angeyo, H. K. (2012). Natural radioactivity and external dose in the high background radiation area of Lambwe East, Southwestern Kenya. *Radiation Protection Dosimetry*, *152*(4), 423-428.

Akenga, T. (2019). Investigation of Selected Heavy Metal Ions in Irrigation Water, Soil, and Managu (Solanum Nigrum) from Homa hills, Homabay County, Kenya.

Akkus, C., and Ozdenerol, E. (2014). Exploring Childhood Lead Exposure through GIS: A Review of the Recent Literature. *International Journal of Environmental Research and Public Health*, 11, 6314-6334. http://dx.doi.org/10.3390/ijerph110606314.

Ali, N., Khan, E. U., Akhter, P., Khan, F., and Waheed, A. (2010). Estimation of mean annual effective dose through radon concentration in the water and indoor air of Islamabad and Murree. *Radiation protection dosimetry*, *141*(2), 183-191.

Asaduzzaman, K., Khandaker, M. U., Amin, Y. M. and Mahat, R. (2015) Uptake and distribution of natural radioactivity in rice from the soil in north and west part of peninsular Malaysia for the estimation of ingestion dose to man. *Annual Nuclear. Energy* 76, 85–93.

Barbier O., Jacquillet G., Tauc M, Cougnon M and Poujel P., (2005). Effects of Heavy Metals on, and Handling by, the Kidney. *Nepgron Physiology*, 99(4): 105-110.

Bavarnegin, E., Moghaddam, M. V., and Fathabadi, N. (2013). Natural radionuclide and radiological assessment of building materials in high background radiation areas of Ramsar, Iran. *Journal of Medical Physics/Association of Medical Physicists of India*, *38*(2), 93.

BEIR VII, (2006). Health Risks from Exposure to Low Levels of Ionizing Radiation. Health risks from low levels of ionizing radiation: BEIR VII, Phase 2.

Beretka, J., and Mathwew, P. J. (1985). Natural Radioactivity of Austrian Building Materials, Industrial Waste, and By-Products, Health Phys., 48, 87.

Carrer, P., Wargocki, P., Fanetti, A., Bischof, W., De Oliveira Fernandes, E., Hartmann, T.,Seppa¨nen,Cember, H., and Thomas, J. E. (2006). Physics by Introduction to Health Physics, 4th Edition.

CEN 15251. (2007). European Committee for Standardization, "EN 15251: 2007. Indoor environmental input parameters for design and assessment of energy performance of buildings addressing indoor air quality, thermal environment, lighting and acoustics," CEN, 2007.

Chege, M. W., Hashim, N., Nyambura, C., Mustapha, A., Hosoda, M., and Tokonami, S. (2019). Radon and Thoron; Radioactive Gases Lurking in Earthen houses in Rural Kenya. Frontiers in public health, 7: 113.

Chege, M. W. (2015). *Modelling radon and thoron exhalation and measurement of total natural radiation exposure in Mrima Hill, Kenya*, (PhD Thesis, Kenyatta University).

Chege, M. W., Hashim, N. O., and Merenga, A. S. (2013). Physio-Chemical Analysis of Groundwater in the Gazi-Mrima Hill Region of Kwale County, Kenya. *Asian journal of Science and Technology*, *4*(05), 055-058.

Chege, M. W., Hashim, N., Nyambura, C., Mustapha, A., Hosoda, M., and Tokonami, S. (2019). Radon and Thoron; Radioactive Gases Lurking in Earthen Houses in Rural Kenya. *Frontiers in public health*, ***7***: 113.

Chen, J., Bergman, L., Falcomer, R., and Whyte, J. (2014). Results of simultaneous radon and thoron measurements in 33 metropolitan areas of Canada. *Radiation protection dosimetry* ***163*****(2)**: 210-216.

Colgan P. A., Organo C., Hone C. and Fenton D., (2008). Radiation Doses Received by the Irish Population: *Radiological Protection Institute of Ireland*: PPII08/01.

Cozmuta, I., Van der Graaf, E., and De Meijer, R. (2003). Moisture dependence of radon transport in concrete: Measurements and Modeling. *Health Physics.* 85: 438-456.

Crameri, R. and Burkart, W. (1989) 'The radon problem,' International Journal of Radiation Applications and Instrumentation, Part C, *Radiation Physics and Chemistry, Elsevier*, Vol. 34, No. 2, pp.251–259.

Currie, L. A. (1968). "Limits for qualitative detection and quantitative determination. Application to radiochemistry.". *Analytical Chemistry* 40.3, 586-593.

Cuttler, J. M. (2013). Commentary on Fukushima and the beneficial effects of low radiation. *Canadian Nuclear Society Bulletin*, 34(1), 27-32.

De Jong, P., and Van Dijk, W. (2008). Modeling Gamma Radiation Dose in Dwellings due to Building Materials, *Health Physics* 94, 33.

De Jong, P., Van Dijk, W., van der Graaf, E. R., and de Groot, T. J. (2006). National survey on the natural radioactivity and 222Rn exhalation rate of building materials in the Netherlands. *Health physics 91*(3), 200-210.

De With, G., Smetsers, R. C. G. M., Slaper, H., and De Jong, P. (2018). Thoron exposure in Dutch dwellings–An overview. *Journal of environmental radioactivity*, *183*, 73-81.

DURRIDGE Co. (2015). RAD7 *Electronic Radon detector user manual*.

DURRIDGE Co. (2015). *RAD7 CAPTURE software manual version 4.7.5, 2012.*

DURRIDGE Co. (2015). *Big Bottle System High Sensitivity Radon in Water Accessory for the RAD7 With Aerator Cap Revision B User Manual*.

Eisenbud, M., and Gesell, T. (1997). Environmental Radioactivity from Natural, Industrial and Military Sources: From Natural, Industrial and Military Sources. California, USA: Academic Press.

Elzain, A. E. A., Idriss, H., Mohammed, Y. S., Mohamed, K. S., Ali, M. A. E. M., Elkhalig, M. M. S. H., and Rabih, M. N. A. (2019). Assessment of radioactivity from selected soil samples from Halfa Aljadida area, Sudan *Radiochemical Acta*, *107*(6), 489-502.

Elzain, A. E. A. (2014). Measurement of Radon-222 concentration levels in water samples in Sudan. *Advances in Applied Science Research*, *5*(2), 229-234.

EN-15251, CEN. (2007). "Indoor environmental input parameters for design and assessment of energy performance of buildings - Addressing indoor air quality, thermal environment, lighting, and acoustics," Brussels: CEN.

European Society of Radiology (ESR) communications@ my ESR. org. (2015). Summary of the European Directive 2013/59/Euratom: essentials for health professionals in radiology. *Insights into imaging*, *6*, 411-417.

Euratom. (2014). Laying down basic safety standards for protection against the dangers arising from exposure to ionizing radiation. European Union Council.

Feinendegen, L. E., Pollycove, M., and Neumann, R. D. (2012). Hormesis by low-dose radiation effects: Low-dose cancer risk modeling must recognize up-regulation of protection. Therapeutic Nuclear Medicine.

Frutos-Puerto, S., Pinilla-Gil, E., Andrade, E., Reis, M., Madruga, M. J., and Rodríguez, C. M. (2020). Radon and thoron exhalation rate, emanation factor and radioactivity risks of building materials of the Iberian Peninsula. *Peer Journal*, *8*, e10331.

Hassan, N. M., Hosoda M., Iwaoka K., Sorimachi A., Janik M., Kranrod C., Sahoo S. K., Ishikawa T., Yonehara H., Fukushi M. And Tokonami S., (2011). Simultaneous Measurement of Radon and Thoron Released from Building Materials Used in Japan. *Progress in Nuclear Science and Technology* **1**: 404-407.

IAEA, GSR Part 3. (2014). IAEA Safety Standards for protecting people and the environment. Radiation Protection and Safety of Radiation Sources: International Basic Safety Standards. General Safety Requirements Part 3. VIENNA ISBN 978–92 –0–135310–8 ISSN 1020–525X No. GSR Part 3:

IAEA-TRS 474. (2013). Measurement and Calculation of Radon Release from NORM Residues. IAEA Technical Reports Series No. 474. Vienna: IAEA.

ICRP. (1991). Recommendations of the International Commission on Radiological. Publication 60. Oxford: Pergamon Press.

ICRP. (1995). Age-dependent doses to members of the public from intake of radionuclides: Part 4. Inhalation dose coefficients. ICRP Publication 71. Annals of the ICRP 25(3-4). Oxford: International Commission on Radiological Protection, Pergamon Press,

ICRP. (1995). Basic anatomical and physiological data for use in radiological protection: the skeleton. ICRP Publication 70. Annals of the ICRP 25(2). International Commission on Radiological Protection, Pergamon Press, Oxford,

ICRP. (1996). Conversion coefficients for use in radiological protection against external radiation. ICRP Publication 74. Annals of the ICRP 26(3-4). Oxford, International Commission on Radiological Protection, Pergamon Press.

ICRP. (2005). Low-dose extrapolation of radiation-related cancer risk. ICRP Publication 99. Annals of the ICRP 35(4).,. International Commission on Radiological Protection, Elsevier Ltd.

ICRP. (2007). Recommendations of the International Commission on Radiological Protection. Publication.

ICRP. (2010). Recommendations of the International Commission on lung cancer risk from radon, progeny, and Statement on Radon. ICRP Publication 115.

Ismail, N. F., Hashim, S., Sanusi, M. S. M., Abdul Rahman, A. T., and Bradley, D. A. (2021). Radon Levels of Water Sources in the Southwest Coastal Region of Peninsular Malaysia. *Applied Sciences*, *11*(15), 6842.

Iwaoka, K., Hosoda, M., Suwankot, N., Omori, Y., Ishikawa, T., Yonehara, H., and Tokonami, S. (2015). Natural radioactivity and radon exhalation rates in man-made tiles used as building materials in Japan. *Radiation protection dosimetry*, *167*(1-3), 135-138.

Jafir, A. O., Ahmad, A. H., and Saridan, W. M. (2016). Seasonal radon measurements in Darbandikhan Lake water resources at Kurdistan region-northeastern of Iraq. In *AIP Conference Proceedings* (Vol. 1718, No. 1, p. 050001). AIP Publishing LLC.

James M. (2006). Physics for radiation protection, 2nd Edition.

Karangelos, D., Petropoulos, N., Anagnostakis, M., Hinis, E., and Simopoulos, S. (2004). Radiological characteristics and investigation of the radioactive equilibrium in the ashes produced in lignite-fired power plants. *Journal of Environmental Radioactivity*., 77, 233-246.

Kebwaro J. M., Rathore I. V. S., Hashim, N. O. and Mustapha A. O., (2011). Radiometric Assessment of Natural Radioactivity Levels Around Mrima Hill, Kenya. International Journal of the Physical Sciences, 6: 3105–3110.

Kies, A., Massen, F., and Tosheva, Z., (2002). Influence of variable stress on underground radon concentrations. *Geophysical International* **41(3)**: 325-329.

Khandaker, M. U., Wahib, N. B., Amin, Y. M., and Bradley, D. A. (2013). Committed effective dose from naturally occurring radionuclides in shellfish. *Radiation Physics and Chemistry, 88*, 1-6.

Khan MS, Srivastava D.S., and Azam A (2012). Study of radium content and radon exhalation rates in soil samples of Northern India. *Environmental Earth Science* 67(5):1363–1371.

Knoll, F. G. (2010). Radiation Detection and Measurement, 4th Edition. John Wiley and Sons.

Kranrod, C., Tamakuma, Y., Hosoda, M., and Tokonami, S. (2020). Importance of discriminative measurement for radon isotopes and its utilization in the environment and lessons learned from using the RADUET monitor. *International Journal of Environmental Research and Public Health, 17*(11), 4141.

Kumar, A., Chauhan, R., Joshi, M., and Sahoo, B. (2014). Modelling of indoor radon concentration from radon exhalation rates of building materials and validation through measurements, (2014) 50–55. *Journal of Environmental Radioactivity*., 127, 50-55.

Kurttio P., Komulainen H., Leino, A., Salonen L., Auvinen A. and Saha H., (2005). Bone as a Possible Target of Chemical Toxicity of Natural Uranium in Drinking Water. *Environmental Health Perspectives*, 113: 68-72.

Løvborg, L., Bøtter-Jensen, L., and Kirkegaard, P. (1978). Experiences with concrete calibration sources for radiometric field instruments. *Geophysics*, *43*(3), 543-549.

Le Bas, M. J. (1977). *Carbonatite-nephelinite volcanism: an African case history* (p. 347). London: Wiley.

Maina, J. A. (2008). Concentrations of radionuclides in selected foodstuffs and consumer products in Nairobi using gamma-ray spectroscopy (Doctoral dissertation, University of Nairobi, Kenya).

Mayaka, G. N., Hashim, N. O., and Angeyo, H. K. (2015). Measurement of radon activity concentration in waters from Homa Mountain South Western Kenya. *International Journal of Science, Environment and Technology* **4**: 2278-7798.

McCall, G. J. H. (1958). Geology of the Gwasi area: Geol. *Survey Kenya, Report, 45*, 88.

Meisenberg O., Gierl S. and Tschiersch J., (2013). Measurement of Thoron and its Progeny in Traditional and Modern Earthen Buildings in Germany: Methodology and Results. 2013 International Radon Symposium: Creating New Opportunities for the Radon Professional Measurement and Mitigation. September 22-25, 2013, Springfield, Illinois.

Ministry of Land, Housing and Urban Development [MOLHUD]. (2012/13). Kenya National Housing Survey Report, 2012/2013. Nairobi: Kenya National Bureau of Statistics.

Mlwilo N. A., Mohammed N. K. and Spyrou N. M., (2007). Radioactivity Levels of Staple Foodstuffs and Dose Estimates for Most of the Tanzanian Population. Journal of Radiological Protection, 27: 741-744.

Mohanty A. K., Sengupta D., Das S. K., Vijayan V. and Saha S. K., (2004). Natural Radioactivity in the Newly Discovered High Background Radiation Area on the Eastern Coast of Orissa India. *Radiation Measurements*, 38(2004): 153-165.

Momodu M. A. and Anyakora C. A., (2009). Heavy Metal Contamination of Ground Water: The Surulere Case Study. *Research Journal Environmental and Earth Sciences*, 2(1): 39-43.

Moura, C., Artur, A., Bonotto, D., Guedes, and Mar-tinelli, C. (2001). Natural radioactivity and radon exhalation rate in Brazilian igneous rocks. *Applied Radiation. Isotopes*., 69, 1094–1099.

Mubarak, F., Fayez-Hassan, M., Mansour, N. A., Salah Ahmed, T., and Ali, A. (2017). Radiological investigation of high background radiation areas. *Scientific reports*, *7*(1), 15223.

Mwamburi, J., and Oloo, F. N. (1996). The distribution and concentration levels of trace metals in water and sediments of Lake Victoria, Kenya. *African Journal of Tropical Hydrobiology and Fisheries*, *7*(1), 37-48.

National Research Council [NRC], BEIR VII. (2006). Health risks from exposure to low levels of ionizing radiation. Committee to Assess Health Risks from Exposure to Low Levels of Ionizing Radiation, BEIR VII - Phase 2. Washington D.C, National Research Council, The National Academies Press.

Nawrot T., Plusquin M., Hogervovst J.,and Roels H. A.(2006). Environmental Exposure to Cadmium and Risk of Cancer: Perspective Population-Based Study. *Lancet Oncology*, 7(2):119-126.

Nyambura, C., Hashim, N. O., Chege, M. W., Tokonami, S., and Omonya, F. W. (2020). Cancer and non-cancer health risks from carcinogenic heavy metal exposures in underground water from Kilimambogo, Kenya. *Groundwater for Sustainable Development*, *10*, 100315.

Nyambura, C., Tokonami, S., Hashim, N. O., Chege, M. W., Suzuki, T., Kudo, H., and Hosoda, M. (2019). Annual effective dose assessment due to radon and Thoron progenies in dwellings of Kilimambogo, Kenya. *Radiation protection dosimetry* ***184*****(3-4):** 430-434.

Ogoyi, D. O., Mwita, C. J., Nguu, E. K., and Shiundu, P. M. (2011). Determination of heavy metal content in water, sediment, and microalgae from Lake Victoria, East Africa. *Journal* of *Environmental Engineering* 4(1)156-161.

Omori, Y., Tokonami, S., Sahoo, S. K., Ishikawa, T., Sorimachi, A., Hosoda, M., ... and Akiba, S. (2016). Radiation dose due to radon and thoron progeny inhalation in high-level natural radiation areas of Kerala, India. *Journal of Radiological Protection*, *37*(1), 111.

Okungu, J. O., Njoka, S., Abuodha, J. O. Z., and Hecky, R. E. (2005). An introduction to Lake Victoria catchment, water quality, physical limnology, and ecosystem status (Kenyan sector).

Opiyo, A. S. (2009). *Radioactivity and elemental analysis of carbonatite rocks from parts of the Gwasi area, South Western Kenya* (Ph.D.Thesis , University of NAIROBI).

Orabi, M. (2017). Radon release and its simulated effect on radiation doses. *Health Physics*, *112*(3), 294-299.

Orabi, M. (2019). Modeling the indoor gamma-radiation dose: A review of refinements and application. *The European Physical Journal Plus*, *134*(6), 290.

Otwoma D., Patel J. P., Bartilos S. and Mustapaha A. O., (2012). Radioactivity and Dose Assessment of Rock and Soil Samples from Homa. XI Radiation Physics and Protection Conference, 25-28 November, Nasr city, Cairo, Egypt.

Otwoma, D., Patel, J., Bartilol, S., and Mustapha, A. (2013). Estimation of Annual Effective Dose and Radiation Hazards due to Natural Radionuclides in Mount Homa, Southwestern Kenya. Radiation Protection Dosimetry, 1–8.

Otwoma, D., Patel, J. P., Bartilol, S., and Mustapha, A. O. (2012). Radioactivity and dose assessment of rock and soil samples from Homa Mountain, Homa Bay County, Kenya.

Otwoma, D., and Mustapha, A. O. (1998). Measurement of $^{222}$Rn concentration in Kenyan groundwater. *Health physics*, *74*(1), 91-95.

Outa, J. O., Kowenje, C. O., Plessl, C., and Jirsa, F. (2020). Distribution of arsenic, silver, cadmium, lead and other trace elements in water, sediment, and macrophytes in the Kenyan part of Lake Victoria: spatial, temporal and bioindication aspects. *Environmental Science and Pollution Research*, *27*(2), 1485-1498.

Pandey, B., Sarma, H., Shukla, D., and Mishra, K. (2006). Low-dose radiation-induced modification of ROS and apoptosis in thymocytes of whole body irradiated mice. International Journal of Low Radiation, 2(1-2), 111-118.

Patra, A. C., Mohapatra, S., Sahoo, S. K., Lenka, P., Dubey, J. S., Tripathi, R. M., and Puranik, V. D. (2013). Age-dependent dose and health risk due to intake of uranium in drinking water from Jaduguda, India. *Radiation protection dosimetry*, *155*(2), 210-216.

Prasher D. (2009). Heavy Metals and Noise Exposure: Health Effects. Noise Health, 1(44): 141-4.

Quashie, K., Akortia, E., and Asumadu-Sakyi1, A. B. (2011). A preliminary comparative study of indoor radon measurement in Sakumono and Kassena Nankana area of Ghana. Elixir Pollution. 39, 4860–4864.

Ramola, R. C., Mukesh, P., Tushar, K., Preeti, P., Bossew, P., Rosaline, M. and Tokonami, S (2016). *Dose estimation derived from the exposure to radon, thoron, and their progeny in the indoor environment*. Sci. Rep. 6, 1–16.

Saad, A., Al-Awami, H., and Hussein, N. (2014). Radon exhalation from building materials used in Libya.

Sabath E and Robles O. M. L., (2012). Renal Health and the Environment: Heavy Metal Nephrotoxicity. *Nefrologia*, 32(3): 279-286.

Salwa, M.K., Sara, A.M., Samia, H.A., Abdalla, E.B., Manal, Y.I., (2016). Heavy metals contaminants in water and fish from four different sources in Sudan. *Infectious Diseases Therapy*. 4, 275.

Serge Didier, T. S., Saïdou, Tokonami, S., Hosoda, M., Suzuki, T., Kudo, H., and Bouba, O. (2019). Simultaneous measurements of indoor radon and thoron and inhalation dose assessment in Douala City, Cameroon. *Isotopes in environmental and health studies*, *55*(5), 499-510.

Shang B., Chen B., Gao Y., Wang Y., Cui H. and Li Z., (2005). Thoron Levels in Traditional Chinese Residential Dwellings. *Radiation and Environmental Biophysics*, 44(3): 193-199.

Sitoki, L., Gichuki, J., Ezekiel, C., Wanda, F., Mkumbo, O. C., and Marshall, B. E. (2010). The environment of Lake Victoria (East Africa): current status and historical changes. *International Review of Hydrobiology*, *95*(3), 209-223.

Smith M. A., Grant L. D., and Sors A., (1989). Lead Exposure and Child Development: An International Assessment. Kleven Academic Publishers.

Somalai, K, Tokonami S, Ishikawa T, Vancsura P, Gaspar M, Jobbagy V, Somalai Jand Kovacs T. (2007) $^{222}$Rn concentration of water in the Balaton Highland and in the southern part of Hungary, and the assessment of the resulting dose, *Radiation measurements*, 42:491-495.

Stranden, E. (1979). Radioactivity of building materials and the gamma radiation in dwellings. *Physics in Medicine and Biology*, 24, 921-930.

TALLING, J. F., (1966) The annual cycle of stratification and phytoplankton growth in Lake Victoria (East Africa). − Int. Revue ges. Hydrobiology. 51: 545–621.

Tokonami, S., Takahashi, H., Kobayashi, Y., Zhuo, W., and Hulber, E. (2005). Up-to-date radon-thoron discriminative detector for a large-scale survey. *Review of Scientific Instruments*, *76*(11), 113505.

Tokonami, S. (2020). Characteristics of thoron (220Rn) and its progeny in the indoor environment. *International Journal of Environmental Research and Public Health*, *17*(23), 8769.

Tole, M. P., and Shitsama, J. M. (2003). Concentrations of heavy metals in water, fish, and sediments of the Winam Gulf, Lake Victoria, Kenya. *Lake Victoria Fisheries: Status, Biodiversity, and Management. Aquatic Ecosystem Health and Management Society*, 1-9.

Tzortzis T. and Haralabos T. H., (2002). Gamma-Ray Measurements of Naturally Occurring Radioactive samples from Cyprus Characteristic Geological Rocks. Medical Physics Department, Nicosia General Hospital, Nicosia, Cyprus; UCY−PHY− 02/02 (Revised version: 2/12/2002): 1-27.

UNSCEAR, (2000). United Nations Scientific Committee on the Effects of Atomic Radiation. Sources and Effects of Ionizing Radiation. UNSCEAR 2000 Report to the General Assembly, with Scientific Annexes, (I): New York: United Nations, 2000.

UNSCEAR, (2008). United Nations Scientific Committee on the Effects of Atomic Radiation. Sources and Effects of Ionizing Radiation. UNSCEAR 2008 Report to the General Assembly, with Scientific Annexes, (I): New York: United Nations, 2008.

UNSCEAR. (1993). Sources and Effects of Ionizing Radiation. United Nations Scientific Committee on the Effects of Atomic Radiation. Report to the General Assembly with scientific annexes. United Nations Scientific Committee.

UNSCEAR. (2000). United Nations Scientific Committee on the Effects of Atomic Radiation. Exposures from Natural Radiation Sources, Annex B., New York: United Nations.

UNSCEAR. (2009). 2006 Report Volume II. Effects of ionizing radiation. Annex E. Sources-to-Effects Assessment for Radon in Homes and Workplaces. New York: United Nations.

UNSCEAR. (2013). United Nations Scientific Committee on the Effects of Atomic Radiation. Sources, effects, and risks of ionizing radiation report to the General Assembly, Volume II Scientific Annex B: Effects of radiation exposure of children.

US EPA (1991). National primary drinking water regulation, radionuclides (proposed rules), Vol. 56. US Environmental Protection Agency, Federal Register, p. 138.

USEPA, (2003). National Primary Drinking Water Standards. U.S. Environmental Protection Agency.

USEPA, (2004). Drinking Water Advisory for Manganese. U.S. Environmental Protection Agency, 2004.

US EPA (United States Environmental Protection Agency). *Exposure Factors Handbook: 2011 Edition*. Office of Research and Development, United States Environmental Protection Agency, Washington, DC, EPA/600/R-09/052F, 2011a.

WHO, (2009) World Health Organization Handbook on Indoor Radon: A Public Health Perspective. World Health Organization, 2009.

William J. Makofske and Michael R. Edelstein (1991) Radon and the Environment, Noyes publication, Park Ridge, New Jersey, U.S.A.pp50.

World Health Organization (WHO, 2011*). Guidelines for Drinking Water Quality. Chapter 9. Radiological Aspects, fourth edition. Geneva.*

World Health Organization. (2008). Chemical fact sheets. *Guidelines for drinking-water quality, third edition, incorporating first and second addenda*, 326-329.

Wongsasuluk, P., Chotpantarat, S., Siriwong, W., and Robson, M. (2014). Heavy metal contamination and human health risk assessment in drinking water from shallow groundwater wells in an agricultural area in Ubon Ratchathani province, Thailand. *Environmental geochemistry and health*, *36*(1), 169-182.

Xiaofeng, H., and Guosheng, W. (2011). Surface radon exhalation rates of building material and soil effect on indoor air radon concentration. *Procedia Engineering*, *18*, 122-127.

Yamada Y., Sun Q., Tokonami S., Akiba S., Zhuo W., Hou C., Zhang S., Ishikawa T., Furukawa M., Fukutsu K. and Yonehara H., (2006). Radon-Thoron Discriminative Measurements in Gansu Province, China, and their Implication for Dose Estimates. *Journal of Toxicology and Environmental Health, Part A*, 69(7):723-34.

Yamaguchi, Y. (1994). Age-dependent effective doses for external photons. *Radiation Protection Dosimetry*, 55(2): 123-129.

Zamora M. L., Tracy B. L., Zielinski J. M., Meyerhof, D. P. and Moss M. A. (1998): Chronic Ingestion of Uranium in Drinking Water: A Study of Kidney Bioeffects in Humans. *Toxicological Sciences*, 43: 68-77.

# APPENDICES

## Appendix I: $^{238}U$ Decay chain

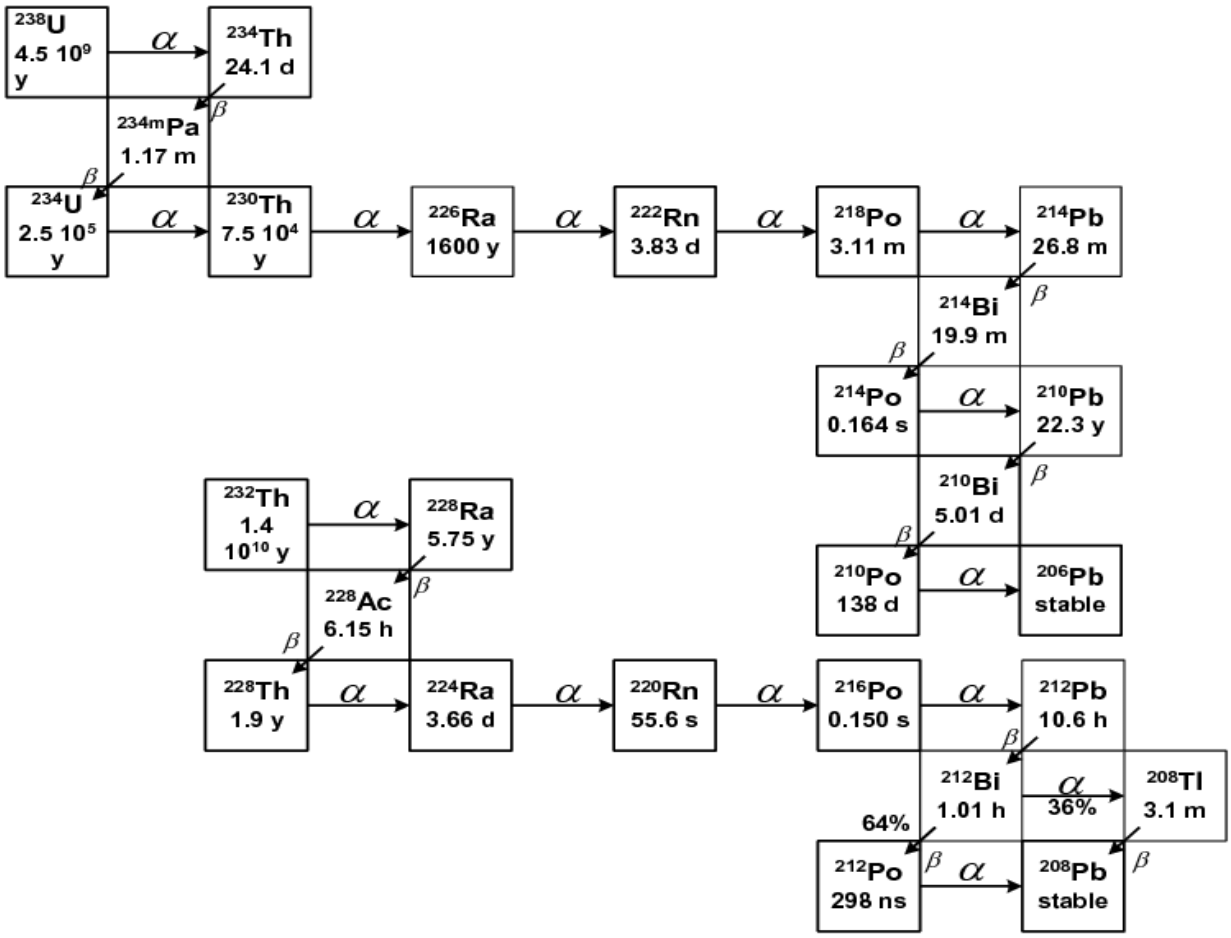


**Source: https://www.researchgate.net/figure/Decay-series-of-238-U-a-and-232-Th-b-with-half-lifes-in-years-y-months-m-days_fig4_321576814**

## Appendix II: $^{232}$Th Decay chain

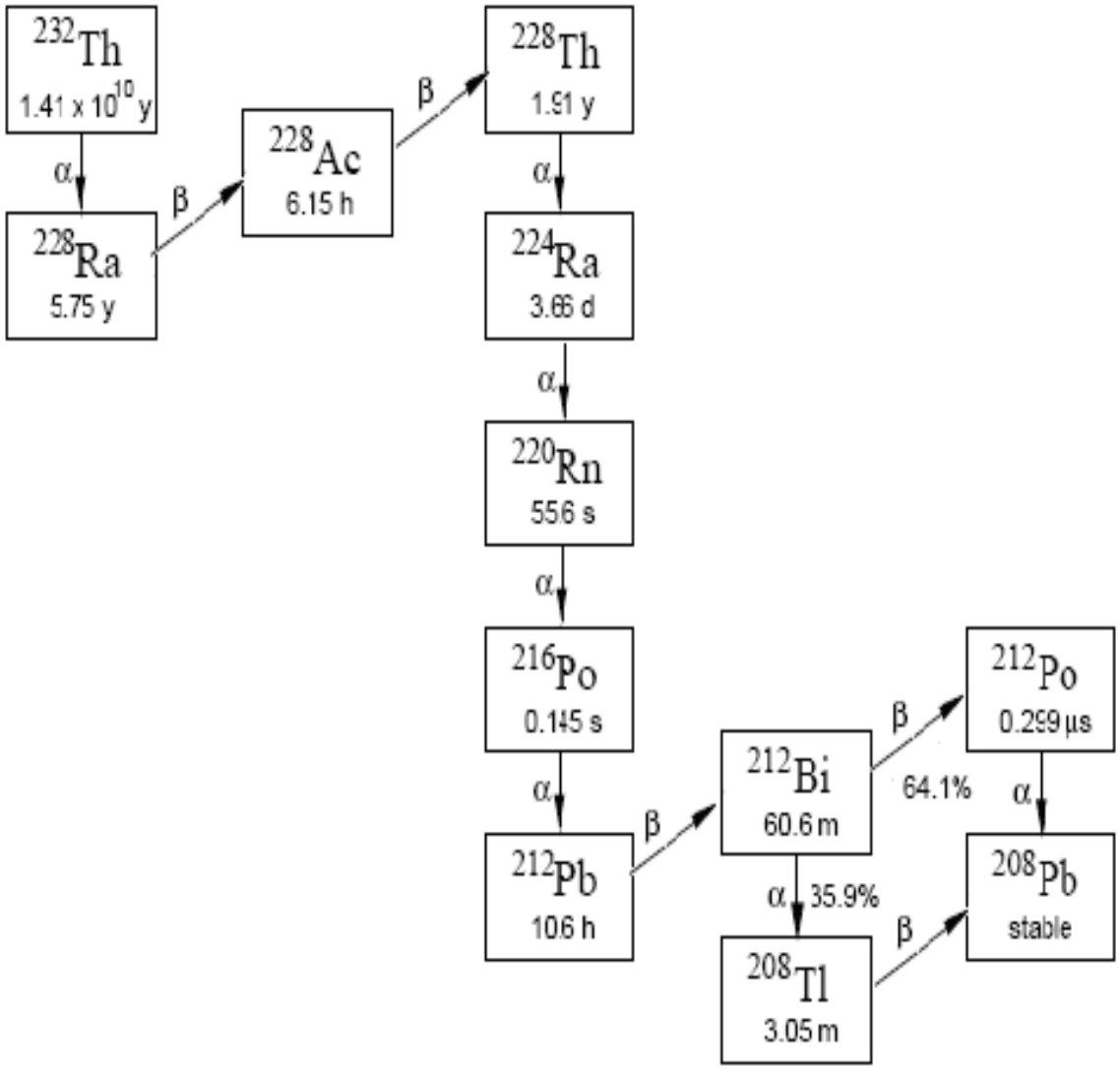


**Source: https://www.researchgate.net/figure/Decay-series-of-238-U-a-and-232-Th-b-with-half-lifes-in-years-y-months-m-days_fig4_321576814**

**Appendix III: Installation of a RADUET monitor in one of the sampled dwellings for $^{222}Rn$ and $^{220}Rn$ measurements.**

**Appendix IV: Water sample collection using the deep-water sampler in Homa at a 10 m deep point at sample site 4.**

**Appendix V: From the top is the digestion procedure, followed by heating and, lastly, the measurement of the metal concentration in the AAS.**

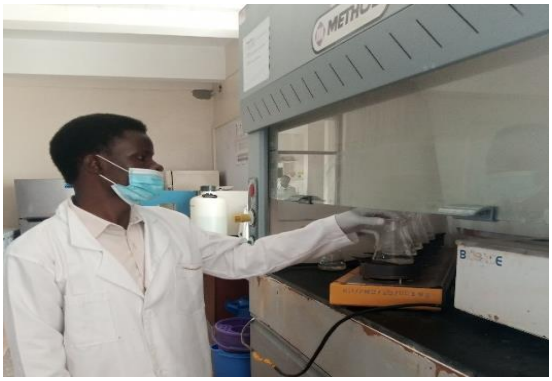

**Appendix VI: Table of Statistics for One-Way ANOVA of activity concentration of $^{226}$Ra between Homa and Ruri**

Null Hypothesis: The means of activity concentration of $^{226}$Ra between Homa and Ruri are equal.

Alternative Hypothesis: The means of activity concentration of $^{226}$Ra between Homa and Ruri are not equal

**SUMMARY**

| *Groups* | *Count* | *Sum* | *Average* | *Variance* |
|---|---|---|---|---|
| Homa | 15 | 1933 | 128.8667 | 6701.552 |
| Ruri | 15 | 1672 | 111.4667 | 3688.267 |

**ANOVA**

| *Source of Variation* | *SS* | *df* | *MS* | *F* | *P-value* | *F crit* |
|---|---|---|---|---|---|---|
| Between Groups | 2270.7 | 1 | 2270.7 | 0.437101 | 0.513929 | 4.195971819 |
| Within Groups | 145457.5 | 28 | 5194.91 | | | |
| Total | 147728.2 | 29 | | | | |

The means of activity concentration of $^{226}$Ra between Homa and Ruri are not significantly different at 0.05 level of significance

## Appendix VII: Published papers

Odongo, W. O. G., Chege, M., Tokonami, S., Hashim, N., Kranrod, C., & Nyambura, C. (2021). Radon and Thoron Exhalation Rates from Earthen Building Materials Used in High Background Radiation Areas of Homa and Ruri, Kenya. *Radiation Protection Dosimetry*, *197*(1), 12-18.

Odongo, W. O. G., Chege, M., Hashim, N., Tokonami, S., Chutima, K., & Rotich, C. (2021). Determination of Activity Concentration of Natural Radionuclides and Radiation Hazards' Assessment of Building Materials in High Background Radiation Areas of Homa and Ruri, Kenya. *The Scientific World Journal*, *2021*.

Odongo, W. O. G., Hashim, N., & Chege, M. W. (2021). Gamma Ray Spectrometric Analysis of Sand Samples from Selected Beaches along Kenyan Coastline. *The scientific world journal*, *2021*, 1-8.

## Appendix VIII: Research Permit

REPUBLIC OF KENYA

NATIONAL COMMISSION FOR SCIENCE,TECHNOLOGY & INNOVATION

Ref No: **374455**

Date of Issue: **21/September/2020**

**RESEARCH LICENSE**

**This is to Certify that Mr.. Willis Otieno Gor Odongo of Kenyatta University, has been licensed to conduct research in Homabay on the topic: DETERMINATION OF EXPOSURE FROM RADON, THORON AND TERRESTRIAL RADIONUCLIDES AND MODELLING INDOOR GAMMA RADIATION DOSE IN HOMA BAY COUNTY, KENYA for the period ending : 21/September/2021.**

License No: **NACOSTI/P/20/6822**

**374455**

Applicant Identification Number

Director General
NATIONAL COMMISSION FOR SCIENCE,TECHNOLOGY & INNOVATION

Verification QR Code

NOTE: This is a computer generated License. To verify the authenticity of this document, Scan the QR Code using QR scanner application.